FLORIDA A&M UNIVERSITY - FLORIDA STATE UNIVERSITY
COLLEGE OF ENGINEERING

INVESTIGATION OF IMPACT FACTORS FOR FDOT BRIDGES

FDOT CONTRACT NUMBER: BDK83, TASK WORK ORDER: 977-03

FINAL REPORT

Submitted to:
William Potter, Project Manager
FDOT Structures Research Laboratory
by
Jerry Wekezer, Ph.D. P.E., Principal Investigator
Eduardo Taft, B.S.
Leslaw Kwasniewski, Ph.D.
Sharnie Earle, M.S.

Tallahassee, December 2010

DISCLAIMER

The study described in this final report was supported by a contract from the Florida Department of Transportation Structures Laboratory titled "Investigation of Impact Factors for FDOT Bridges", contract number BDK83, task work order number 977-03. The project started from January 2009 through December 2010. The opinions, findings, and conclusions expressed in this report are those of the writers and not necessarily those of the sponsoring agency.

CONVERSION TABLES

Table 1. Approximate conversions to US Customary Units

Symbol	When You Know	Multiply by	to Find	Symbol
		LENGTH		
mm	millimeters	0.039	inches	in
m	meters	3.28	feet	ft
m	meters	1.09	yards	yd
km	kilometers	0.621	miles	mi
		AREA		
mm^2	square millimeters	0.0016	square inches	in^2
m^2	square meters	10.764	square feet	ft^2
m^2	square meters	1.195	square yards	yd^2
ha	hectares	2.47	acres	ac
km^2	square kilometers	0.386	square miles	mi^2
		VOLUME		
mL	milliliters	0.034	fluid ounces	fl oz
L	liters	0.264	gallons	gal
m^3	cubic meters	35.314	cubic feet	ft^3
m^3	cubic meters	1.307	cubic yards	yd^3
		MASS		
g	grams	0.035	ounces	oz
kg	kilograms	2.202	pounds	lb
Mg (or "t")	megagrams (or "metric ton")	1.103	short tons (2000 lb)	T
		FORCE and PRESSURE or STRESS		
N	newtons	0.225	pound force	lbf
kPa	kilopascals	0.145	pound force per square inch	lbf/in^2

Table 2. Approximate conversions to SI Units

Symbol	When You Know	Multiply by	to Find	Symbol
		LENGTH		
in	inches	25.4	millimeters	mm
ft	feet	0.305	meters	m
yd	yards	0.914	meters	m
mi	miles	1.61	kilometers	km
		AREA		
in^2	square inches	645.2	square millimeters	mm^2
ft^2	square feet	0.093	square meters	m^2
yd^2	square yard	0.836	square meters	m^2
ac	acres	0.405	hectares	ha
mi^2	square miles	2.59	square kilometers	km^2
		VOLUME		
fl oz	fluid ounces	29.57	milliliters	mL
gal	gallons	3.785	liters	L
ft^3	cubic feet	0.028	cubic meters	m^3
yd^3	cubic yards	0.765	cubic meters	m^3
		MASS		
oz	ounces	28.35	grams	g
lb	pounds	0.454	kilograms	kg
T	short tons (2000 lb)	0.907	megagrams (or "metric ton")	Mg (or "t")
		FORCE and PRESSURE or STRESS		
lbf	pound force	4.45	newtons	N
lbf/in^2	pound force per square inch	6.89	kilopascals	kPa

Technical Report Documentation Page

1. Report No.	2. Government Accession No.	3. Recipient's Catalog No.
FDOT BDK83		

4. Title and Subtitle	5. Report Date
INVESTIGATION OF IMPACT FACTORS FOR FDOT BRIDGES	December 31, 2010
	6. Performing Organization Code
7. Author(s)	8. Performing Organization Report No.
Jerry Wekezer (PI), Eduardo Taft, Leslaw Kwasniewski, Sharnie Earle	
9. Performing Organization Report No.	10. Work Unit No. (TRAIS)
FSU Project number 025159 and 025160 Crashworthiness and Impact Analysis Laboratory FAMU-FSU College of Engineering	11. Contract or Grant No.
12. Sponsoring Agency Name and Address	13. Type of Report and Period Covered
Florida Department of Transportation 605 Suwannee Street, MS Tallahassee, FL 32399	Draft Final 01/01/2009 – 12/31/2010
	14. Sponsoring Agency Code

15. Supplementary Notes

16. Abstract

Modern prestressed reinforced concrete bridges are designed per LRFD standards, and are more efficient with optimum load factors. At the same time they are loaded with heavier vehicles with larger mass when compared to the mass of the bridge. Imperfections in pavement and bridge decks can trigger a significant dynamic load on the bridge with adverse effects. Studying and understanding the actual impact of dynamic loads is critical for design and maintenance of Florida Department of Transportation (FDOT) bridges.

The main objective of this project was to use numerical models of heavy vehicles and bridges to conduct transient analysis of dynamic interaction between the vehicle and the bridge. An assessment of three existing finite element (FE) vehicle models and one bridge model, which were already validated under previous research, was conducted and the necessary improvements were implemented. Two additional bridges were developed according to the American Association of State Highway and Transportation Officials (AASHTO) specifications.

Three FE models of heavy vehicles were used with three different bridges for computational dynamics analysis. The dynamic load allowance (DLA, previously referred to as a dynamic impact factor) was determined for each vehicle-bridge combination. The influence of factors including vehicle mass and speed in the dynamic response of the bridge were studied by analysis using LS-DYNA computer code.

17. Key Word	18. Distribution Statement
Finite element analysis, LS-DYNA, vehicle - bridge interaction, dynamic load.	

19. Security Classif. (of this report)	20. Security Classif. (of this page)	21. No. of Pages	22. Price
Unclassified.	Unclassified.	158	

Form DOT F 1700.7 (8-72) Reproduction of complete page authorized

ACKNOWLEDGEMENTS

This study was completed under direction and in cooperation with Mr. Marc Ansley, the Project Manager and previous Director of the FDOT Structures Laboratory. The research team appreciates his commitment in supporting this research during the past few years, prior to his untimely death. His dedication to the advancement of knowledge in the bridge engineering field will be greatly missed. The support from Mr. William Potter and Mr. Sam Fallaha from the FDOT Structures Research Laboratory throughout the duration of this project is greatly appreciated.

This project was a continuation of earlier FDOT research projects No. BD493 and BD543 carried out by Dr. Hongyi Li, Dr. Leslaw Kwasniewski, Dr. Piotr Szurgott and Dr. Jerry Wekezer.

The Transportation Research and Analysis Computing Center (TRACC), Energy Systems Division, Argonne National Laboratory and the High Performance Computing Laboratory at The Florida State University provided diverse computing resources to aid in the development of the project. Constant technical support and guidance with LS-DYNA was provided by staff member of TRACC, Dr. Cezary Bojanowski.

All the comments, advice, guidance, and technical support provided by this group of professionals were essential in the development of the project and are highly appreciated.

EXECUTIVE SUMMARY

The dynamic load allowance (DLA) is a quantitative measure of dynamic effects exerted in addition to static loads by moving vehicles on highway bridges. The American Association of State Highway and Transportation Officials (AASHTO) recommend using 33% as a maximum value of DLA. This final report presents results of extensive investigation of DLA, which was carried out for the Florida Department of Transportation (FDOT) for a broad class of prestressed reinforced concrete bridges. FDOT manages over 6400 such bridges and precise information about their performance, due to heavy (so called: permit) vehicles, is critical for its Permit Office. Two parallel tracks, experimental and analytical, were designed and implemented as integral parts of this research. Each track resulted in data which was used to calculate DLA. Comparison of these results showed a good correlation between experiments and analyses and was used to verify and validate finite element (FE) models developed.

All experimental tests were carried out on a selected, typical, prestressed, reinforced concrete bridge (#500133) on US 90 in northeastern Florida. It is a newer bridge, built in 1999 with three simply supported spans and AASHTO type III girders. A selected span of the bridge was instrumented with: (a) two linear variable displacement transformers (LVDT), (b) 38 strain gauges and (c) 14 accelerometers installed at the top of the bridge deck. Several static and dynamic tests were carried out with speeds of 48 km/h and 80 km/h. Three representative permit vehicles were used for the tests: (a) a Mack CH613 truck tractor with a single drop trailer, (b) a Terex T-340 crane, and (c) a FDOT truck with a very stiff suspension. Data acquisition from experimental testing allowed for calculation of DLA.

The second research track consisted of FE model development and computational analysis using LS-DYNA computer code. In addition to the bridge #500133, two other local, prestressed, reinforced concrete bridges were selected for analytical studies of DLA. Their superstructure consisted of AASHTO type II and IV prestressed reinforced concrete girders. The FE model of bridge #500133 was validated and verified using experimental data. DLA factors were calculated for all bridges as functions of vehicle types and their velocities. They were determined based on maximum displacements and strains. Strain-based DLA factors appeared to be more reliable, closer to experimental data, and closer to values recommended by AASHTO. Several features were identified as triggering significant DLA. They included: surface

imperfections (joint abutments and bridge approach depression), loosely attached cargo producing so called hammering effect, and characteristics of the vehicle suspension.

TABLE OF CONTENTS

LIST OF TABLES

LIST OF FIGURES

CHAPTER 1

INTRODUCTION

1.1. Problem Statement

This project responds to growing needs to rehabilitate our nation's roads, highways, and bridges. With the recent report card from the American Society of Civil Engineers (ASCE) giving America's roadways and bridges a grade of D, it is more vital than ever to reduce the deterioration of our country's infrastructure. According to ASCE, an estimated $930 billion dollars within 5 years will be needed to improve our nation's roadways and bridges [1]. A price tag like this can be reduced significantly if proper operation and maintenance of highway bridges are carried out. Knowledge of the actual dynamic load effects and structure resistance is necessary to resolve this ongoing problem of deterioration of transportation infrastructure. This information is very useful for determining the load carrying capacity and the condition of the structures. It can also help in making management decisions, such as establishing permissible weight limits for certain roadways and bridges and, most importantly, it provides positive economic and safety implications. Advanced computational mechanics analysis and evaluation procedures can also be applied to a structure that exhibits behavior difficult to explain, such as excessive vibration, deflection, and others.

Bridges are frequently evaluated using simplified static analysis methods. Unfortunately, these methods do not represent what is actually happening in the structure, due to the lack of knowledge of certain dynamic effects. The dynamic essence of live loads as well as the interaction between vehicle and bridge is usually not considered in the design process. Dynamic load allowance, suggested by the design codes currently used, usually leads to conservative designs, especially for very heavy vehicles. More accurate and less expensive methods are needed to assess the actual dynamic effects of heavy vehicles on highway bridges and the impact loads associated with them.

Bridge analysis and design are traditionally based on simplifications of geometry, materials, boundary conditions and loading. The live loads and their dynamic nature are one of the most questionable simplifications. The vehicle load is usually represented as a concentrated and/or uniformly distributed static load applied to the superstructure of the bridge. The dynamic effects of the actual live load are considered by scaling up the static loads by values known as the

dynamic load allowance (DLA), referred to as impact factors in the past. The magnitude of the DLA was usually only related to the length of the bridge without further consideration of the dynamic characteristics of live loads and characteristics of the bridge like road and bridge surface imperfections, among others, which have a large influence on the dynamic effect.

With an increase in computational capabilities of computers and the development of commercial finite element (FE) programs, advanced numerical 3-D dynamic analyses of bridge structures are carried out faster and easier than ever before. Growing knowledge of finite element analysis (FEA) is making it possible to create more detailed 3-D models of bridges that contain a large amount of finite elements with consistent mass and stiffness distributions. Commercial FE software has also allowed for advanced material models of steel and concrete, options for modeling rebar for reinforcement, application of different types of constraints, and damping options, which provide a more accurate description of the actual behavior of the bridge. Available public domain models with varying representations of suspension systems, wheel models, and kinematical characteristics can be used for dynamic truck and bridge analysis, after necessary modifications are applied.

Advanced FE models allow for complex mechanical phenomena such as contact between pavement and wheels, impact forces due to surface imperfections, and dependence of moving live loads on time caused by dynamic interaction among suspended masses which represent the vehicle and the bridge components.

Validated FE models can provide extensive information about the structural behavior, which is both expensive and difficult, if not impossible, to obtain through experimental study only. This project focuses on DLA factors for short and medium span reinforced concrete bridges, involving advanced FEA with well validated FE models of selected permit vehicles and the selected bridges.

1.2. Research Objective

Emphasis of the current research project has been placed on the development of two new FE models of highway bridges in North Florida. The development of the FE models was completed through modifications of a previously validated FE bridge model [26]. The first finite element model of the bridge was developed and validated under a previous Florida Department

of Transportation (FDOT) research project "*Investigation of Impact Factors for Heavy Vehicles*" with the FDOT contract number BD493. Validation of this bridge model was carried out through experimental testing. Once this model was successfully validated, modifications of the original model were carried out to create new FE models of the two new bridges. The two new bridges were specifically chosen to have type II and IV girders according to the American Association of State Highway and Transportation Officials (AASHTO), as compared to the existing bridge model with an AASHTO type III girder. Three different permit vehicles were also modeled and validated under the previous research.

The three different vehicle models and three bridge models were analyzed to capture the dynamic interaction between the vehicles and the bridges. Analyses were based on nonlinear, explicit, dynamic, finite element computation mechanics using the commercial LS-DYNA computer code.

The vehicles and the bridges were selected by the Florida DOT Project Manager. Due to the fact that span length, vehicle speed, suspension parameters, truck weight, truck position on bridge lane, and road surface condition have a significant influence on dynamic responses, emphasis was placed on these specific parameters.

Additional focus on the new FE model of the bridges includes the evaluation and assessment of the elastomeric bearing pads. No testing was previously done for the neoprene bearing pad material properties; therefore the properties in the model were estimated.

Different parameters such as vehicle speed, surface imperfections, and vehicle mass were of major focus in this research. Varying vehicle speeds were studied to analyze the sensibility of the speed on the bridge dynamic response. Also, the increased dynamic effect produced by the bouncing cargo on the truck was included in the current analysis.

The results have been documented in monthly progress reports as well as in this final report submitted to the FDOT Structures Laboratory. Analysis, conclusions and recommendations for further research are presented in the following chapters.

1.3. Research Tasks

The following research tasks were proposed for the study and were approved by the Project Manager:

Task 1 — Literature Review

Task 2 — Assessment and improvements of the existing models

Task 3 — Survey of selected bridges and surface irregularities

Task 4 — Development of FE models of bridges with surface imperfections

Task 5 — FE analysis and validation

Task 6 — Milestone meetings

Task 7 — Quarterly and final reports

Research activities by task as of December 18, 2010 are presented in Table 1.1.

Table 1.1. Major research tasks of the project

RESEARCH TASK	Year:	2008			2009												2010												2011			ESTIMATED % COMPLETION
	Quarter:	1			2			3			4			5			6			7			8			9			10			
	Month:	Oct	Nov	Dec	Jan	Feb	Mar	Apr	May	Jun	Jul	Aug	Sep	Oct	Nov	Dec	Jan	Feb	Mar	Apr	May	Jun	Jul	Aug	Sep	Oct	Nov	Dec	Jan	Feb	Mar	
Task 1																																100%
Literature review			15%			15%			10%			10%			10%			10%			10%			10%			10%					
Task 2																																100%
Assessment of models							20%	20%	20%	20%	20%																					
Task 3																																100%
Survey and selection of bridges										20%	20%	20%	20%	20%																		
Task 4																																100%
Development of FE models												8.3%	8.3%	8.3%	8.3%	8.3%	8.3%	8.3%	8.3%	8.3%	8.3%	8.3%	8.3%									
Task 5																																100%
FE analysis and validation															8.3%	8.3%	8.3%	8.3%	8.3%	8.3%	8.3%	8.3%	8.3%	8.3%	8.3%	8.3%	8.3%					
Task 6																																100%
Milestone meetings			15%			10%			10%			15%			10%			10%			10%			10%			10%					
Task 7																																100%
Quarterly and final reports					5%			5%			5%			5%			5%			5%			5%		10%	15%	10%	10%	15%		5%	

CHAPTER 2

LITERATURE REVIEW

Literature relevant to this project has been reviewed throughout the project duration. Intense literature study was especially conducted at the earlier stages of the research. The review covers such topics as: AASHTO specification of bridge dynamic effects, FE modeling of prestressed concrete girder highway bridges, FE model development and representation of reactions from permit trucks on bridge decks, analysis of elastomeric bearing pads, and validation and verification of FE models.

2.1. AASHTO Specification of Bridge Dynamic Effects

Highway bridges are always subject to dynamic loading produced by vehicles driving over them. These dynamic loads, if not accounted for, can be damaging resulting in deterioration of the structure, increasing its maintenance costs, and decreasing its life span. The main elements of concern in the superstructure include the floor beams, girders, diaphragms, joints, and bearings. With the rapid growth of highway transportation and the fact that vehicles are increasingly heavier, fatigue damage is quickly becoming a serious concern. As a result, bridge maintenance is more difficult and expensive due to the fact that required maintenance, rehabilitation, and/or replacement are more frequent [24].

Since dynamic effects result in accelerated bridge fatigue, it is necessary to consider them when evaluating an existing bridge or designing a new one. The DLA concept is commonly used to assess the dynamic effect of the vehicle load on the structure. The effects are usually seen as a response of the passing vehicles as well as a result from the bouncing of loose cargo which results from factors such as imperfections in the road surface i.e., abutment joints, expansion joints, cracks, potholes, and delamination.

The DLA was originally expressed in the AASHTO Standard Specifications for Highway Bridges by the simplified formula [2]:

$$DLA = \frac{50}{L + 125} \tag{2.1}$$

where *L* is the length in feet of the portion of the span that is loaded to produce the maximum stress in the member. Equation (2.1) is based on field tests for specific trucks. This equation gives only an approximation of the DLA, and it is not clear if this equation can be used to evaluate bridges subjected to very heavy permit vehicles. As suggested from the literature review, DLA is computed using equation 2.2:

$$DLA = \frac{\quad}{\quad} \tag{2.2}$$

where R_d is the dynamic response and R_s is the static response of any physical variable. The quantities most commonly used for R_d and R_s are displacements and strains, from dynamic and static analysis, respectively.

2.2. FE Modeling of Highway Bridges

As we enter a new era of structural analysis and design, it is important to develop techniques that will aide in the speedy development of a product, reduce cost to develop a product, improve quality of a product, increase product life, provide greater product reliability, and increase customer satisfaction. With the development of the finite element method (FEM), one can significantly improve both the standard of engineering design and the methodology of the design process. The Federal Highway Administration (FHWA) has focused much of its attention on developing highly reliable, realistic, and detailed analytical models of highway bridges. By using FE methodology certain key features in a bridge can be modeled accurately. Some of these features are a complete, detailed geometric component, constitutive material models, connections, boundary conditions, and conditions of dynamic loading.

It is a common practice that the effects of torsion in simplified structural analysis are usually neglected, and only bending, shear, and axial forces are taken into account. This leads to cases in which bridges are modeled as simply supported or continuous beams. Simply supported bridge models could only be reasonably accurate if they have a large length to width ratio, uniform stiffness and mass distribution, and the loading acting on them is symmetric [26]. Vehicles usually travel along one of the lanes of the bridge therefore applying a non-symmetric loading condition and introducing torsional loads. This violates the condition for bridges

modeled as simply supported beams and would not provide for accurate results. The simplified condition typically yields more conservative results.

Including torsional behavior of a reinforced concrete member is essential in obtaining accurate results. Even small torsional moments can cause considerable stresses which can change the response of the whole structure. Torsional loads are usually included in 3-D FE analyses, such as in [6]. It is also important to remember that when a bridge is subjected to extreme traffic loads, a nonlinear response is possible either locally or globally. This is usually due to plastic deformation, time varying dependency of materials and aging degradation. With commercial FE codes, materials that exhibit a nonlinear behavior can easily be modeled with a piecewise stress-strain curve.

In dynamic interaction, flexural and torsional stiffness are taken into account in the 3-D FE modeling process. A simple 3-D grillage model provides for a better and more accurate approximation of the response of the slab as compared with a simply supported beam model. A grillage model has been proven to be a reasonably accurate, robust, and useful tool for analysis of bridges [21]. Figure 2.1 shows a single grillage element and a grillage model of a bridge.

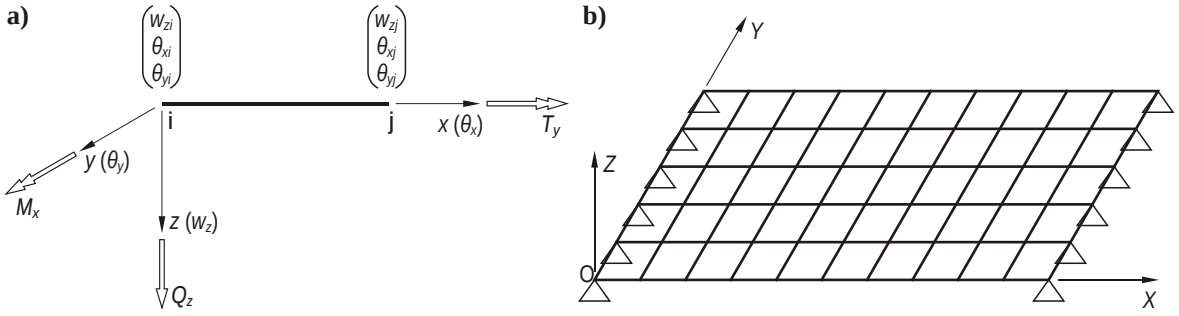

Figure 2.1. Grillage model: a) a single grillage element, b) grillage model of a bridge span [21]

The use of solid elements for bridge deck modeling is currently limited to research and highly specialized applications due to its excessive run time, computer storage requirements, and a shortage of user-friendly software, particularly for the large quantities of output data generated [18]. The elements are connected at joints where loads and constraints are applied. The stiffness of girders was often adjusted to include an effective width of the deck by using a trial-and-error method so that the deflection of the model and the actual behavior were the same.

Connections between components, such as bolts and welds in a bridge, can easily be modeled using commercial FE software. LS-DYNA, 3-D explicit FE software, provides several options when modeling connections [6].

Elastomeric bearing pads are essential in modeling an interface between the superstructure and the pier. These pads allow for translation along the longitudinal direction of the bridge girder. In a FE model, bearing pads can be modeled using their real geometry and by applying the appropriate material model. An example of a FE model of the bridge developed in [22] is shown in Figure 2.2.

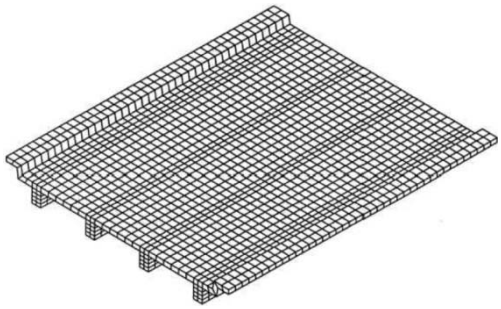

Figure 2.2. An example of an earlier FE model of a bridge [22]

Earlier FE models, such as the one shown in Figure 2.2, were characterized by a fewer number of finite elements due to limited computational efficiency of the computational hardware and software. For comparison, the current FE models of each bridge span included approximately 250,000 finite elements.

2.3. Analysis of Elastomeric Bearing Pads

Elastomeric bearing pads, specifically the laminated neoprene pads, are a subset of the elastomeric pads. These pads are ideal for bridge design because they are economical, effective, and require no maintenance. They deflect in shear to accommodate expansion, contraction, and end rotation of the bridge girders. There is no need for lubrication, cleaning, nor do they have the opportunity to seize [16]. They are also simple solid pads with no moving parts which makes them straightforward when developing their FE models. They were first introduced in 1958 by AASHTO and ever since then, the popularity of these pads grew. When designing bearing pads,

it is important to understand what causes them to fail. These pads may fail due to compression, shear, or rotation. By understanding the modes in which they fail, improvements on these pads can be better understood. Figure 2.3-2.5 illustrates the different modes in which a bearing pad may fail.

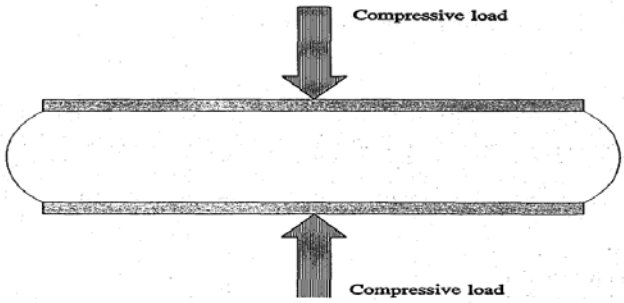

Figure 2.3. Bearing deformation due to compression

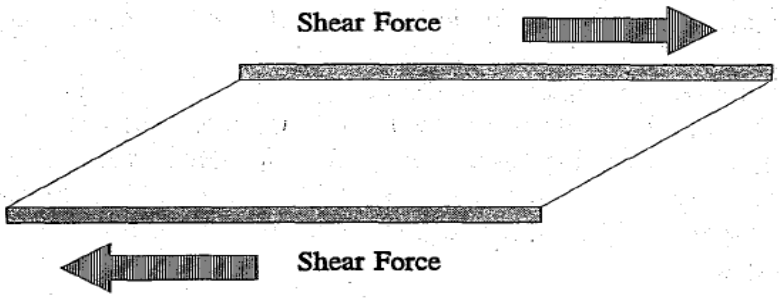

Figure 2.4. Bearing deformation due to shear

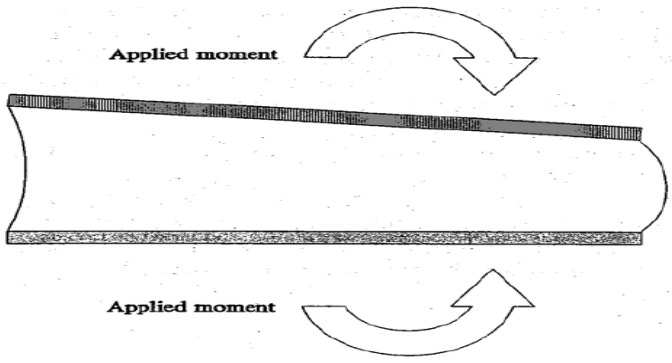

Figure 2.5. Bearing deformation due to rotation

Several factors need to be considered when designing a steel-laminated neoprene bearing pad. These parameters include:

1. shape factor
2. reinforcement type
3. effective rubber thickness
4. hardness
5. compressive modulus.

The shape factor is one of the key parameters in determining vertical deflection characteristics. The shape factor is defined as the ratio of the surface area or plan area of one loaded face to the area free to bulge around the perimeter of one internal elastomeric layer of the pad [16]. As the reinforcement between the layers increases, the shape factor increases thus, reducing the deflection for a given load.

The effective layer of the bearing pad is defined as the combined thickness of all the elastomeric layers in the pad. This is a critical part in design because it determines the amount of horizontal movement a bearing will permit.

The hardness of the elastomeric material in a bearing pad is a relative measure of the modulus of the bearing in both compression and shear. Generally, as hardness increases, modulus increases and deflection decreases [16].

Neoprene, a synthetic rubber, is highly resistant to deterioration by weathering and natural aging. It has a history of long-term service, and with its proven record of durability and economic necessity, it has easily become the elastomer of choice in bridge bearing design. Analyses of these bearings have been conducted with the assumption that they are linearly elastic, isotropic and that the deformations are small enough to be negligible. Unfortunately, this material has highly nonlinear, thixotropic constitutive properties (in which the visco-elastic properties are time dependent, when subjected to loads) and can only be properly analyzed through advanced experiments and commercial FE software. The most common bearing pads include solid elastomeric pads and pads with horizontally placed steel shims. Figure 2.6 illustrates the two most common types of neoprene pads used in bridge construction.

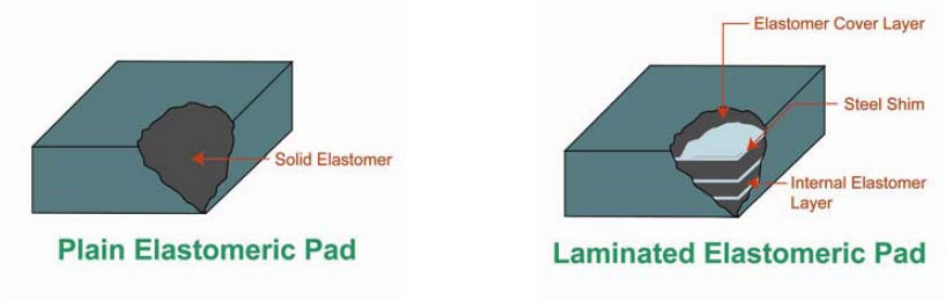

Figure 2.6. Types of neoprene pads

Experimental investigations of material properties of elastomeric pads were of interest to FDOT. Two research projects were contracted by FDOT and their results were presented in [17] and [5].

2.4. Validation and Verification of FE Model

The verification and validation (V&V) of a FE model is increasingly becoming more important in today's research. The V&V process is an essential part when developing a model if it is to be accepted and used to support technology transfer and practical implementation of research results. The verification process is concerned with the specifications being met and making sure that mistakes have not been made in implementing the model. Verification is done to ensure that:

- The model is programmed correctly
- The algorithms have been implemented properly
- The model does not contain errors, oversights, or bugs.

The verification process ensures that all major physical phenomena are well represented in the FE model. On the other hand, the validation process is concerned with building the model right. Its main objective is to determine quantitatively that a model is an accurate representation of the real system. Validation is usually achieved through the calibration of the model, an iterative process of comparing the model to actual system behavior and using the discrepancies between the two and the insights gained to improve the model. Information about the actual system behavior is obtained from experimental testing of the system. This process is repeated until model accuracy is judged to be acceptable [12]. Validation is done to ensure that:

- The model addresses the right problem

- Provides accurate information about the system being modeled
- The model meets intended requirements in terms of results obtained.

A special-purpose computer program called Roadside Safety Verification and Validation Program (RSVVP) has been developed and described in [19] to address the V&V process for roadside safety barriers. The V&V process is carried out by verifying the results of a simulation with another simulation or analytical solution, assessing the repeatability of a physical experiment, and performing a comparison of virtually any pair of curves. This software utilizes statistical techniques in order to verify and validate curves. Statistical tests such as the Analysis of Variance and the Sprague-Geers MPC are used when calculating and comparing curves. The Analysis of Variance (ANOVA) metrics are based on the residuals between the true and test curve while the Sprague and Geers metrics indicate the quality of comparison for the magnitude and phase of the test and a true curve. These tests are described in the RSVVP Manual [19] and are strongly recommended when comparing a full-scale experimental test to a numerical simulation.

2.5. FE Modeling of Vehicles

A strategy used for development of vehicle models is different from the analytical modeling of a bridge. There are several approaches that can be used which are numerically small and simple, yet they contain the most essential elements of the vehicle such as the body with its mass, wheels and suspension systems. As can be found in literature, bodies are commonly represented by masses subjected to rigid body motions. Suspensions are assumed to be the combination of springs and dampers dissipating energy during oscillation. One of the simplest two-dimensional analytical models is depicted in Figure 2.7. In the first case, the body is modeled with a rigid bar while the suspension unit is composed of a spring and a damper [27].

Figure 2.7, part (a), represents the body of the vehicle which is modeled by a rigid bar, while the suspension unit is composed of a spring and a damper on a 2-D plane. These three parts are the main elements when building a 2-D analytical vehicle model. Part (b) shows a further simplification of this system. By using lumped masses at the ends of the bar, while excluding the rotational degrees of freedom, a more simplified model is obtained [28]. Some of these models are still used for the study of vehicle-bridge interaction [25].

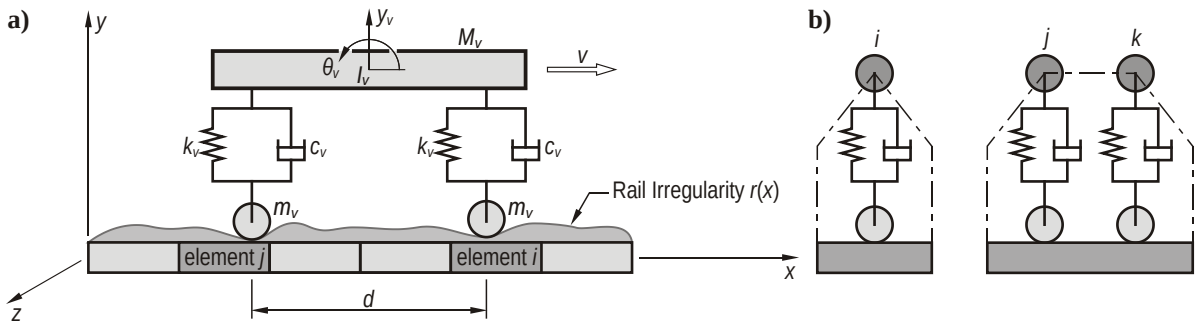

Figure 2.7. Simplified analytical vehicle models [27], [28]

Three-dimensional systems are required for more complex analytical vehicle models. These systems are modeled as a rigid chassis subjected to rigid body motions, which include pitching and rolling rotations. These models have seven degrees of freedom which makes them more accurate than the simplified models in Figure 2.7. The seven degrees of freedom include vertical displacement at the chassis center, pitching and rolling rotation about the two axles of the chassis, and four vertical displacements at each of its wheel locations. The tires (wheels) are modeled as point followers with springs under the axles. Suspension systems are represented by springs with a nonlinear relationship between load and deflection [26]. Figure 2.8 illustrates an example of a 3-D vehicle model with its suspension [6].

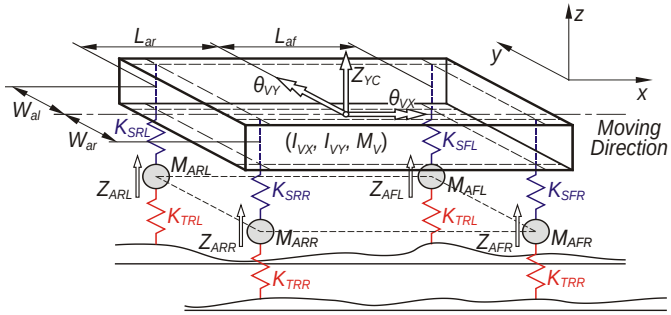

Figure 2.8. Three-dimensional analytical vehicle model [21]

Another analytical model was also developed for the Florida Department of Transportation by the Florida International University in order to create a simple dynamic model of an AASHTO HS20-44 truck [6]. This model has 11 degrees of freedom and was used to evaluate the dynamic response of highway girder bridges. Figure 2.9 illustrates this system.

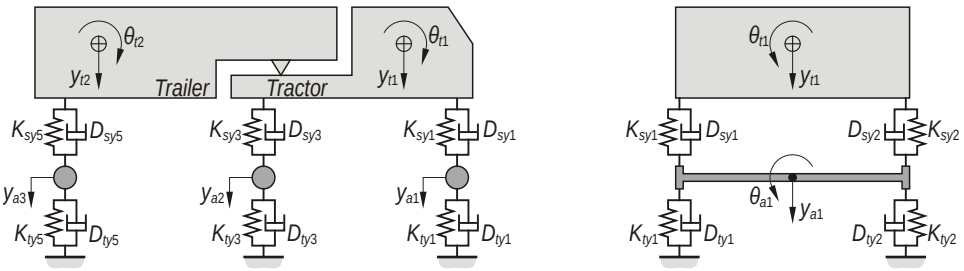

Figure 2.9. Analytical model of an AASHTO HS20-44 truck [23]

Analytical models of this type are treated as a multi-body system, which is suitable for simple analytical studies of vehicle-bridge interactions. However, since the number of degrees of freedom is limited for mathematical convenience, the method has significant limitations. Since most parts of these analytical models are assumed to be rigid, finite element software is needed for additional modeling of non-rigid bodies, such as vehicle tires.

FE modeling becomes convenient for modeling complicated parts such as the transmission, suspension system, etc. Very often, FE models are available in public domain for immediate use. These models are realistic because more structural components can be included as compared with other analytical vehicle models presented thus far. Components that are included in these models are detailed suspension systems with correct spring and damper characteristics of suspension and with rotating and pneumatic wheel models [26]. These models are frequently developed for crashworthiness analysis, but they can also be used when studying vehicle-bridge interaction. Examples of FE models, that are available on-line, are presented in Figure 2.10 [9].

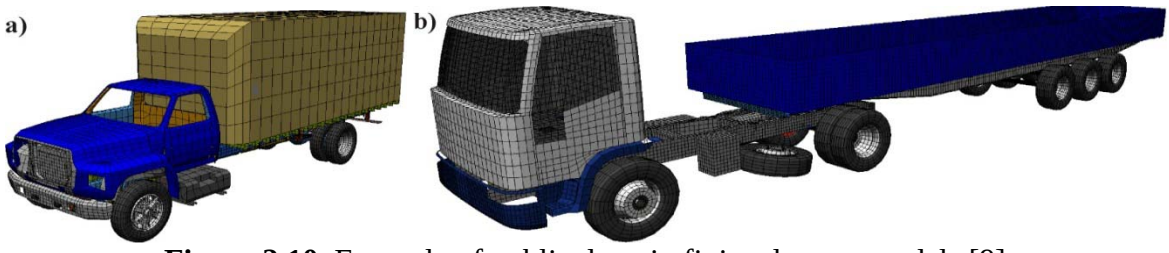

Figure 2.10. Example of public domain finite element models [9]

2.6. 3-D Modeling of Vehicle – Bridge Interaction

The most recent AASHTO LRFD codes allow for more economic and efficient bridges with optimum load factors. At the same time, these bridges are loaded with heavy trucks as compared to the weight of the bridge. It was shown for example in [20] that the mass of a permit truck considered in the paper constitutes as much as 17% of the total mass of the vehicle-bridge system. Therefore, both the truck and the bridge should be included in the comprehensive 3-D computational dynamic analysis.

Such an approach was made possible with recent advances of computational software and hardware. It was adopted in earlier studies carried out for FDOT through two previous research contracts: BD493 and BD542, [25] and [26]. respectively. A heavily used reinforced concrete bridge, made of AASHTO type III girders, was selected for both studies. The selected bridge (#500133), shown in Figures 2.11 and 2.12, was a 3-span bridge with two lanes of traffic and built in 1999 on US 90 near Chattahoochee.

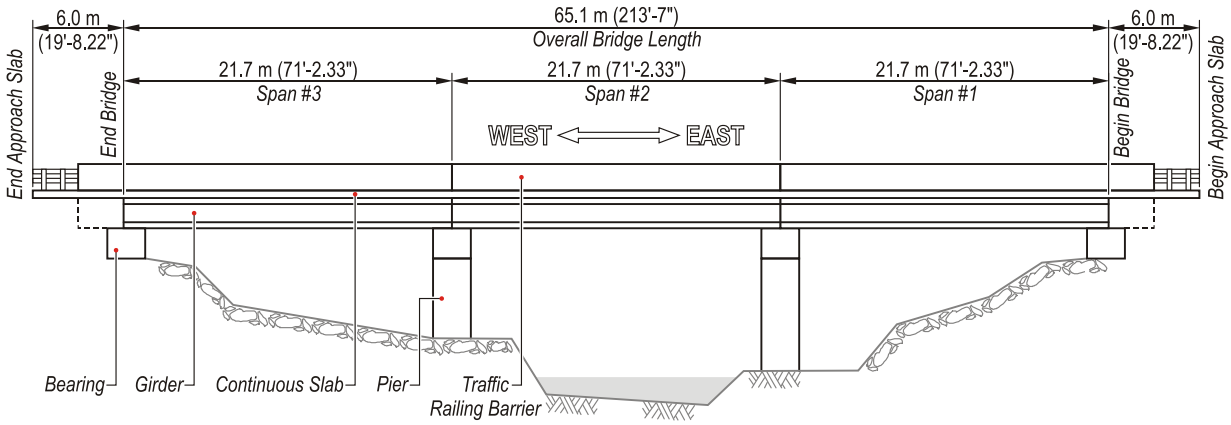

Figure 2.11. Elevation of the tested bridge [26]

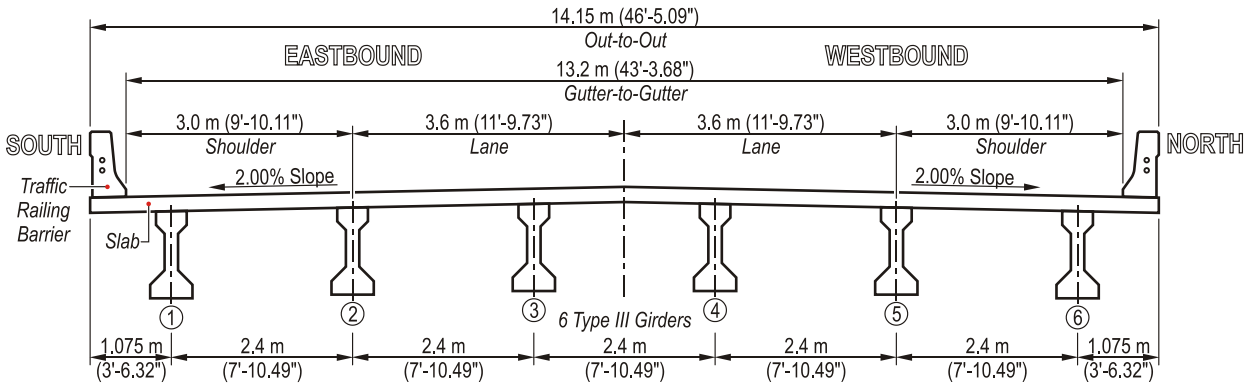

Figure 2.12. Bridge cross-section [26]

A typical span of the bridge was modeled using 204,000 finite elements. Most of these elements were 3-D quadrilateral solid elements which were used for modeling concrete. The model of the bridge span included: six AASHTO type III girders, a concrete deck, diaphragms, rails, elastomeric pads and a bridge approach depression with a distinct abutment joint. In addition, a simple FE model of the FDOT truck, consisting of 12,934 finite elements was also developed. The model of the truck was relatively simple. During its development an emphasis was placed on correct mass distribution and reactions under each axle. Efforts were also made to accurately model the truck suspension with accurate spring and damping characteristics. Constitutive rubber material and pneumatic rotating wheels were used with an airbag model. A complete permit truck – bridge finite element model is described in detail in [25] and [12] and is depicted in Figure 2.13.

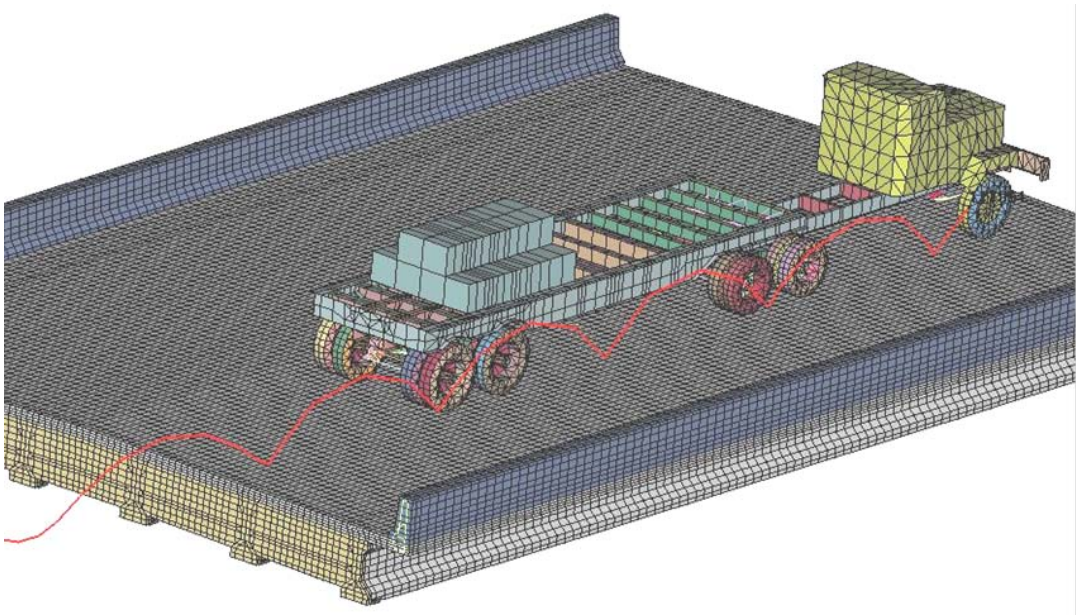

Figure 2.13. A FE model of a complete vehicle – bridge system [25], [14], [12]

A red curve in Figure 2.13 represents a trajectory of a point on the front, right tire of the tractor. It is referred to as a cycloid and it represents rotation of the wheels. The vehicle-bridge FE model was verified and validated through an experimental testing program carried out in Fall 2003 on bridge #500133. Data acquisition included displacements, strains and accelerations of the selected points of the vehicle and the bridge. The strain data was particularly useful for DLA calculations. Validation and verification of the FE models were based on comparison of strain time histories from experiments and from FE analyses, which showed a very good correlation. Detailed, 3-D models of pneumatic and rotating tires allowed for capturing physics of wheels rolling over an abutment joint with up to 20 mm difference in elevation between asphalt approach and the bridge concrete deck. This impact was shown in [25] and [12] as triggering significant dynamic response of the bridge and high DLA.

To further validate the FE models developed, a simple grillage model of the bridge span (similar to the one presented in Figure 2.1) and a vehicle model similar to that depicted in Figure 2.8 was developed for the MatLab program in [14]. Results were consistent with those obtained earlier from LS-DYNA analysis. This simple model allowed for fast, multiple runs to calculate DLA for the same vehicle at speeds varying every 5 mph. Two major conclusions were drawn from this effort:

1. DLA is not necessarily directly proportional to the vehicle speed for the same vehicle-bridge configurations. Several instances were noted where DLA locally decreased with the increase of the vehicle velocity.
2. Further research on detailed vehicle models, with improved suspension, would be justified to gain a better insight into the dynamic vehicle – bridge interaction.

Further research on selected vehicles was carried out in the FDOT sponsored project BD543 [26]. The major objective of the project was to develop three well-validated FE models of the vehicles for LS-DYNA analyses. Of particular interest were heavy permit vehicles popular on Florida highways. Permit vehicles were defined as those which need special permits from the Maintenance Office of the Florida Department of Transportation due to their gross vehicle weight (GVW) exceeding posted capacity of bridges that they cross. FDOT processes over 90,000 requests per year for such overload permits and decisions have to be made very quickly. Three permit vehicles were selected for FE modeling. They included: Mack CH613 truck tractor with a three-axle single drop lowboy trailer, a Terex T-340 crane, and the FDOT tractor-trailer, as shown in Figure 2.14. Mack is a popular tractor-trailer with GVW (per FDOT records) exceeding 200,000 lbs. Fortunately, its total mass is well distributed through six axles, twenty-two tires, and is supported by well-designed spring suspensions and shock absorbers. Although the Terex crane has a smaller GVW, it is supported by only three axles with a smaller bridge distance (i.e. distance between the two most distant axles), which ignited the FDOT interest in this vehicle. Finally, the FDOT truck was selected due to its very stiff (almost non-existent) suspension.

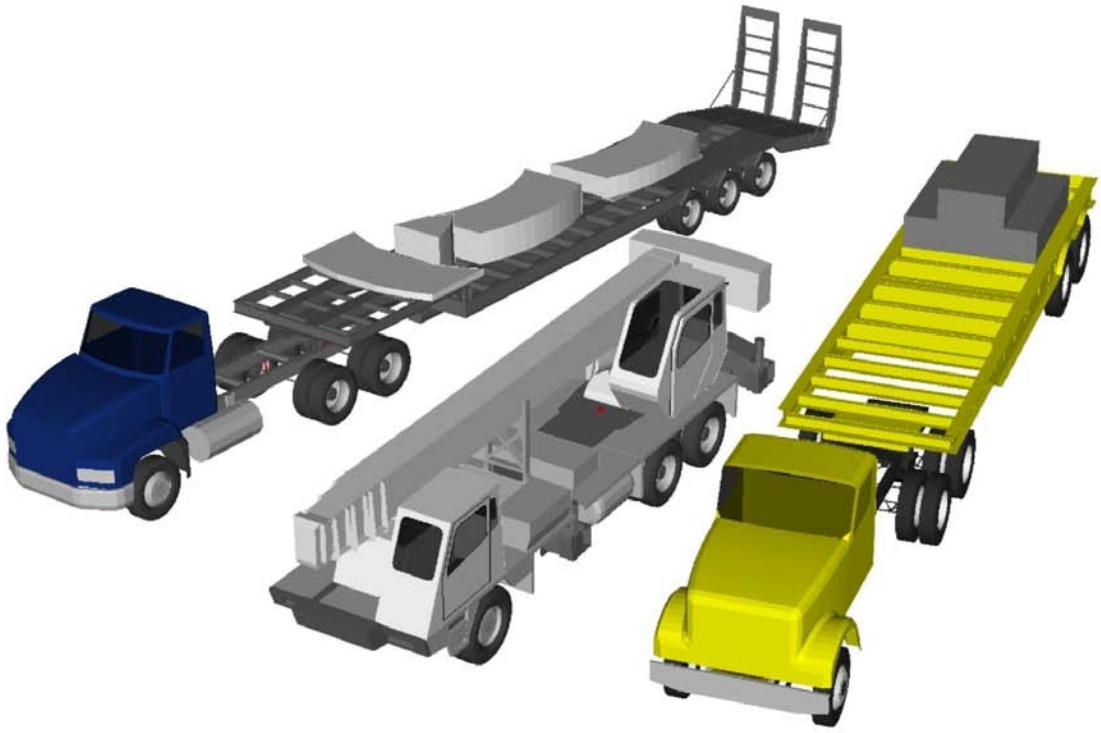

Figure 2.14. FE model of three heavy vehicles [26], [20]

This truck is frequently used by the FDOT Structures Lab for bridge testing. Development of its FE model was critical to assess the importance of the truck suspension. The vehicle models developed and described in [26] and [20] were computationally small and efficient. Each consisted of less than 25,000 finite elements. In addition to rotating and pressurized tires introduced earlier in [25], [14], [12], an emphasis was placed on correct characterization of the spring and damping properties of each suspension. To achieve this goal, a series of tests were carried out on several speed bumps located in Broadmoor Estates in Tallahassee in 2007. Three vehicles were rented and were driven over the speed bumps with velocities ranging from 5 to 20 mph. Higher speeds were eliminated due to the concern of damaging the vehicle suspension. Data acquisition included displacement and acceleration time histories of several points located on each vehicle. A FE model of the speed bump was also developed. Its geometry was based on a point cloud collected from a laser scan using an Optech Intelligent Laser Ranging and Imaging System (ILRIS) laser scanner. The speed bump was

modeled with approximately 300 2-D shell finite elements. The first round of V&V consisted of analysis of acceleration time histories of selected points from experiments and LS-DYNA analysis. Additional field tests were carried out with all three vehicles on bridge #500133 in 2008. The experimental tests consisted of 35 static and dynamic runs. The tests were conducted with different vehicle positions across the bridge, at speeds of 30 and 50 mph (48 and 80 km/h). The most important conclusions were listed in [26] and [20] and are summarized below:

1. All three FE vehicle models were verified and validated through experimental testing at Broadmoor Estate (speed bumps) and at bridge # 500133.
2. Significant dynamic loading triggered on bridge #500133 was primarily by the abutment joint and by the hammering effect of loosely attached cargo.
3. The dynamic response of a bridge can be efficiently controlled by well-designed vehicle suspension.
4. DLA calculated based on strains in the girders are more reliable as compared with those obtained based on the displacement time histories.
5. It was confirmed that DLA may not always be directly proportional to the vehicle speed. Some instances were found for the same vehicle-bridge configuration where increased vehicle speed led to a reduced DLA.

Prior research experience gained from the recent FDOT projects BD493 and BD543 were instrumental in carrying out the current research project. More detailed background information can be found in [26], [25], [14], [12], and [20].

2.7. Effect of Vehicle Speed on DLA

AASHTO LRFD specifications suggest a value of 33 percent as a dynamic amplification factor for the design of highway bridges. The current factor provides a good specification for design of new bridges, which have good road surface conditions. The average age of all the bridges across the United States is over forty-three years old, with deteriorated road surfaces according to a recent AASHTO report [1]. The vehicle speed is significant in evaluating DLA, but its effect may be amplified depending on the road surface condition.

Dynamic interaction between bridge and vehicle on bridges with several types of girders was studied focusing on different factors such as vehicle speed, vehicle damping ratio, mass ratio of vehicle and bridge and others. Numerical 3-D models of coupled bridge-vehicle systems were developed to evaluate dynamic impact factors. Analysis using the FE method and the results are reported in [10], [7], and [13]. The spectral method, which calculates the dynamic force induced by the vehicle mass and the random interaction force induced by the vehicle vibrations separately, has also been implemented in the study of this system with similar results [8].

It can be intuitively expected that a dynamic response of a bridge is amplified with the increase of the vehicle speed. In most cases the DLA associated with higher vehicle speeds tend to be more pronounced than those for lower vehicle speeds. However, it can hardly be described as a constant, directly proportional trend, and usually local fluctuations occur [7].

Recent research on the effect of the vehicle speed on DLA has shown that in some cases the increase of vehicle speed reduces the response of the bridge, while in others it amplifies it, and these variations may be significant [10]. The research, using numerical models, has shown that the average DLA may vary as the vehicle speed increases. Therefore it is difficult to uniquely describe the DLA trend as a function of the vehicle speed [10], [7], [13].

Vehicle speed is an important factor in the determination of DLA factors. The response resulting from the speed is generally triggered by other factors such as abutment joints, bridge approach depression, and road surface irregularities [8].

The speed of the vehicles is just one of the several significant factors that have to be taken into account when studying dynamic interaction between a vehicle and a bridge. As shown in [7], attention has to be paid to other factors such as road surface condition, span length, bearing pad condition, vehicle mass, and vehicle suspension characteristics. The influence of these factors is presented and discussed in further parts of this report.

CHAPTER 3

ASSESSMENT OF EXISTING BRIDGE AND VEHICLE MODELS

3.1. Chattahoochee Bridge

A FE model of bridge #500133 which was developed and validated under previous FDOT research project was acquired for use in the current research project [26]. It is a simple model consisting of five major structural components: a slab, railing barriers, AASHTO type III beams, diaphragms, and neoprene pads. Geometric data was obtained from blueprints provided by the FDOT. The bridge elevation and cross section are presented in section 2.6.

The FE model of one span of the bridge was developed using mostly 8- and 6-node 3-D, fully integrated solid elements for the concrete parts. An elastic material model was chosen for the analysis, with the properties for concrete obtained from cylinder testing conducted by the FDOT Structures Research Laboratory. Three different reinforcing bars for the bridge were modeled using 1-D beam elements with their respective diameters according to AASHTO specifications [2]. An elastic material model was chosen for the analysis, with material properties for steel. The prestressed concrete girders also consisted of prestressing strands, modeled as 1-D beam elements. The prestressing strands used a special material model that inserts a prestressing force on the girder and allows the strands to carry tensile loads, without any bending or compression stiffness. The FE model of the Chattahoochee Bridge is summarized in Table 3.1.

Table 3.1. Summary of the complete FE model of one span of the bridge [26]

Specification		Specification	
Number of parts	13	Total number of elements	145,600
Number of nodes	107,378	- solid elements	84,694
Number of material models	8	- beam elements	60,906

The FE model of the bridge was also introduced with the bridge approach depression, and abutment joint between the asphalt and the concrete. The approach used for the FE model is the actual approach profile which was scanned by the FDOT Structures Research Laboratory using Optech's ILRIS scanner. The profile was modeled using 6-node 3-D, solid fully integrated elements. More detailed information on modeling of the bridge is available in [26]. The final FE model of the bridge is presented in Figure 3.1.

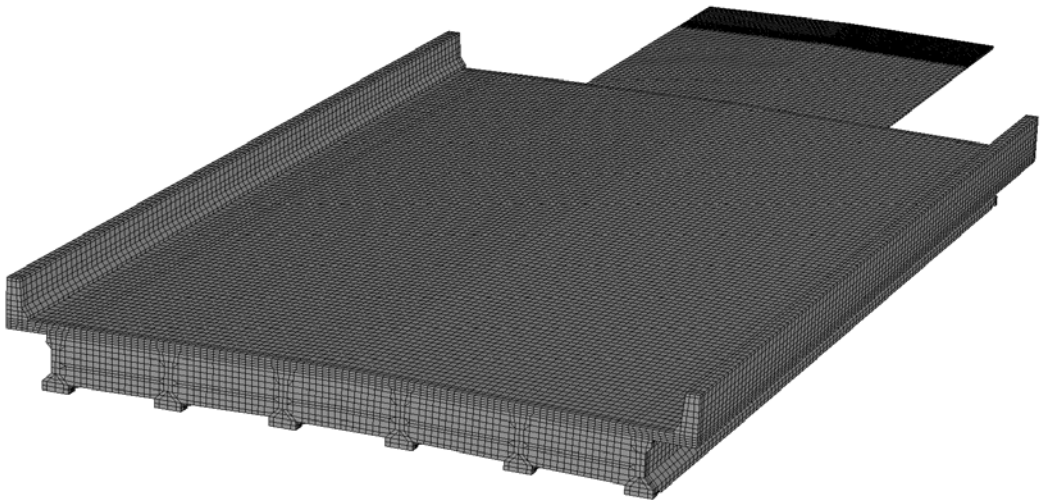

Figure 3.1. A FE model of the Chattahoochee Bridge

The FE model of the bridge was validated and is available for use in further dynamic analysis of vehicle-bridge interaction. The use of this bridge model provides accurate results, because comparison from the results of the full-scale field test on the actual bridge and FE models is satisfactory in most of the cases. Strains and displacements were the primary measure of validation and verification. Strain and displacement histories from the analysis of the three vehicles are presented for the full-scale experiment and FE model in Figures 3.2, 3.3 and 3.4.

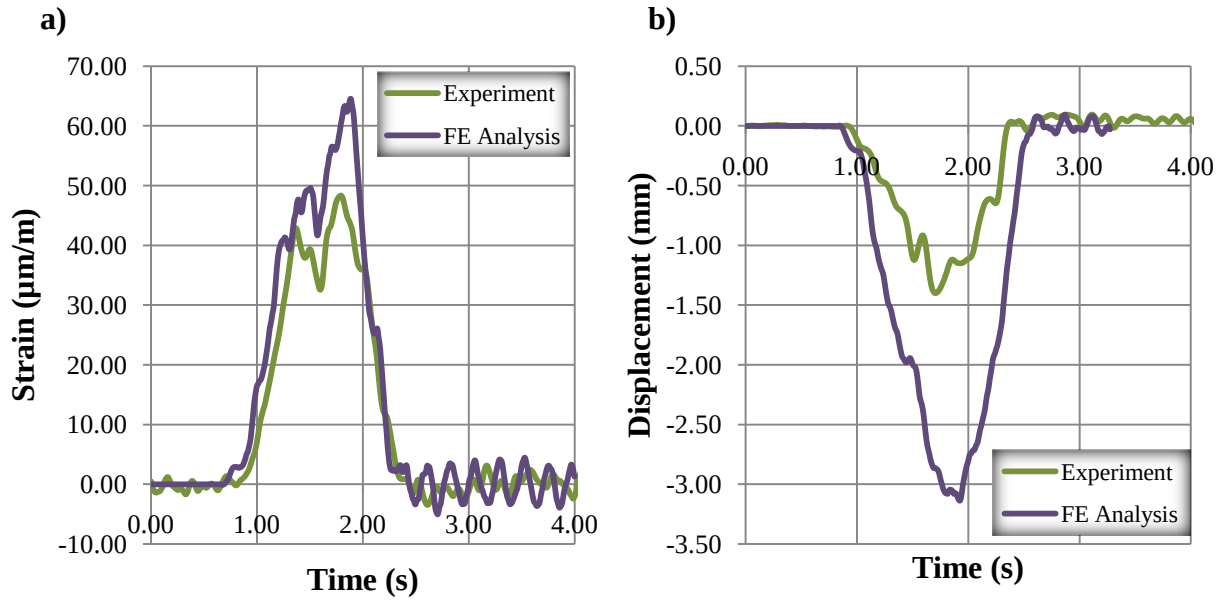

Figure 3.2. Time histories for the tractor-trailer in the center of the westbound lane at 80 km/h (50 mph): a) strains, b) displacements

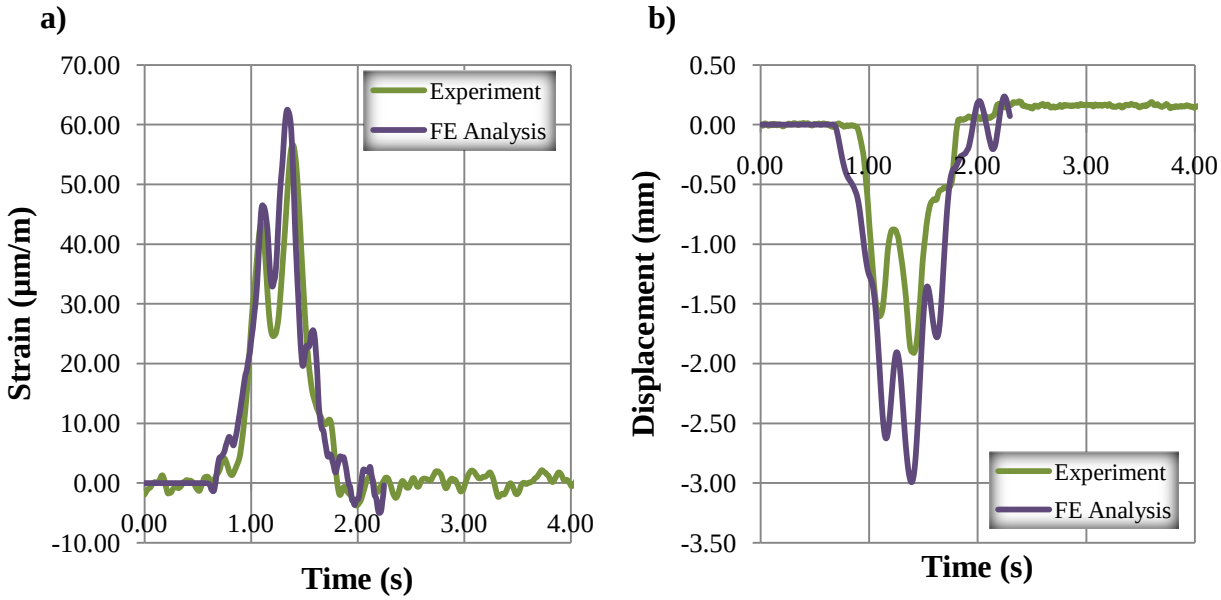

Figure 3.3. Time histories for the Terex crane in the center of the westbound lane at 80 km/h (50 mph): a) strains, b) displacements

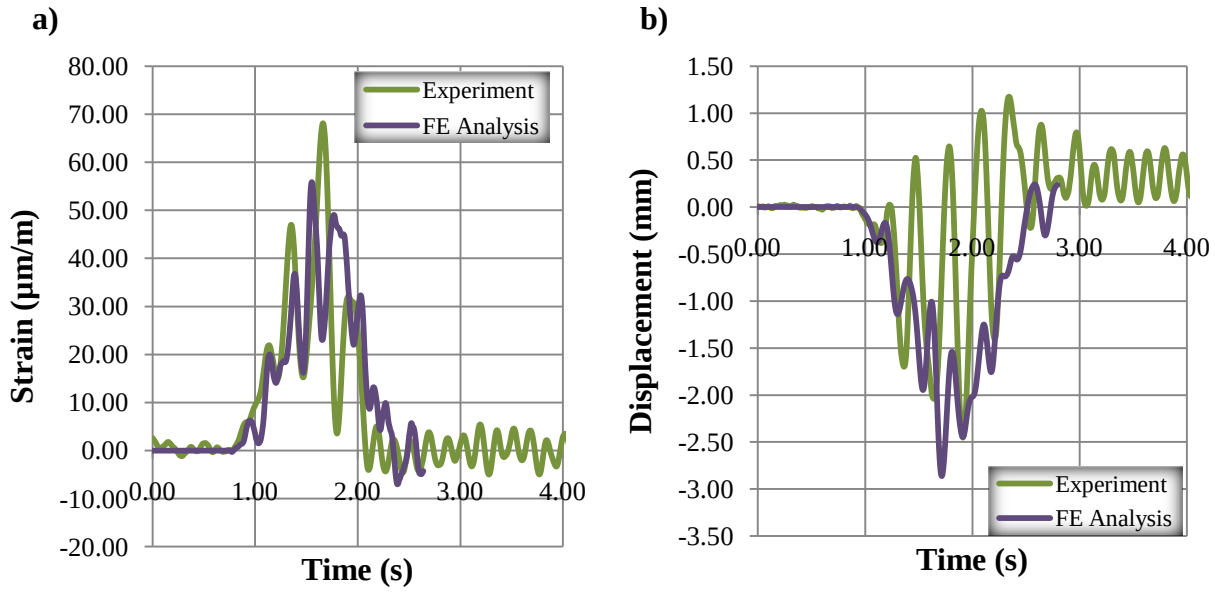

Figure 3.4. Time histories for the FDOT truck in the center of the westbound lane at 80 km/h (50 mph): a) strains, b) displacements

To ensure the level of conformity of the results RSVVP V&V software was used to compare each pair of curves, with predefined criteria. NCHRP 22-24 acceptance criteria proposed for the V&V of finite element models in roadside safety was considered [19]. The results are presented in Appendix A and summarized in Table 3.2.

Table 3.2. Results of RSVVP V&V software for the bridge

		Sprague & Geers Metric			Anova Metric		Passing Metrics
		Magnitude	Phase	Comprehensive	Average	Std	
Strains	Tractor-tr.	27.2	5.7	27.8	0.06	0.12	4/5
	Crane	9.1	7.8	12	0.03	0.09	5/5
	FDOT tr.	-0.2	19.7	19.7	0.01	0.18	5/5
Displacements	Tractor-tr.	154.2	7.1	154.4	-0.41	0.49	1/5
	Crane	72.5	9.3	73.1	-0.19	0.23	2/5
	FDOT tr.	33.2	33.7	47.3	-0.19	0.34	3/5

The results from the two tests for all three vehicles were deemed satisfactory; it's observed that the values are between ranges of measurement error. Displacements of the tractor-trailer showed the biggest discrepancy which was attributed to error in the displacement gauges as well as small relative error from the simplification of the numerical models. Strain measurements proved to be a more reliable method for calculating the dynamic effect on the

bridge. Still with some of the error observed, the values are accepted as qualitative rather than quantitative.

The results from the software provide an unbiased comparison of the two curves. A minimum of 4 out of 5 passing criteria is observed in the comparison of the strains. This suggests that the FE models are accurate, while also once again emphasizing the fact that strain measurements from the bridge experimental testing were more accurately gathered than displacements.

3.2. Neoprene Bearing Pads

The neoprene bearing pads were modeled using 3-D fully integrated solid elements as presented in Figure 3.5.

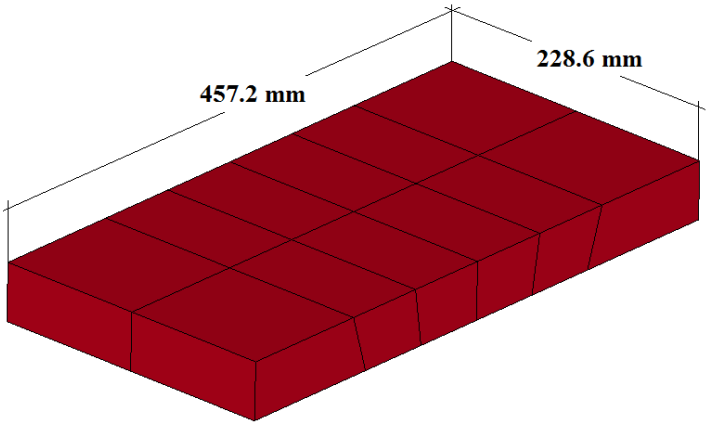

Figure 3.5. A FE model of a neoprene bearing pad

The FE model of the bridge consisted of 12 typical 9” x 18” unreinforced elastomeric bearing pads, with a total of 12 finite elements for each pad. With so few finite elements, the correct material characterization is very important. A viscoelastic material model was selected for analysis. The material properties of the bridge’s neoprene bearing pads were not known and were obtained through a parametric study. The FE models of the pads were assessed to ensure the material properties initially used for analysis were appropriate. Due to gravity loads and dynamic vibrations, the elastomeric pads undergo compression and shear deformations. Therefore, determination of shear and Young’s modulus is critical for bearing pad analysis. The viscoelastic material model is defined by short-time shear modulus and long-time or infinite

shear modulus. To evaluate the accuracy of the elastomeric pad properties used for analysis, the shear moduli were calculated using new design criteria for typical steel-reinforced elastomeric bearing pads subjected to compression and rotation obtained from [17].

Elastomeric bearing pads are usually designed by one of two approaches referred to as Method A or Method B. These two methods usually differ in the typical section of the pad including the reinforcements and the equations used for design. The typical sections of the two methods for reinforced bearing pads are presented in Figure 3.6.

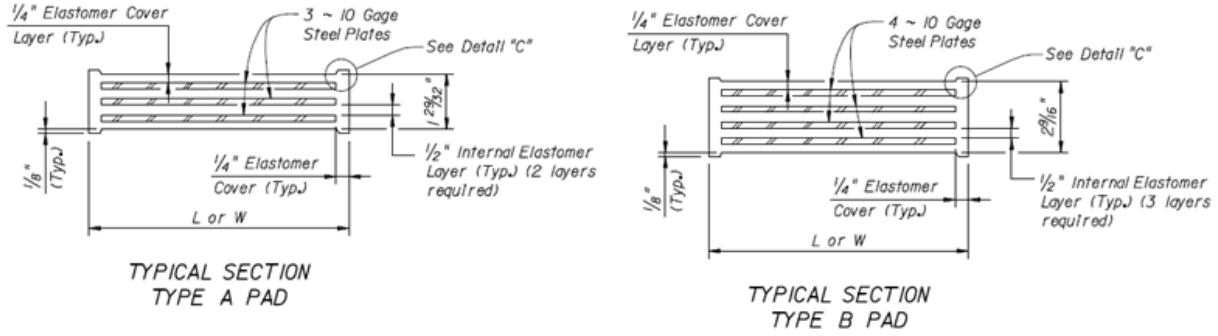

Figure 3.6. Typical section of elastomeric bearing pads [3]

The bridge bearing pads are assumed to have been designed using Method B, the most current method of design, which in most cases results in a higher bearing capacity than Method A. Previous research on elastomeric bearing pads show that the AASHTO specification equation for bearing capacity usually results in lower values than what is observed in the field [17] ,[21]. AASHTO LRFD Bridge design specifications suggest that for Method B, the shear modulus of the neoprene should range from 0.175 MPa to a maximum of 1.3 MPa [2].

The shape factor is a key geometric parameter in bearing pad design because to a large extent it determines the vertical deflection characteristics of the bearing. The shape factor is defined as follows:

(3.1)

where S is the shape factor, L is the length parallel to the flow of traffic, W is the width perpendicular to the flow of traffic, and h_{ri} is the height of the internal elastomer layer, or the layer between two steel plates.

A linear relationship between the steel-reinforced elastomeric bearing pad shape factor and the material shear modulus was obtained in [17]. The relationship showed a correlation coefficient of 0.73. The shear modulus dependent on the bearing pad shape factor is calculated with the following equation:

$$G = 0.0332(S) + 0.0239 \quad [MPa] \tag{3.2}$$

where G is the shear modulus and S is the shape factor. Then the initial Young's modulus is calculated from the shear modulus obtained with the following equation:

$$E_o = 4.515(G) - 0.448 \quad [MPa] \tag{3.3}$$

where E_o is the initial Young's modulus which is dependent on the shape factor. To account for the rotation of the girder on the bearing pad, the degree of rotation Φ is calculated. The degree of rotation is also known as the material compressibility coefficient and is calculated with the following equation:

$$\Phi = 0.445 + \frac{\quad}{\quad} \quad [MPa] \tag{3.4}$$

From these parameters calculated, an effective Young's modulus that includes the effect of the girder rotation as well as the pad shape and reinforcement is calculated. With the effective Young's modulus, determination of effective short-time and long-time shear moduli for the viscoelastic material model was possible. The effective Young's modulus and the shear moduli were determined with the following equations:

$$E_c = E_o(1 + 2*\Phi*S^2) \quad [MPa] \tag{3.5}$$

$$G_o = \frac{\quad}{\quad} \quad [\text{MPa}] \tag{3.6}$$

$$G_\infty = \frac{\quad}{\quad} \quad [\text{MPa}] \tag{3.7}$$

where E_c is the effective Young's modulus, and G_o and G_∞ are the short-time and long-time shear moduli respectively.

Poisson's ratio for neoprene is usually in the range of 0.3 – 0.49. The following assumptions were made for the purpose of the assessment:

- Bearing Pad Length, L = 18"
- Bearing Pad Width, W = 9"
- Bearing Pad Internal Elastomer Layer Height, h_{ri} = 0.5".
- Poisson's Ratio, υ = 0.4.

The results of the assessment of the neoprene bearing pad properties are presented in Table 3.3.

Table 3.3. Results of bearing pad assessment

	S	G (MPa)	Eo (MPa)	Φ	Ec (MPa)	Go (MPa)	G∞ (MPa)
Bridge Bearing Pads	6	0.223	0.559	1.162	47.359	16.914	15.786

The initial shear modulus falls in between the range specified by AASHTO. A comparison between the two models is shown in Table 3.4.

Table 3.4. Comparison of bearing pad properties

	Go (MPa)	G∞ (MPa)
Assessment	16.914	15.786
Numerical Model [26]	17.000	16.000

The results obtained for the short-time and long-time shear moduli from the assessment are comparable to the properties used for the viscoelastic material model in the analysis.

Therefore, the properties for the viscoelastic material model used initially for analysis are well-founded.

3.3. Tractor-Trailer

An FE model of a tractor-trailer developed under previous FDOT research project was acquired for use in the current research project. It is a very simple model consisting of two models, the truck tractor and the lowboy trailer.

Extensive efforts were made on the vehicle's components that have significant influence in the interaction between the vehicle and the road. These components include the vehicle chassis, wheels, elastic tires, single and tandem axles, and the suspension system.

The tractor-trailer was modeled using 3- and 4-node 2-D, shell elements, and 6- and 8-node 3-D, fully integrated solid elements for most of the vehicle's components. The suspension system was modeled using 1-D, discrete beam elements. Material models included elastic materials for steel and aluminum, fabric and rubber materials for the wheels, and discrete spring and damper materials for the suspension system. More detailed information on the development of the tractor-trailer FE model is available in [26]. The final FE model of the tractor-trailer is summarized in Table 3.5 and presented in Figure 3.7.

Table 3.5. Summary of complete FE model of the tractor-trailer [26]

Specification		Specification	
Number of parts	204	Number of elements	26,194
Number of nodes	19,941	- solid elements	1128
Number of material models	38	- shell elements	24,790
		- beam elements	248
		- discrete elements	22
		- mass elements	6

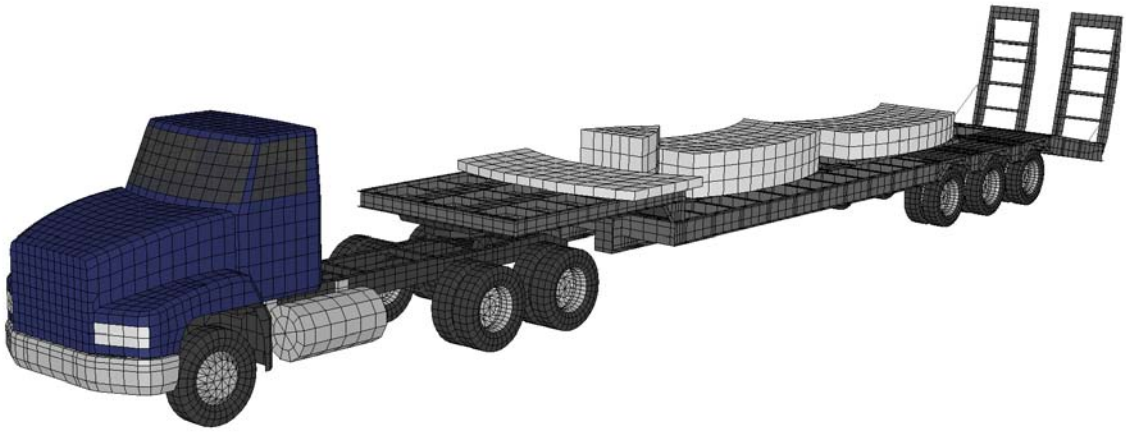

Figure 3.7. A FE model of the tractor-trailer [26]

Efforts were made to simulate the original mass of each vehicle component, paying special attention to the center of gravity of the vehicle. The position of the mass for each component was important to maintain the FE model's sprung and unsprung masses consistent with the actual vehicle.

The FE model of the tractor-trailer was validated and made available for further dynamic analysis of vehicle-bridge interaction. The verification and validation process had two stages, first the scaling of the vehicle's axles for validation of the masses presented in Table 3.6. Second, full-scale testing of the vehicle crossing over a speed bump for validation of the suspension system is presented in Figure 3.8.

Table 3.6. Axle loads for the tractor-trailer in experiment and FE analysis

Axle No.	Axle type	Axle load (kN / Kips)		Relative error (%)
		Measurements	FE model	
1	Front steer axle	42.18 / 9.48	42.29 / 9.51	0.25
2	Forward tandem drive axle	89.44 / 20.11	89.44 / 20.11	0.00
3	Rear tandem drive axle	94.96 / 21.35	95.01 / 21.36	0.05
4	First trailer axle	94.60 / 21.27	93.95 / 21.12	-0.69
5	Second trailer axle	98.52 / 22.15	97.91 / 22.01	-0.62
6	Third trailer axle	100.83 / 22.67	101.75 / 22.87	0.92
TOTAL		520.51 / 117.03	520.35 / 116.98	-0.04

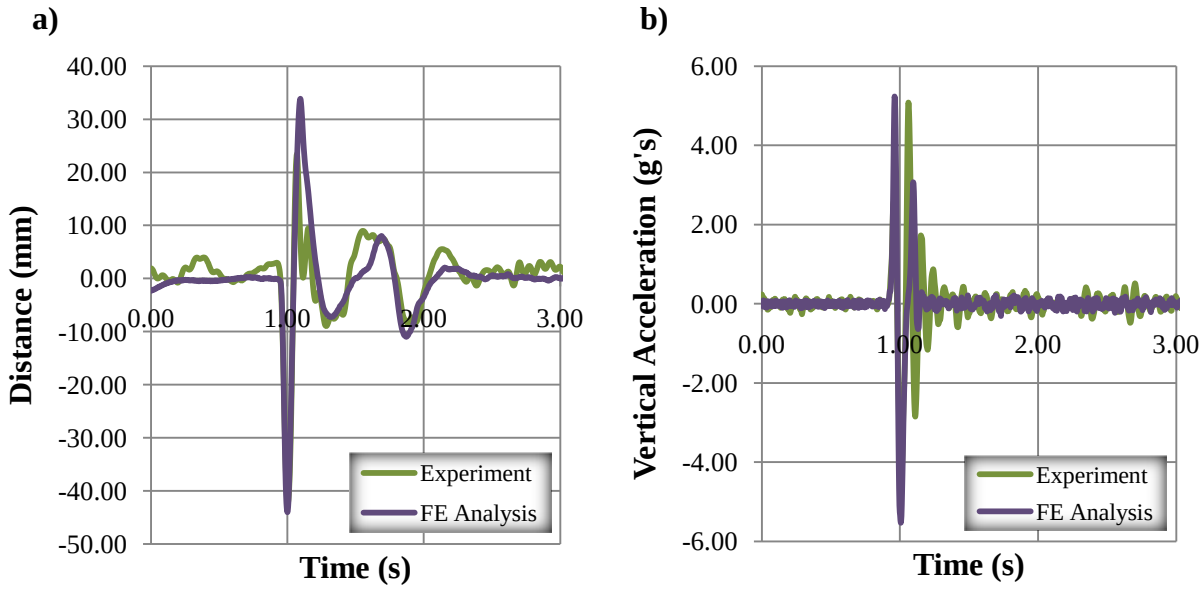

Figure 3.8. Time histories from experiment and FE analysis for the front axle at 24 km/h (15mph): a) change in distance between axle and frame, b) vertical acceleration of the axle

Only time histories for the front of the vehicle are shown, more test results are available in [26]. The tractor-trailer shows a very small relative error when comparing the measurement of the vehicle's axles. The correlation coefficient was measured previously between the two as 0.85 for the front axle. As for the bridge model, the results were compared using the RSVVP V&V software, using the same acceptance criteria [19]. The results are presented in Appendix A and summarized in Table 3.7.

Table 3.7. Results of RSVVP V&V software for the tractor-trailer

	Sprague & Geers Metric			Anova Metric		Passing Metrics
	Magnitude	Phase	Comprehensive	Average	Std	
Change in Distance	12.4	19.4	23	-0.01	0.08	5/5
Vertical Acceleration	0.8	30.9	30.9	0	0.11	5/5

As the results from the software show, with all the acceptance criteria met, the vertical acceleration of the axle as well as the change in distance between the axle and the frame are very satisfactory. The values are accepted and the FE model is validated and verified due to their qualitative similarity.

3.4. Terex Crane

An FE model of the Terex crane was also developed under a previous FDOT research project and was acquired for analysis in the current research project. The model of the crane is the simplest of the three, with most of its components being modeled as rigid elements.

As for the tractor-trailer, emphasis was put on the development of components that influence the interaction between the vehicle and the road surface. The modeling methodology for the wheels and suspension was similar to that of the tractor-trailer.

The Terex crane was modeled using 3- and 4-node 2-D, shell elements, and 6- and 8-node 3-D, fully integrated solid elements. The suspension was also modeled using 1-D, discrete beam elements. Material models included the same as for the tractor-trailer, although properties of the steel could vary. More detailed information about the material models and development of the Terex crane is available in [26]. The final FE model of the Terex crane is summarized in Table 3.8 and presented in Figure 3.9.

Table 3.8. Summary of complete FE model of the Terex crane [26]

Specification		Specification	
Number of parts	153	Number of elements	20,837
Number of nodes	17,401	- solid elements	1,338
Number of material models	29	- shell elements	19,323
		- beam elements	142
		- discrete elements	28
		- mass elements	6

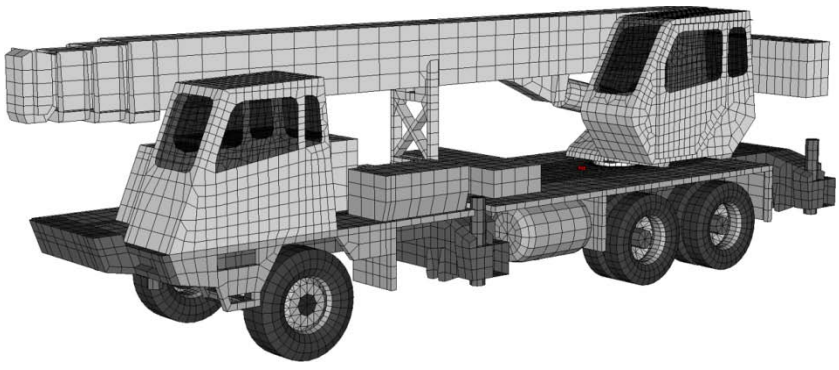

Figure 3.9. A FE model of the Terex T-340 crane [26]

The FE model of the Terex crane is validated and was therefore used in this research for dynamic analysis of vehicle-bridge interaction. Validation and verification also occurred in two stages; first scaling each of the vehicle's axles to validate the mass is presented in Table 3.9. Second, runs of the vehicle in full scale testing over a speed bump for the experiment and FE analysis are compared in Figure 3.10.

Table 3.9. Axle loads for the Terex crane in experiment and FE analysis

Axle No.	Axle type	Axle load (kN / Kips)		Relative error (%)
		Measurements	FE model	
1	Front steer axle	85.26 / 19.17	85.25 / 19.16	-0.01
2	Forward tandem drive axle	93.71 / 21.07	93.72 / 21.07	0.00
3	Rear tandem drive axle	92.47 / 20.79	92.48 / 20.79	0.01
TOTAL		271.44 / 61.03	271.45 / 61.02	0.002

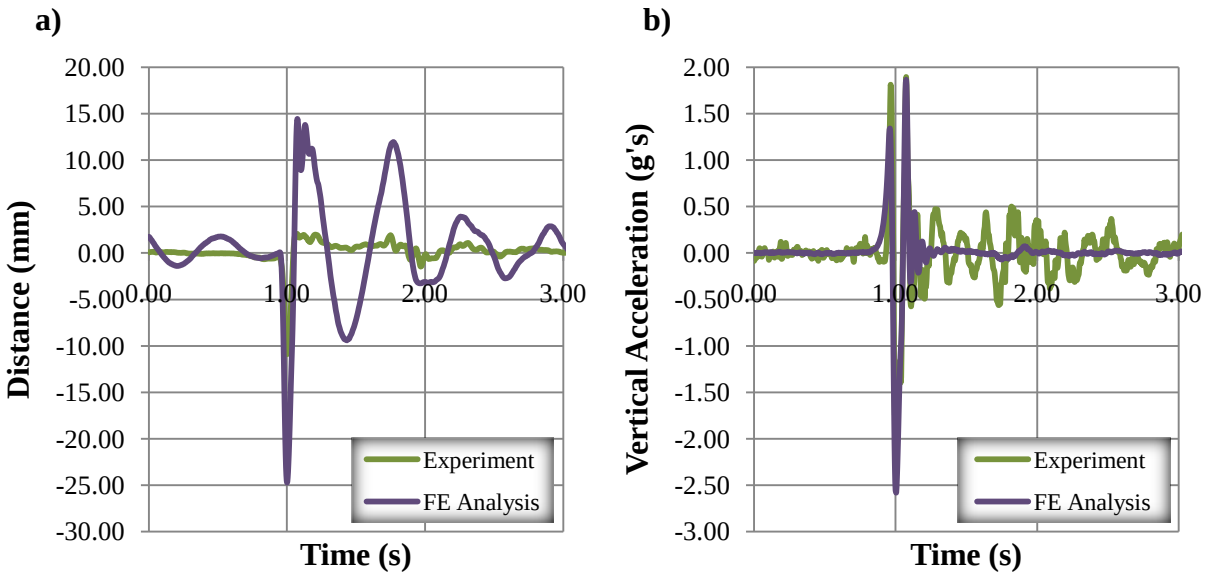

Figure 3.10. Time histories from experiment and FE analysis for the front axle at 24 km/h (15 mph): a) change in distance between axle and frame, b) vertical acceleration of the axle

There is a satisfactory comparison of the axle loads of the FE model and the crane, with small relative errors. Discrepancy in the experiment and FE analyses was attributed to simplification of the vehicle's suspension system, as the lack of a bump stop in the vehicle's FE model. The correlation coefficient was measured previously between the two as 0.7 for the front

axle. The results were then compared using the RSVVP V&V software, using the same acceptance criteria as for the past two cases [19]. The results are presented in Appendix A and summarized in Table 3.10.

Table 3.10. Results of RSVVP V&V software for the Terex crane

	Sprague & Geers Metric			Anova Metric		Passing Metrics
	Magnitude	Phase	Comprehensive	Average	Std	
Change in Distance	255	27.4	256.5	0.01	0.32	3/5
Vertical Acceleration	1.8	21.8	21.9	0	0.1	5/5

For this case, the comparison of numerical analysis and experimental test meet 8 of the total 10 acceptance criteria. The differences between the deflections of the numerical analysis and experimental test are related to simplification of the suspension in the FE model. The values were accepted qualitatively and the FE models were validated and verified.

3.5. FDOT Truck

The third vehicle model assessed was the FDOT truck also developed in a previous FDOT research project [25]. The FE model of the FDOT truck was subjected to some minor modifications.

As for the two other vehicles a lot of emphasis was put on developing the components that influence the interaction between the vehicle and the road. The methodology used for modeling of the wheels is similar to that of the other two vehicle models. The FDOT truck has a very simple suspension system including two tandem axles, which were easier to model.

The FDOT truck was modeled using the same type of elements as the two other vehicles, for most of the components. The material models also include elastic, fabric, rubber and the same type of material models as the other vehicles for most of its components. More detailed information about the development process of the FDOT truck is available in [25] and [26]. The final FE model of the FDOT truck is summarized in Table 3.11 and presented in Figure 3.11.

Table 3.11. Summary of complete FE model of the FDOT truck [26]

Specification		Specification	
Number of parts	181	Number of elements	18,569
Number of nodes	13,031	- solid elements	926
Number of material models	25	- shell elements	17,137
		- beam elements	440
		- discrete elements	58
		- mass elements	8

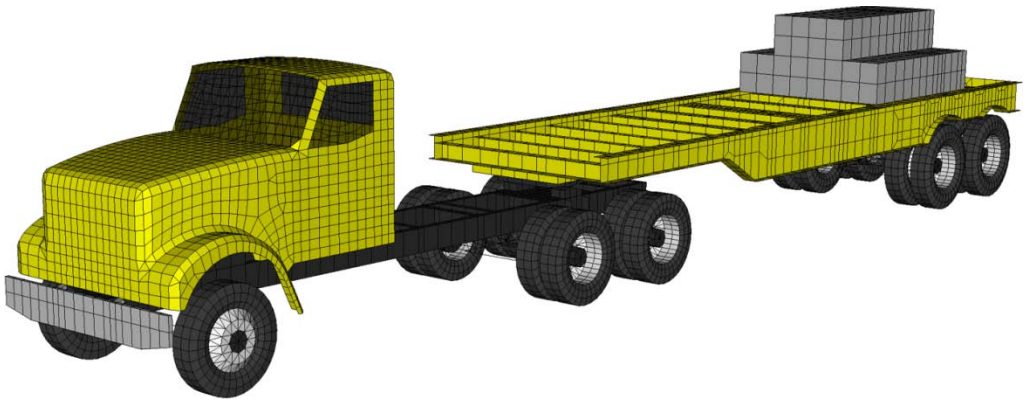

Figure 3.11. A FE model of the FDOT truck [26]

The FE model of the FDOT truck was also validated and was used for the dynamic analysis of vehicle-bridge interaction performed in this research project. The validation and verification process for the FDOT truck was only based on distribution of the masses, because the vehicle was not included in the speed bump testing like the other two. To achieve good correlation of the mass, material densities were changed and mass elements were attached where necessary. The final results of the load measurements are presented in Table 3.12.

Table 3.12. Axle loads for the FDOT truck in experiment and FE analysis

Axle No.	Axle type	Axle load (kN / Kips)		Relative error (%)
		Measurements	FE model	
1	Front steer axle	50.10 / 11.26	50.10 / 11.26	0.00
2	Forward tandem drive axle	48.06 / 10.80	48.07 / 10.81	0.02
3	Rear tandem drive axle	48.06 / 10.80	48.05 / 10.80	-0.02
4	Forward tandem trailer axle	84.50 / 18.99	84.51 / 18.99	0.01
5	Rear tandem trailer axle	84.50 / 18.99	84.50 / 18.99	0.00
TOTAL		315.22 / 70.84	315.23 / 70.85	0.003

The measurements of the axle loads were satisfactory with the largest relative error being 0.02 percent. With the validation and verification criteria, the vehicle was successfully validated and therefore data obtained is assumed to be accurate.

CHAPTER 4

SELECTION OF BRIDGES FOR FURTHER ANALYSIS

4.1. Survey of Local Bridges

One of the main objectives of this research is to develop additional FE models of FDOT bridges. Past research (FDOT projects BD493 and BD543, [25] and [26]) was focused on the FDOT Bridge #500133 made of AASHTO type III girders. A FE model of that bridge was developed and well validated ([26], [25], [14], [12], [20]). The main focus of this research was placed on identification and development of supplementary models of prestressed reinforced concrete bridges made of AASHTO type II and type IV girders. Bridges with poor road surface imperfections, abutment joints with large difference in elevation between asphalt pavement and bridge decks, and other bridge approach irregularities were identified as those of special interest to FDOT. Several highway bridges were surveyed around the northern part of Florida in 2009. The close proximity of the selected bridges to Tallahassee was essential to reduce time and cost of local trips to take detailed bridge measurements and to possibly carry out additional testing, if required. Newer, more recently built bridges were also of interest. The newer bridges can be closely monitored during a longer period of time of their remaining life span. In addition, their FE models are more reliable as compared with older bridges, as bridge fatigue and fracture phenomena need not be addressed yet. The survey resulted in five bridges as good candidates for final selection. The locations of all surveyed bridges, with respect to Tallahassee as a reference, are presented in Figure 4.1. The distances from the FSU campus in Tallahassee to all bridges ranged from 15 miles to 22 miles.

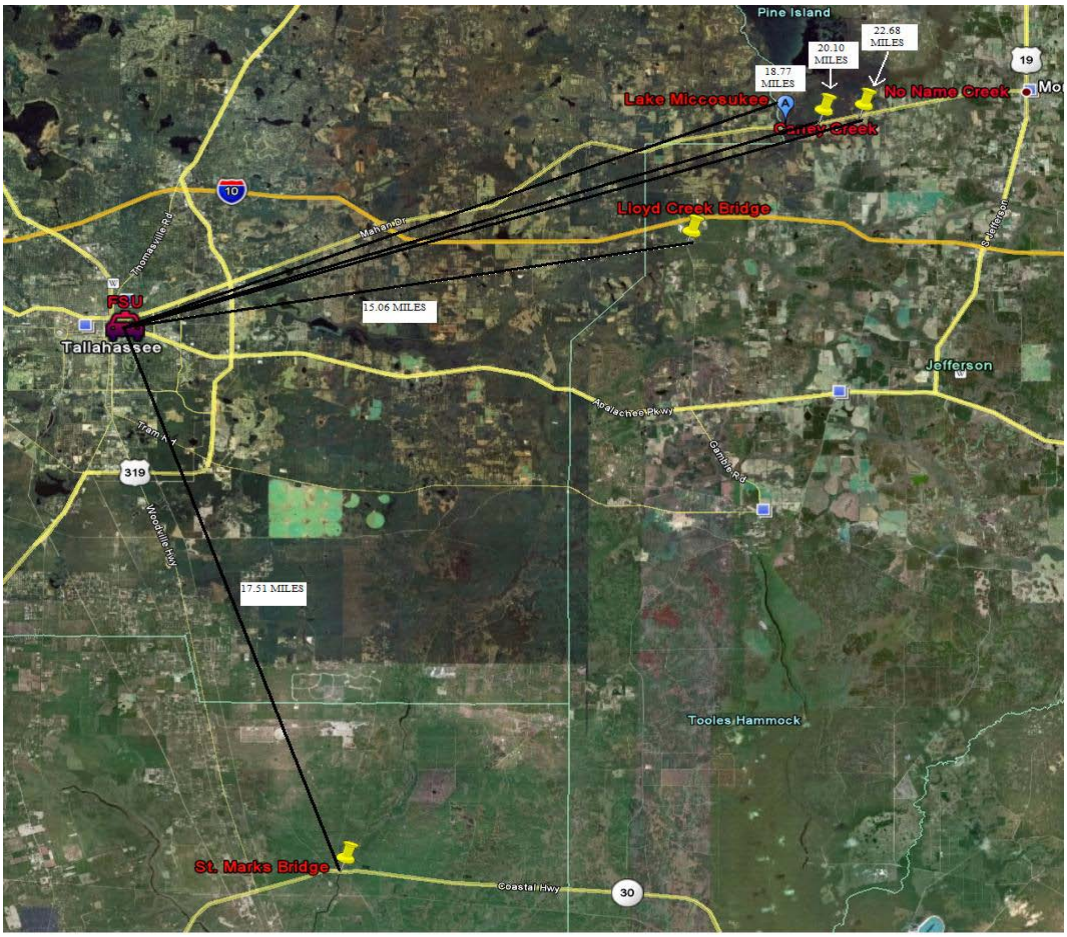

Figure 4.1. Location of bridges included in the survey

The first bridge surveyed was bridge #540072 built in 1997 at Lake Miccosukee. The bridge is located at US 90, Mahan Drive, 30.2 km (18.77 mi) from Tallahassee. The bridge is a two-lane, two-way structure consisting of 8 spans, each 12.2 m (40’-0”) long. AASHTO type II girders with a depth of 0.9 m (3’-0”) were used as a main part of the superstructure. The road and the bridge deck surfaces were in good condition. The small abutment joint has an average difference of elevation between asphalt pavement and the concrete bridge deck of about 5 mm. In addition, the bridge has 7 expansion joints between adjacent bridge spans. The Lake Miccosukee Bridge is shown in Figures 4.2 and 4.3.

Figure 4.2. A side view of bridge #540072

Figure 4.3. An abutment joint of bridge #540072

The second bridge surveyed was bridge #540073 built in 1996 over Caney Creek, shown in Figures 4.4 and 4.5. This bridge is also located on Mahan Drive, US 90, close to Monticello, 32.3 km (20.1 mi) from Tallahassee. The two-way, two-lane bridge consists of 2 spans with a length of 12.2 m (40’-0”) each. The bridge superstructure consisted of AASHTO type II girders with a depth of 0.9 m (3’-0”). An average difference between elevations of the asphalt pavement and the bridge deck abutment was measured and recorded as 6 mm.

Figure 4.4. An approach of bridge #540073

Figure 4.5. A view under bridge #540073

The third bridge surveyed was bridge #540074 built in 1996 over No Name Creek, shown in Figures 4.6 and 4.7. This bridge is also located on Mahan Drive, US 90, close to Monticello, 36.5 km (22.7 mi) from Tallahassee (see Figure 4.1). The two-way, two-lane bridge consists of 2

spans with a length of 12.2 m (40’-0”) each. The bridge superstructure consists of AASHTO type II girders with a depth of 0.9 m (3’-0”). An average difference in abutment joint elevations was approximately 7.5 mm.

Figure 4.6. An approach of bridge #540074

Figure 4.7. AASHTO type II girders of bridge #540074

The next bridge surveyed was the Lloyd Creek Bridge identified with FDOT #540061. The bridge was built in 1977 and is shown in Figures 4.8 and 4.9. The bridge is located on County Road 158 close to Monticello, 24.2 km (15.1 mi) from Tallahassee. The bridge consists of 2 spans with a length of 12.2 m (40’-0”) each. The bridge superstructure consists of precast prestressed panels with a depth of 0.9 m (3’-0”). An average difference in elevation of 13 mm was measured and recorded between two adjacent parts of the abutment joint.

Figure 4.8. An approach of bridge #540061

Figure 4.9. A view under bridge #540061

Another bridge surveyed was bridge #590056. The bridge was built in 2001 over St. Marks River and is shown in Figures 4.10 and 4.11. The bridge is located on US 98 close to the St. Mark's area, 28.2 km (17.5 mi) southeast of Tallahassee. The bridge consists of 3 spans with a length of 29.3 m (96'-0") each, AASHTO type IV girders with a depth of 1.4 m (4'-8"). An average vertical difference in elevation of 13 mm was measured between the asphalt approach and the bridge deck.

Figure 4.10. An approach of bridge #590056

Figure 4.11. A view under bridge #590056

4.2. Selection of Bridges

Five bridges, as described in Section 4.1, were discussed during one of the milestone meetings. Several factors were taken into consideration such as the approach depression, the year built, and the type of girder for each of the bridges. The selection criterion for the new bridges was then narrowed down to bridges with AASHTO type II and type IV girders. The new FE models were to complement an FE model of bridge #500133 with AASHTO type III girders, which was already developed and validated in [14], [12], and [20]. An assessment of the surveyed bridges resulted in the selection of the two following bridges for development of their FE models:

1. Bridge #540074 over No Name Creek, and
2. Bridge #590056 over St. Mark's River.

4.3. No Name Creek Bridge

Bridge #540074 is a 2-span bridge with two lanes of traffic. It was built over a creek known as "No Name Creek" in 1996 on US 90, approximately 50 km (30 mi) east of Tallahassee. The total length of the bridge is 24.3 m (79'-6") with each span having a length of 12.1 m (39'-7") and a width of 11.6 m (38'-0"). Each span of the bridge consists of six AASHTO type II prestressed girders, which are simply supported and spaced at 1.4 m (4'-6"). The concrete slab is cast as continuous and the bridge is in fairly new condition without any significant deterioration.

A picture of the bridge location and detailed drawings are presented in Figures 4.12 to 4.14.

Figure 4.12. Location of bridge #540074

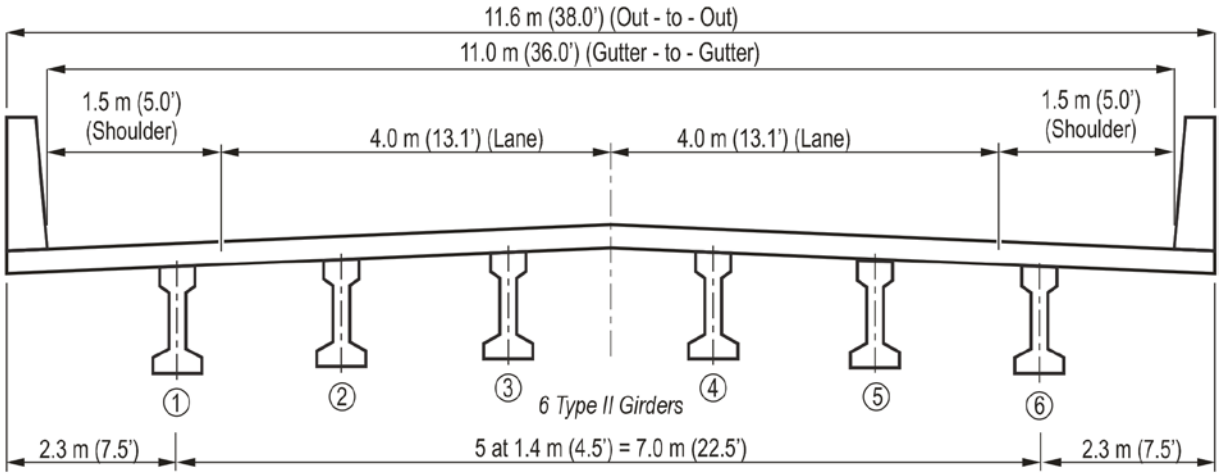

Figure 4.13. Cross section of bridge #540074

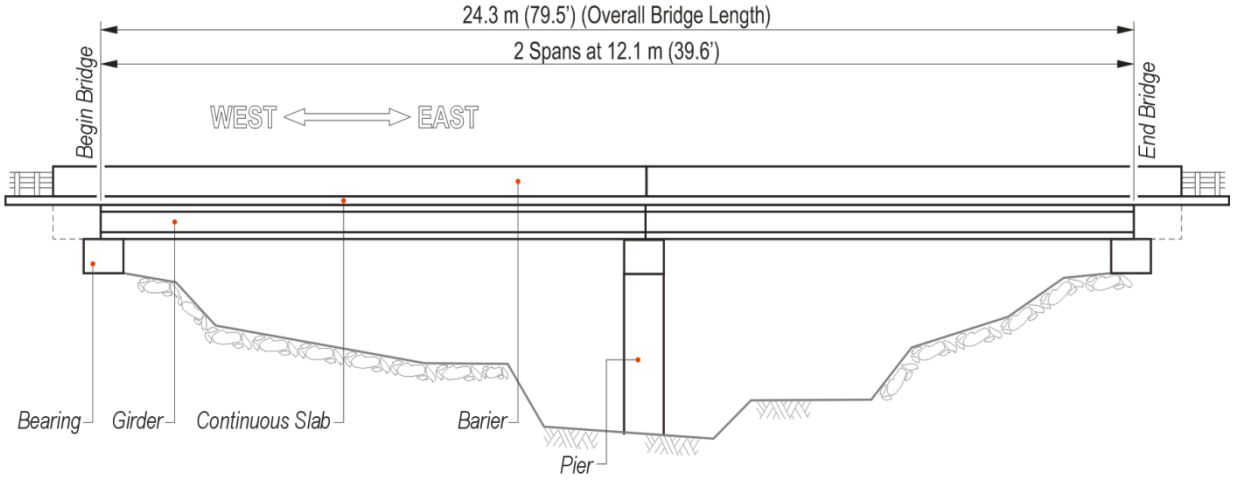

Figure 4.14. Elevation of bridge #540074

4.4. St. Mark's Bridge

Bridge #590056 is a 3-span bridge with two lanes of traffic. It was built in 2001 and crosses St. Mark's River on US 90. The total length of the bridge is 87.3 m (286'-6") with each span having a length of 29.1 m (95'-6") and a width of 12.6 m (41'-4"). Each span of the bridge consists of six AASHTO type IV prestressed girders, which are simply supported and spaced at 2.0 m (6'-6"). The concrete slab is cast as continuous and the bridge is in good condition without any significant deterioration.

A picture of the bridge location and detailed drawings are presented in Figures 4.15 to 4.17.

Figure 4.15. Location of bridge #590056

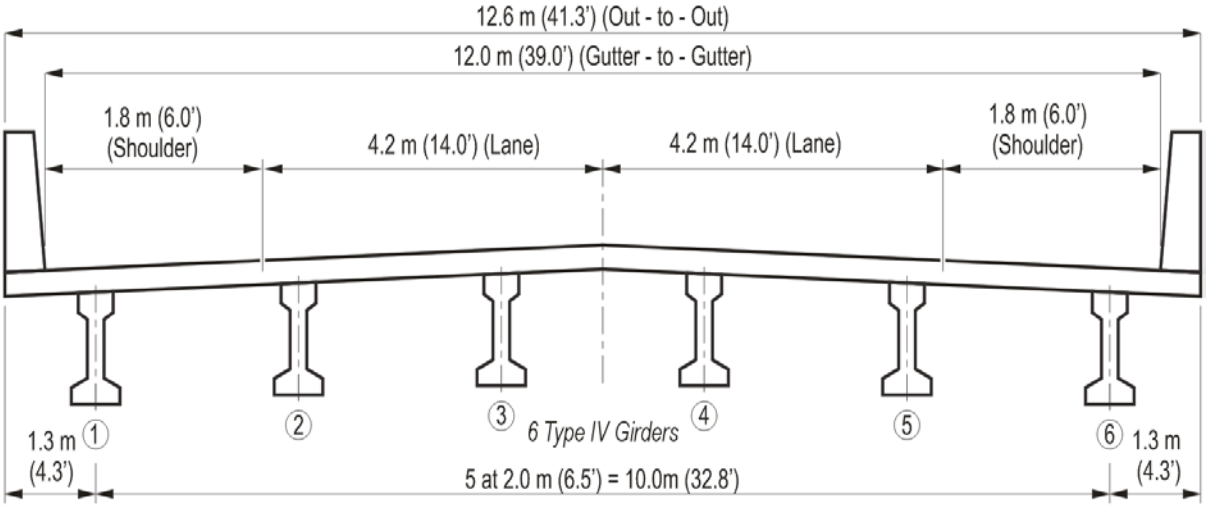

Figure 4.16. Cross section of bridge #590056

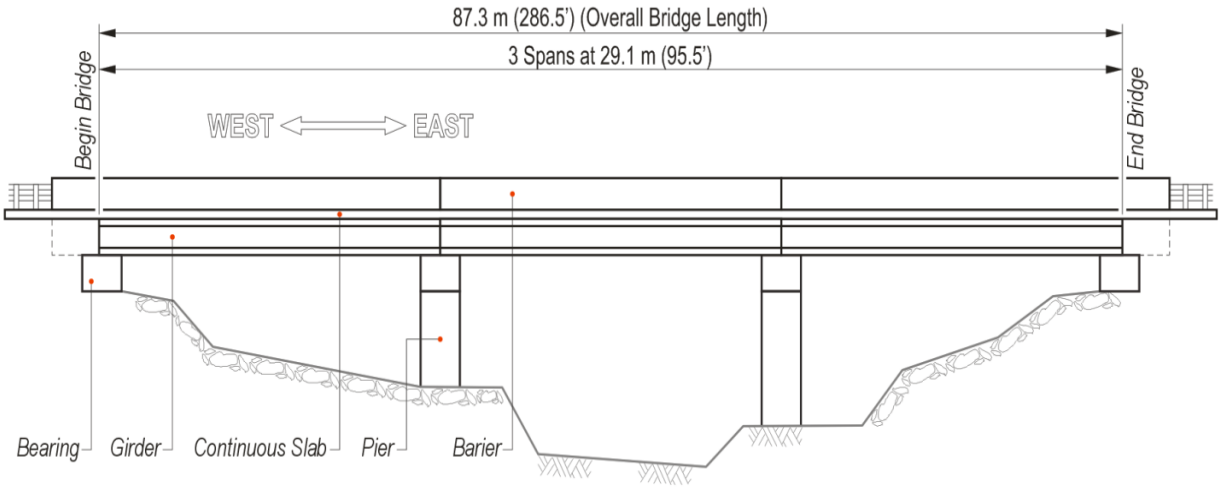

Figure 4.17. Elevation of bridge #590056

CHAPTER 5

DEVELOPMENT OF FE MODELS OF BRIDGES

One of the main objectives of this research was to develop additional FE models of bridges for further analysis of different types of structures. As described in Chapter 4 the bridges selected for the project included the No Name Creek Bridge (#540074, with AASHTO type II girders) and the St. Mark Bridge (#590056, with AASHTO type IV girders). The new FE models were individually developed from the existing FE model of the Chattahoochee Bridge (#500133) [26], [25], that includes AASHTO type III girders. Only one span of each bridge was developed. Additional spans (with the same lengths) are generated, as needed, through a copying process. The Chattahoochee Bridge FE model was validated as a part of the previous project, and the same constitutive material models and the same material characteristics were used for the two new models. The research team believes that this process ensured a high level of confidence so that results for the new FE models of the bridges are valid and accurate.

For the purpose of modeling the bridges with different girder dimensions, the dimensions are presented in Table 5.1 and represented in Figure 5.1.

Table 5.1. AASHTO girder section properties [2]

Girder Type	H1 (mm)	H2 (mm)	H3 (mm)	H4 (mm)	H5 (mm)	H6 (mm)	W1 (mm)	W2 (mm)	W3 (mm)	W4 (mm)	W5 (mm)
II	914.4	152.4	152.4	381	76.2	152.4	457.2	304.8	152.4	152.4	76.2
III	1143	177.8	190.5	482.6	114.3	177.8	558.8	406.4	177.8	190.5	114.3
IV	1371.6	203.2	228.6	584.2	152.4	203.2	660.4	508	203.2	228.6	152.4

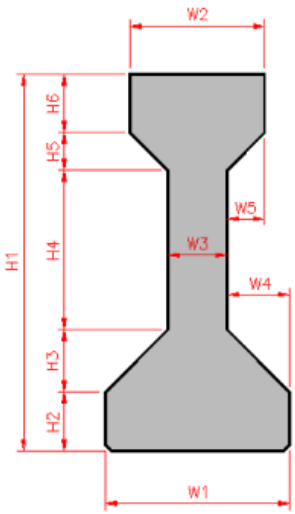

Figure 5.1. AASHTO girder section properties [2]

5.1. Development of No Name Creek Bridge Model

Development of the No Name Creek Bridge (#540074) with six AASHTO type II girders was carried out by making necessary geometric and material adjustments to the existing FE model available for bridge #500133. The process used for the modeling of the new bridge was possible due to significant similarities between the two bridges. Prestressed concrete bridge behavior is governed by the span length and the type of girders used. Usually short span bridges are designed with smaller size girders to carry the loads applied to them. The development of the new bridge FE model also takes into account that the bridge is shorter in length and narrower in width than the existing FE model.

The modeling process was started by using LS-Prepost preprocessor, which is a useful tool in handling a finite element model definition file. All necessary parameters for simulation of FE models including element properties, material properties, contact definitions, boundary conditions, solution type, and others were defined using the LS-Prepost preprocessor.

FE analysis depends on the integrity, grid size and aspect ratio of the elements used to ensure accurate results. Parts of the FE model sharing nodes with another part were modified as one in order to keep the integrity of the model.

The six major bridge elements that needed to be modified include parts such as: barriers, bridge deck, AASHTO girders, diaphragm, neoprene pads, and approach surface. The properties

of the three types of rebar that were used in the reinforcement of the bridge structure are summarized in Table 5.2.

Table 5.2. Nominal dimensions of ASTM standard reinforcing bars in bridge structures [26]

Bar size designation	Mass (kg/m) / (lb/ft)	Diameter (mm) / (in)	Area (mm2) / (in2)
10M	0.785 / 0.527	11.3 / 0.445	100 / 0.155
15M	1.570 / 1.055	16.0 / 0.630	200 / 0.310
20M	2.355 / 1.582	19.5 / 0.768	300 / 0.465

The discrete location of the nodes and dimensions of the elements in the FE model were determined by the actual location of the reinforcement, in accordance to the design plans.

Geometric modifications to the bridge were carried out as necessary with the obtained dimensions from the bridge selection survey. This was done by using the scale option in LS-Prepost preprocessor, which provides a tool to resize the elements as necessary to the desired area. A scale factor was calculated from a ratio between the dimensions of both bridges. Each dimension was processed individually, first the length in the longitudinal axis, and second, the width in the transverse axis of the bridge. The final dimensions of the FE models of the Chattahoochee Bridge and the No Name Creek Bridge span and width are summarized in Table 5.3.

Table 5.3. Summary of FE models dimensions

Bridge FE model	Span length (m) / (ft.)	Span width (m) / (ft.)
Chattahoochee	21.0 / 69.0	13.1 / 45.0
No Name Creek	12.1 / 40.0	11.6 / 38.0

Geometric modifications of the AASHTO girders were the most important in modeling of the bridge. This process is further discussed in detail in section 5.1.3.

5.1.1. Concrete Slab

The reinforced concrete slab was modeled using four layers of 3-D, fully integrated 8-node solid elements. The elastic material properties for the concrete slab were obtained from cylinder testing of the Chattahoochee bridge (#500133) slab conducted by the FDOT Structures Research Laboratory. No testing was carried out for the No Name Creek Bridge (#540074), therefore the same material properties for the concrete slab of the Chattahoochee Bridge were assumed. Material properties for the bridge concrete slab were adopted from [25], and are summarized in Table 5.4.

Table 5.4. Material properties of the concrete slab [26]

Specification	Units	Value
Young's modulus, E	(GPa) / (Ksi)	40.5 / 5871.8
Poisson's ratio, ν	-	0.2
Cylinder compressive strength, fc'	(MPa) / (Ksi)	55.9 / 8.11

Two types of reinforcement bars were used in the concrete slab: size 10M and 15M. They were modeled using 1-D bar elements with elastic material models with properties for steel. The concrete slab dimensions were measured at 10.2 m (34.0 ft.) wide and 12.1 m (40.0 ft.) long, narrower and shorter than bridge #500133 as specified in Table 5.3. The bridge concrete slab and its reinforcements were scaled down accordingly to the desired new length. The complete FE models of the concrete slab and its reinforcement are presented in Figures 5.2 and 5.3.

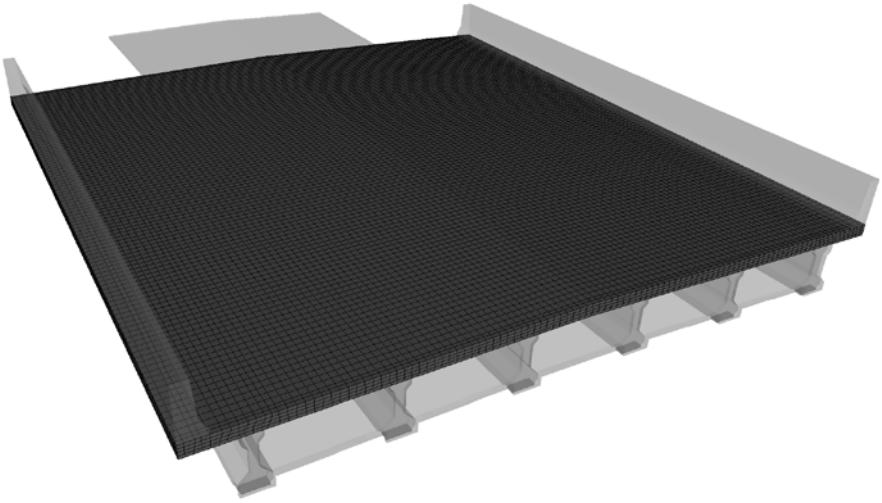

Figure 5.2. A FE model of the bridge concrete slab

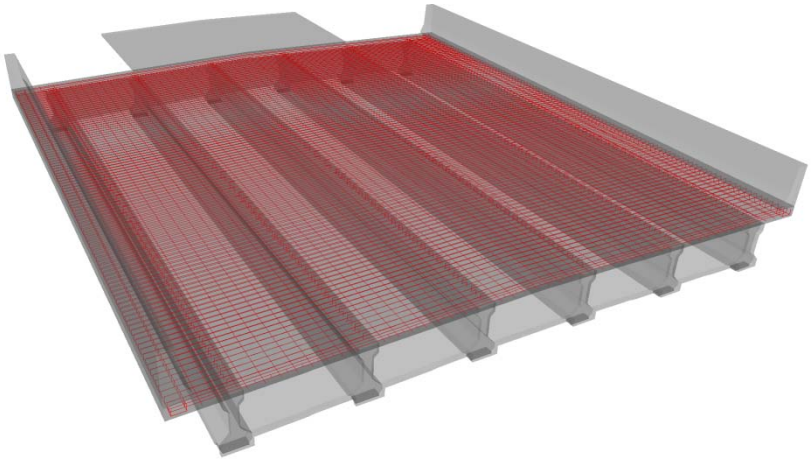

Figure 5.3. A FE model of the bridge deck steel reinforcement

5.1.2. Traffic Railing Barriers

The reinforced concrete railing barriers were modeled using 3-D, fully integrated solid elements. An elastic material model with properties for concrete was used for this part. The reinforcing bars were modeled using 1-D elements with two types of reinforcing bars, 10M and 15M. Due to the position of the nodes, minor geometric adjustments were necessary for the reinforcement of the railing barrier. The complete FE model of the railing barrier with the reinforcement is presented in Figures 5.4 to 5.6.

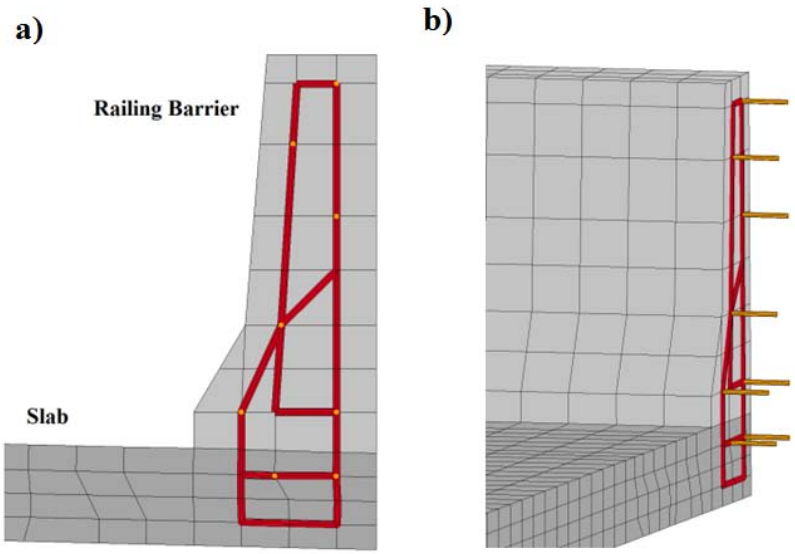

Figure 5.4. Traffic railing barrier reinforcement: a) cross section, b) side view

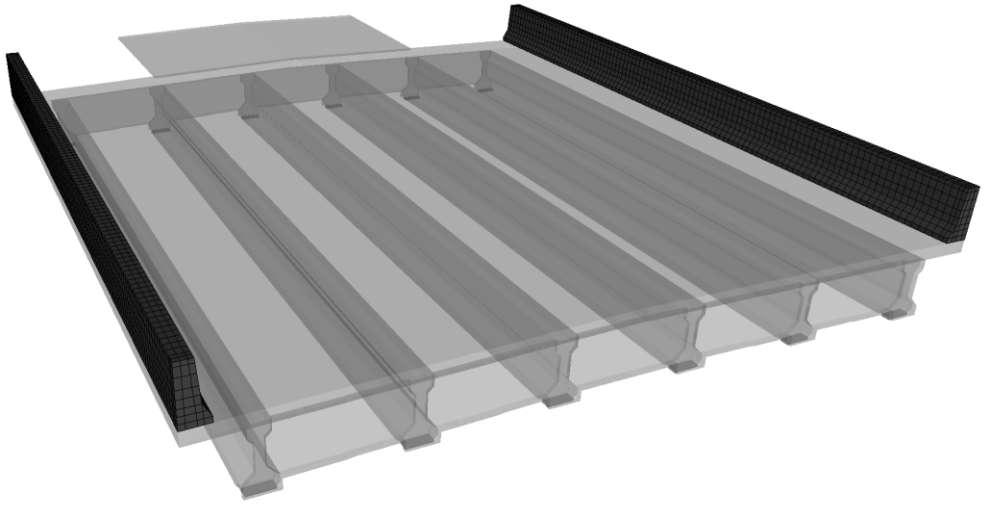

Figure 5.5. A FE model of the traffic concrete barrier

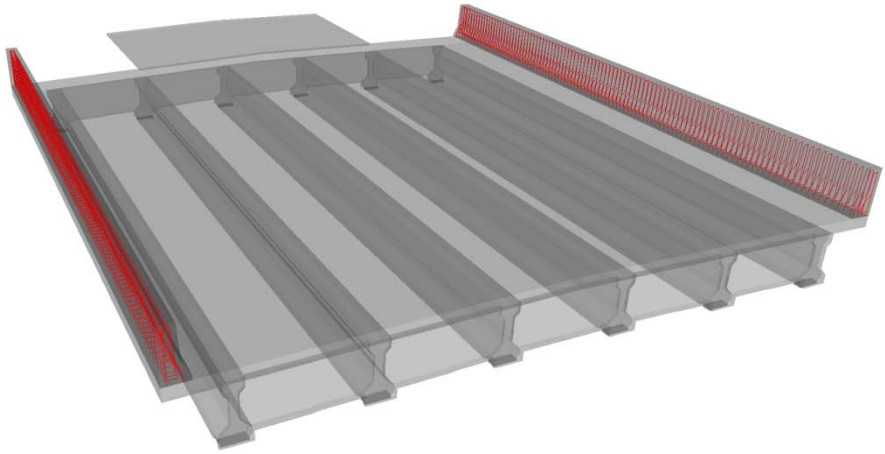

Figure 5.6. A FE model of the traffic railing barrier reinforcement

5.1.3. AASHTO Type II Girders

The size of the girders has the biggest effect on the strength and structural response of a bridge subjected to dynamic loads. Therefore the development of the new AASHTO type II girders was the most important component in the process of creating the new FE model.

Six AASHTO type II concrete girders were modeled using 3-D, fully integrated 8- and 6-node solid elements. An elastic material model was adopted for the FEM of the bridge. The material properties were obtained from cylinder testing of the concrete by the FDOT Structures Research Laboratory [26], and they are presented in Table 5.5.

Table 5.5. Material properties of the concrete girders [26]

Specification	Unit	Value
Young's Modulus, E	(GPa) / (Ksi)	37.5 / 5441.9
Poisson's ratio, ν	-	0.22
Specify compressive strength, fc'	(MPa) / (Ksi)	63.7 / 9.24

Reinforcement of the bridge girders included reinforcing bars and prestressing strands. The bars and strands were modeled as 1-D bar elements. Two no. 9 strands at the top and twenty-four no. 13 strands at the bottom of the girder were required. Due to the discrete location of the model nodes, only one strand at the top and thirteen strands at the bottom were used in the FE model. Although fewer strands were used in the FE model than needed, the strands are

equivalent to the necessary reinforcement. They were grouped and their properties distributed into equivalent locations while making sure the behavior represents that of a real girder. The locations of the prestressing strands in the girder cross section are presented in Figures 5.7 and 5.8. Material model MAT_CABLE_DISCRETE_BEAM was used for the strands to introduce prestressing forces in the bar elements. The model also allows for the cables to carry tensile loads only, without any stiffness for compression [15]. Reinforcing bars included an elastic material model with properties for steel. Location of reinforcing bars in the girder cross section, and FE model are presented in Figure 5.9. The FE model of the concrete girders and the girder reinforcements are presented in Figures 5.10 and 5.11 respectively.

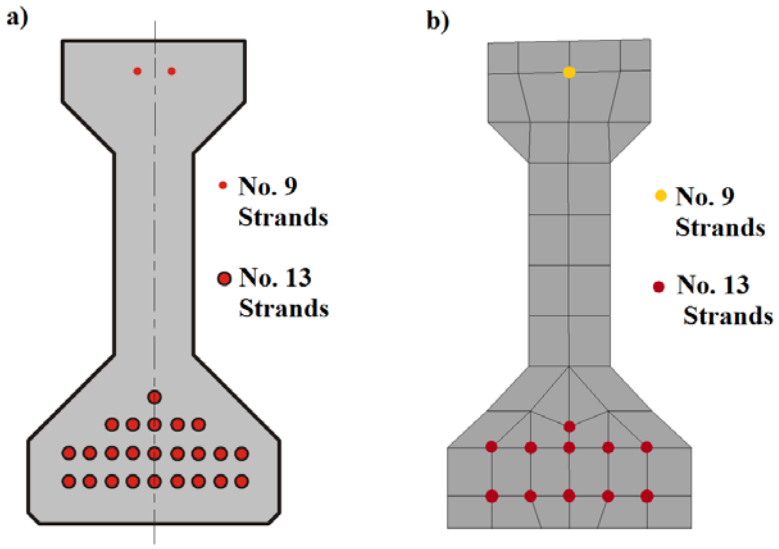

Figure 5.7. Prestressing strands in AASHTO type II girder: a) actual location of strands in girder, b) equivalent location of strands in FE model

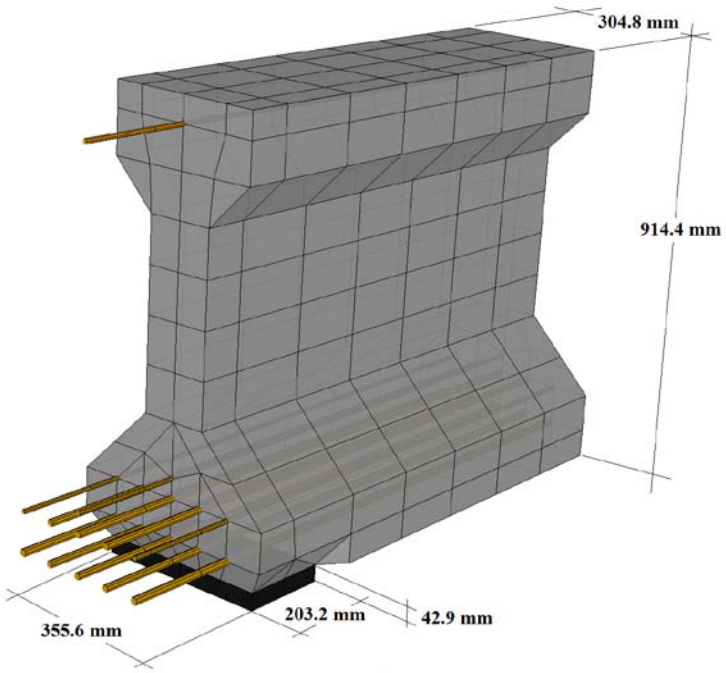

Figure 5.8. A FE model of AASHTO type II girder with prestressing strands

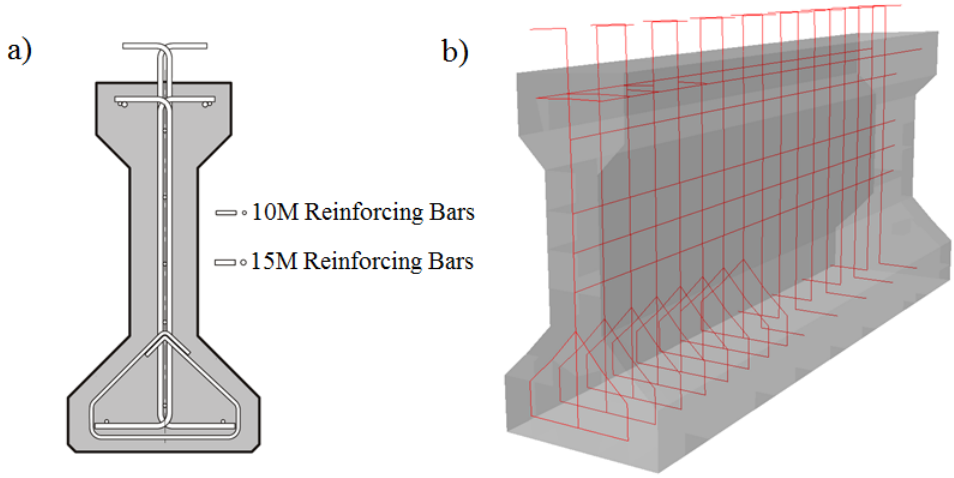

Figure 5.9. Reinforcement bars in the AASHTO type II girder: a) girder cross section, b) FE model of girder reinforcement

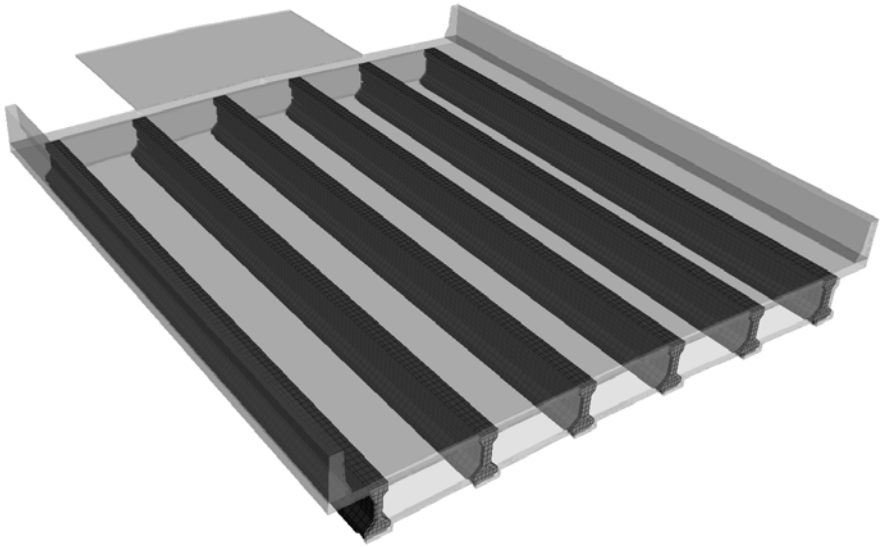

Figure 5.10. A FE model of the concrete girder

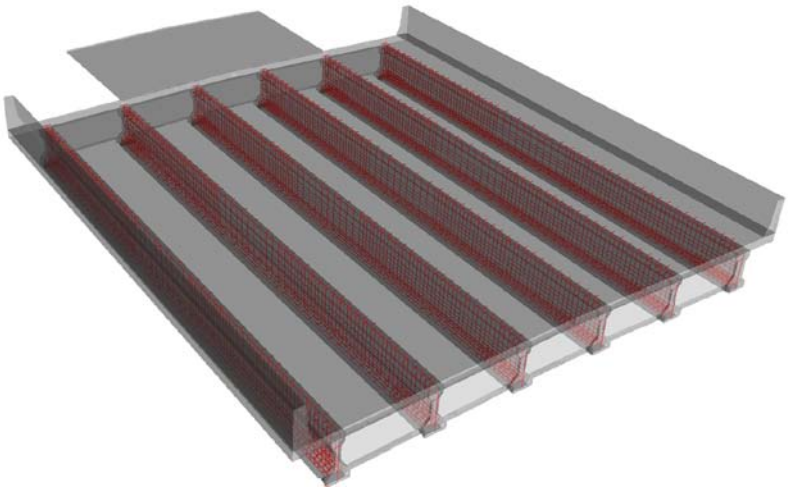

Figure 5.11. A FE model of the girder reinforcement

Geometric modifications of the AASHTO girders were done separately from the rest of the bridge. The girders were selected from the key file and isolated in order to keep the slab dimensions untouched. AASHTO type II girders are shorter and thinner than the type III girders, therefore AASHTO specification for prestressed concrete highway girders were used to find the adequate scaling factors [2]. One scale factor for the complete girder would not provide the required dimensions for each of the sections presented in Figure 5.1. Therefore, each one of these sections was scaled separately with their adequate scaling factor. The modification process was

divided in two parts, first in the vertical axis or height of the girder, and second, in the transverse axis or width of the girder.

For the vertical axis, the process went from top to bottom. Before scaling each section, a reference point was chosen on the top center of the section. This allowed the girder to move from the bottom up when scaled, while keeping the referenced point intact. This process was significant to prevent the movement of the top nodes of the girder, which connect the girder to the slab. The same process was repeated for each vertical section of the girder.

For the transverse axis, the process went from the center of the girder towards the outside. For each section, a reference point was chosen in the center of the section. This allowed for transverse movement of the section towards the center, keeping the distance between girders intact. The same process was repeated for each transverse section of the girder.

The FE models of the type II and III girders are compared in Figure 5.12.

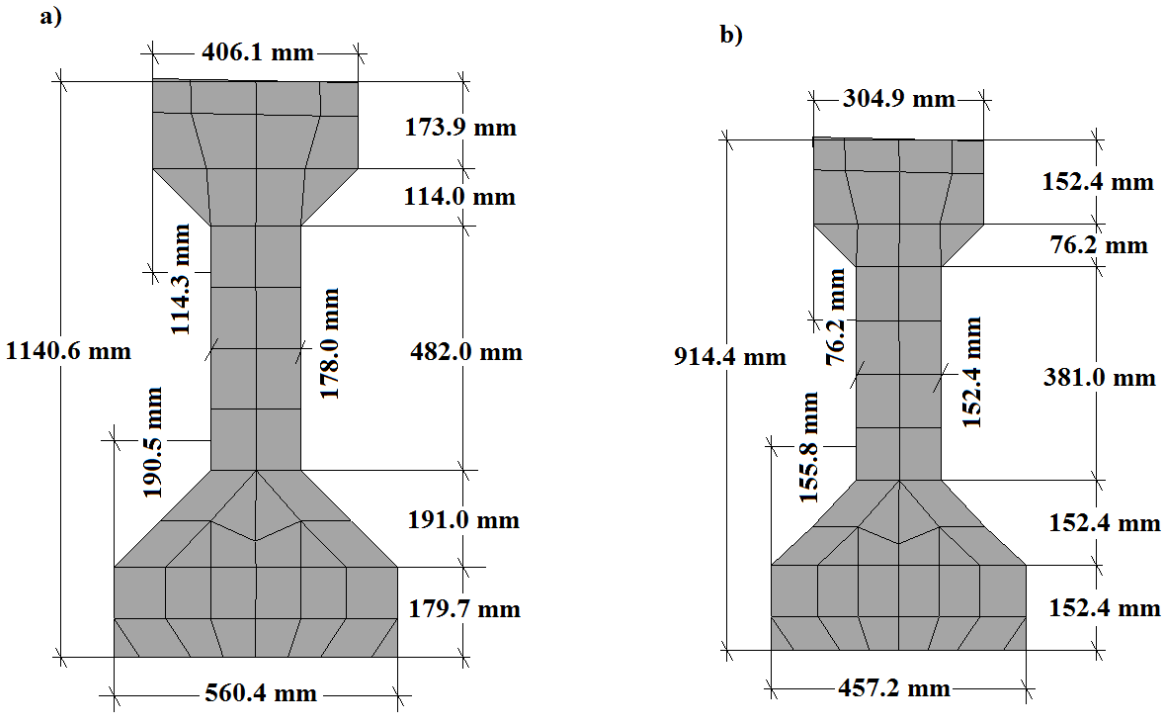

Figure 5.12. A FE model of an AASHTO girder: a) type III, b) type II

5.1.4. Diaphragms

The bridge concrete diaphragm was modeled using 3-D, fully integrated solid elements. An elastic material model was used for the FEA with properties for concrete. The reinforcing bars were modeled as 1-D bar elements, with an elastic material model with properties for steel. The complete FE model of the concrete diaphragm and its reinforcement are shown in Figures 5.13 and 5.14.

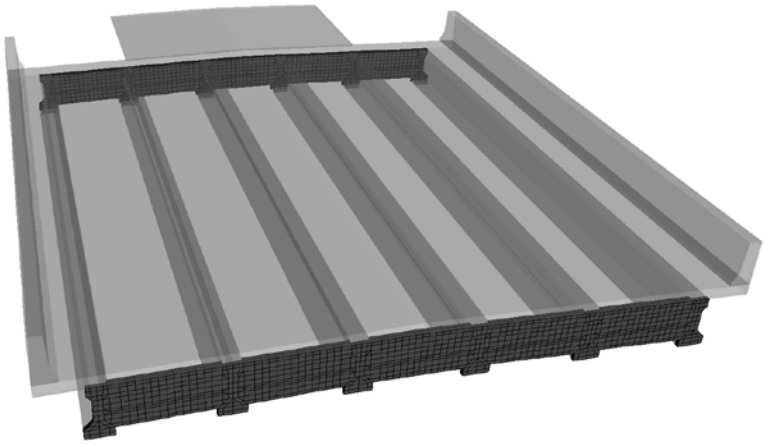

Figure 5.13. A FE model of the concrete diaphragm

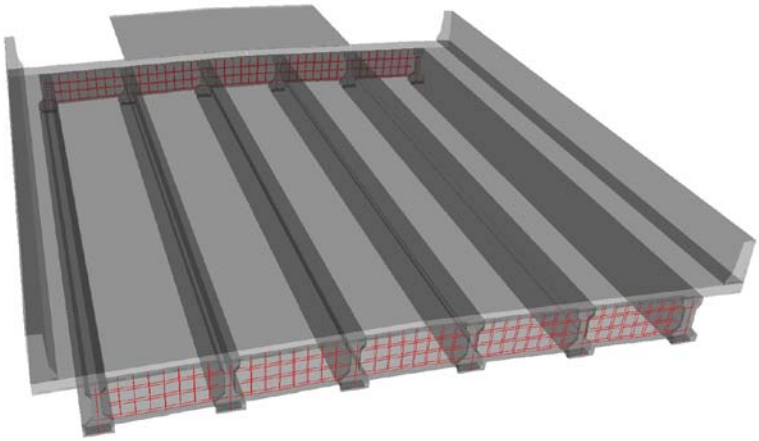

Figure 5.14. A FE model of the diaphragm reinforcement

5.1.5. Neoprene Pads

Neoprene bearing pads were used to support the girders on the piers. The neoprene bearing pads were modeled using 8-node 3-D, fully integrated solid elements. A viscoelastic material model was adopted for the neoprene pads and its properties were obtained from a parametric study. The complete model of the neoprene pads and their location are presented in Figure 5.15.

Figure 5.15. A FE model of neoprene bearing pads and its location

5.1.6. Approach Surface

The modeling of the road approach surface is important, as was explained in chapter 2.6 of the literature review. The approach surface is made of two parts, asphalt and concrete surfaces. The concrete surface was modeled using 3-D solid elements with an elastic material model with properties for concrete. The asphalt surface was modeled based on actual geometry using a laser scanner. Methodology of the modeling of the asphalt approach is discussed in detail in [26]. The FE model of the approach surface is presented in Figure 5.16.

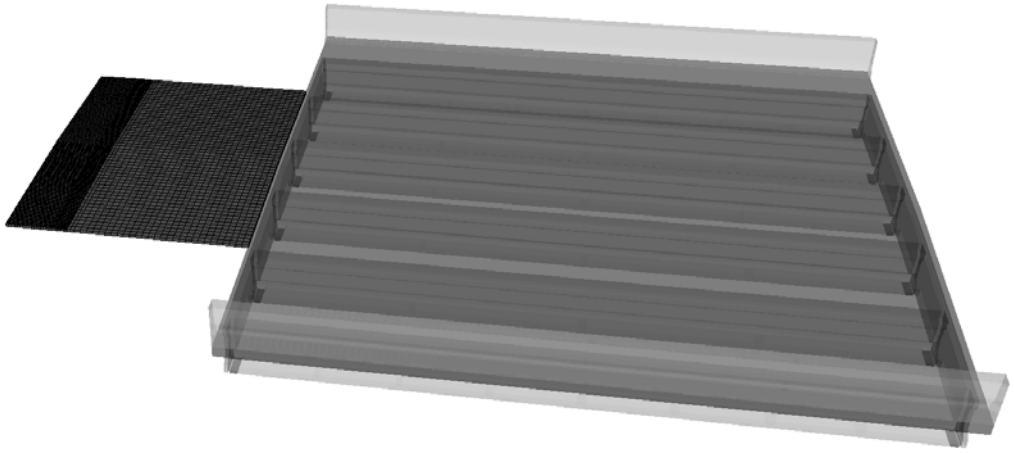

Figure 5.16. A FE model of the bridge approach surface

The FE model of bridge #540074 is summarized in Table 5.6. In the FE model, some elements are shared between parts; therefore the total number of elements may not equal the sum of all individual elements.

Table 5.6. A summary of the FE model of bridge #540074

	Slab	Railing	Girders	Diaphragms	Bearing Pads	Approach	Total
Number of nodes	57770	8269	35137	8011	504	3410	107378
Number of elements	76522	9486	47700	7794	144	1620	145604
- solid elements	45360	5670	26172	5732	144	1620	84698
- beam elements	37192	12076	31560	3870	0	0	60906

5.2. Development of St. Mark's Bridge Model

Development of the St. Mark's Bridge (#590056) with six AASHTO type IV girders also started from the existing FE model of the Chattahoochee Bridge (#500133). The modeling process followed the same methodology as the No Name Creek Bridge (#540074) for each of the parts of the bridge. The two new models consist of the same material properties, and the same number of nodes and elements.

St. Mark's Bridge has a longer span than the Chattahoochee Bridge, therefore it was built with larger girders to carry the heavier load. The final dimensions of the FE models of the Chattahoochee Bridge and the St. Mark's Bridge span and width are compared in Table 5.7.

Table 5.7. Summary of FE models dimensions

Bridge FE model	Span Length (m) / (ft.)	Span width (m) / (ft.)
Chattahoochee	21.0 / 69.0	13.1 / 45.0
St. Mark's	29.3 / 96.0	12.6 / 41.3

Geometric modifications of the AASHTO type IV girders followed the same methodology as for the type II girders. The FE model of the type III and IV girders are compared in Figure 5.17. The FE model of the St. Mark's Bridge is presented in Figure 5.18.

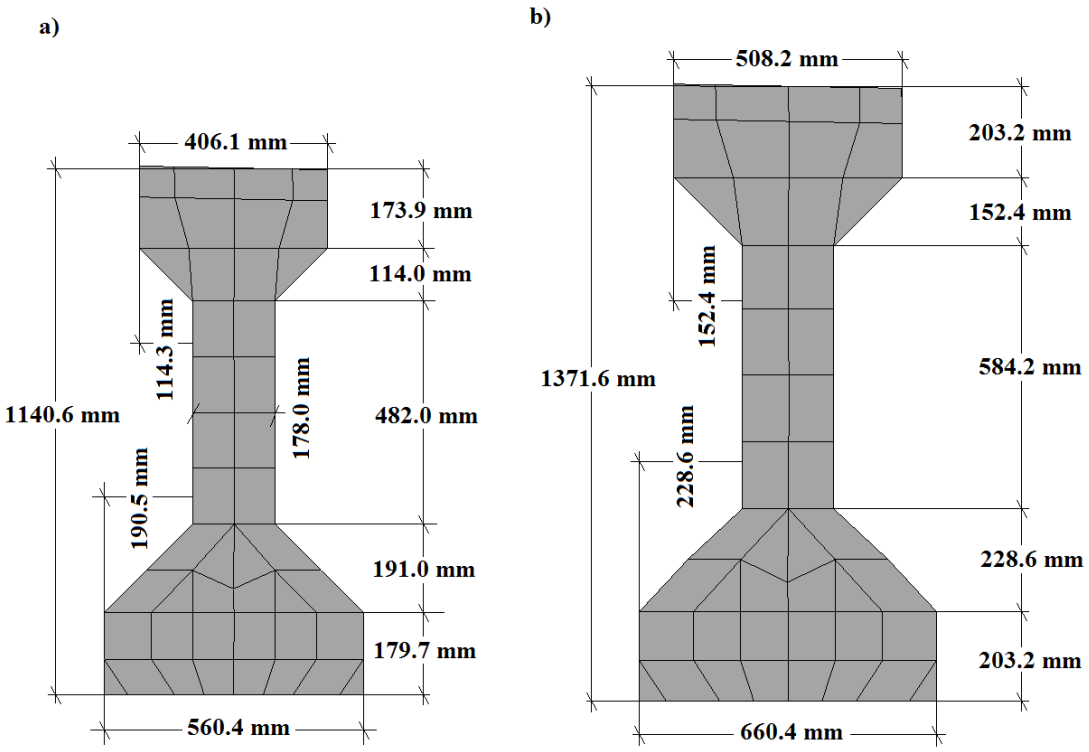

Figure 5.17. A FE model of an AASHTO girder: a) type III, b) type IV

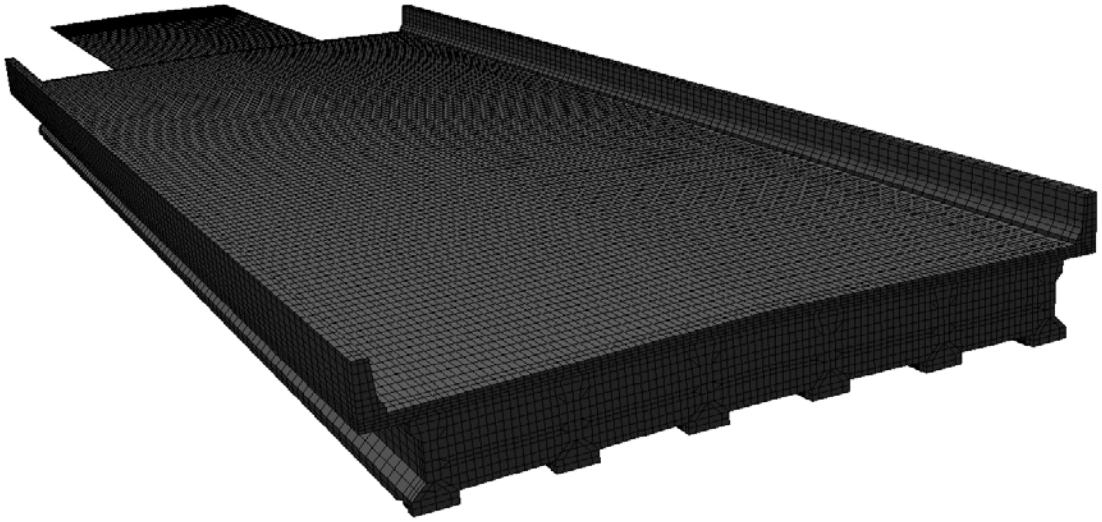

Figure 5.18. An FE model of St. Mark's Bridge

CHAPTER 6

FE ANALYSES OF VEHICLE-BRIDGE INTERACTION

FE analyses were performed on the three FE models of bridges using the three available FE models of heavy vehicles. Analysis of the three different bridges provided information about the effect of bridge characteristics on the dynamic response of bridges.

Analysis of DLA versus speed was performed for each bridge with the three heavy vehicles. The analyses included static and dynamic runs with varying speeds ranging from 24 km/h (15 mph) to 96 km/h (60 mph) with an 8 km/h (5 mph) increase between each run. The FE analysis included runs in the center of the westbound lane of traffic for all the cases. The transverse position of the vehicle in the bridge and the girder numbers used for the analysis are presented in Figure 6.1.

The complete FE analyses including all the six models totaled nine different cases, with over one hundred simulations computed. Time histories of strain and displacement in the girders were obtained from the numerical analysis. It was proven in previous research [26] that in testing, maximum displacement readings come from displacement of various components. Therefore, readings of displacement are not very reliable as the readings of strains in the girders, so the maximum strains were used to compute the DLA.

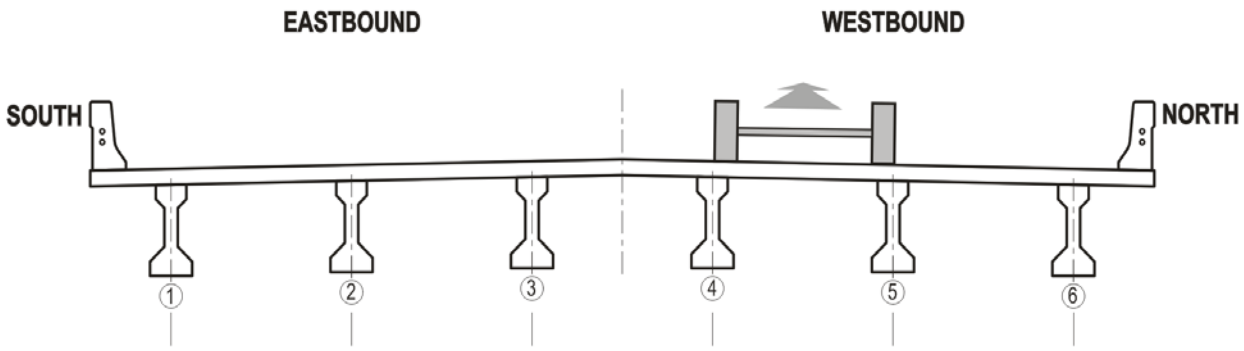

Figure 6.1. Transverse position of the vehicles in the FE analysis (figure not to scale)

6.1. FE Analysis of No Name Creek Bridge (#540074)

6.1.1. Longitudinal Position for Static Tests

The obtained results of the FE analyses are taken from the middle of the span length. The longitudinal position of the vehicles for the static tests is based on the theory of influence lines for statically determinate structures [11]. The bridge span is considered a simply supported beam, and the maximum bending moment, in the middle of the span, occurs when the major concentrated load near the resultant force is located in the centerline of the span.

Tractor-trailer. For the tractor-trailer – bridge system, the maximum moment in the middle of the span occurs when the fifth axle is located in the centerline of the span. The location of the tractor-trailer in the FE model of the No Name Creek Bridge for the static test is presented in Figure 6.2.

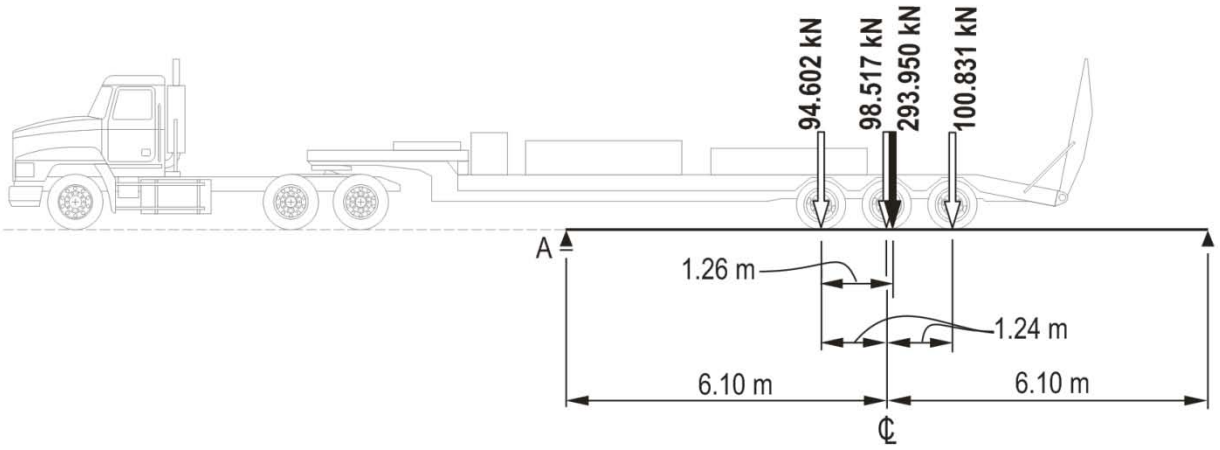

Figure 6.2. Position of the tractor-trailer in the No Name Creek Bridge FE model resulting in the maximum moment in the middle of the span with the resultant force shown as a black arrow

The resultant force from the vehicle configuration is

and the location of the resultant force, defined as the distance from the fourth axle is

The reaction at point A is then

The maximum moment in the middle of the span is then measured as

Terex crane. For the Terex crane – bridge system, the maximum moment in the middle of the span occurs when the second axle is located in the centerline of the span. The location of the Terex crane in the FE model of the No Name Creek Bridge for the static test is presented in Figure 6.3.

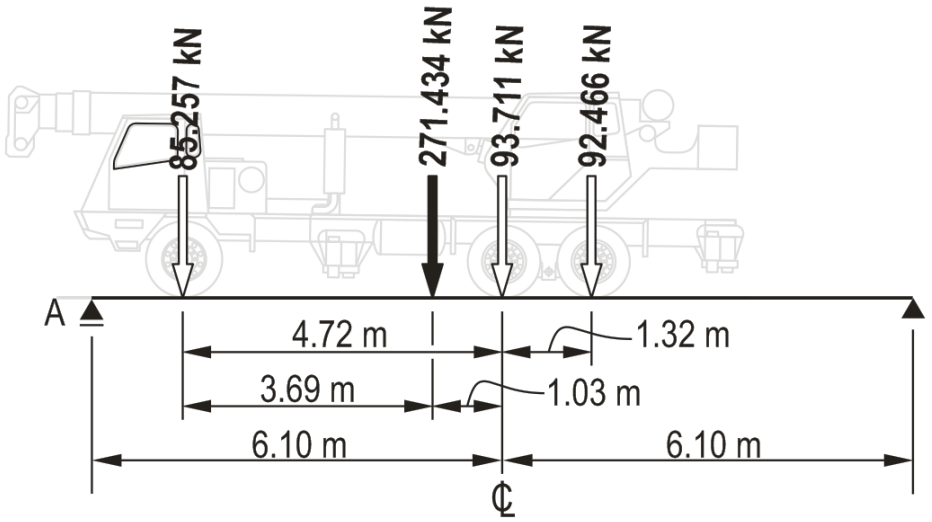

Figure 6.3. Position of the Terex crane in the No Name Creek Bridge FE model resulting in the maximum moment in the middle of the span with the resultant force shown as a black arrow

The resultant force from the vehicle configuration is

and the location of the resultant force, defined as the distance from the first axle is

The reaction at point A is then

The maximum moment in the middle of the span is then measured as

FDOT truck. For the FDOT truck – bridge system, the maximum moment in the middle of the span occurs when the fourth axle is located in the centerline of the span. The location of the FDOT truck in the FE model of the No Name Creek Bridge for the static test is presented in Figure 6.4.

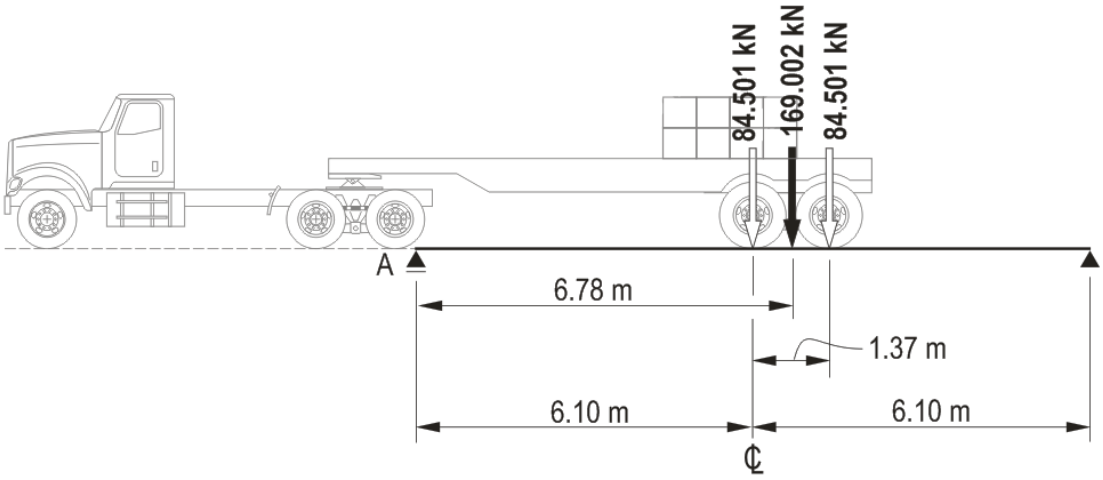

Figure 6.4. Position of the FDOT truck in the No Name Creek Bridge FE model resulting in the maximum moment in the middle of the span with the resultant force shown as a black arrow

The resultant force from the vehicle configuration is

and the location of the resultant force, defined as the distance from the point A is

The reaction at point A is then

The maximum moment in the middle of the span is then measured as

6.1.2. FE Analysis of the Tractor-Trailer

The analysis of the tractor-trailer included eleven runs with the static analysis and varying speeds with an 8 km/h (5 mph) increase between each run. Longitudinal strains in the bottom of the fourth and fifth girders for all the vehicle speeds are presented in Figure 6.5. The strains range from 52 to 67 μm/m, without a strong correlation to the vehicle speed. The fourth and fifth girders result in the highest dynamic response due to the position of the vehicle. Time histories of strain and displacements for selected speeds of 48 km/h (30 mph) and 80 km/h (50 mph) are presented in Figures 6.6 and 6.7.

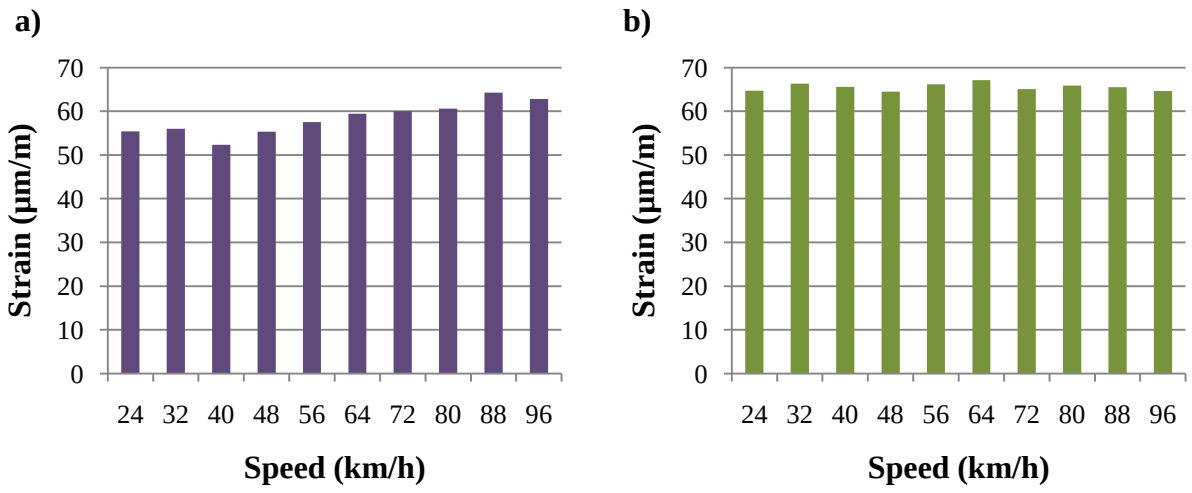

Figure 6.5. Longitudinal strains from FE analyses in the bottom of the girder for the tractor-trailer in the center of the westbound lane: a) girder #4, b) girder #5

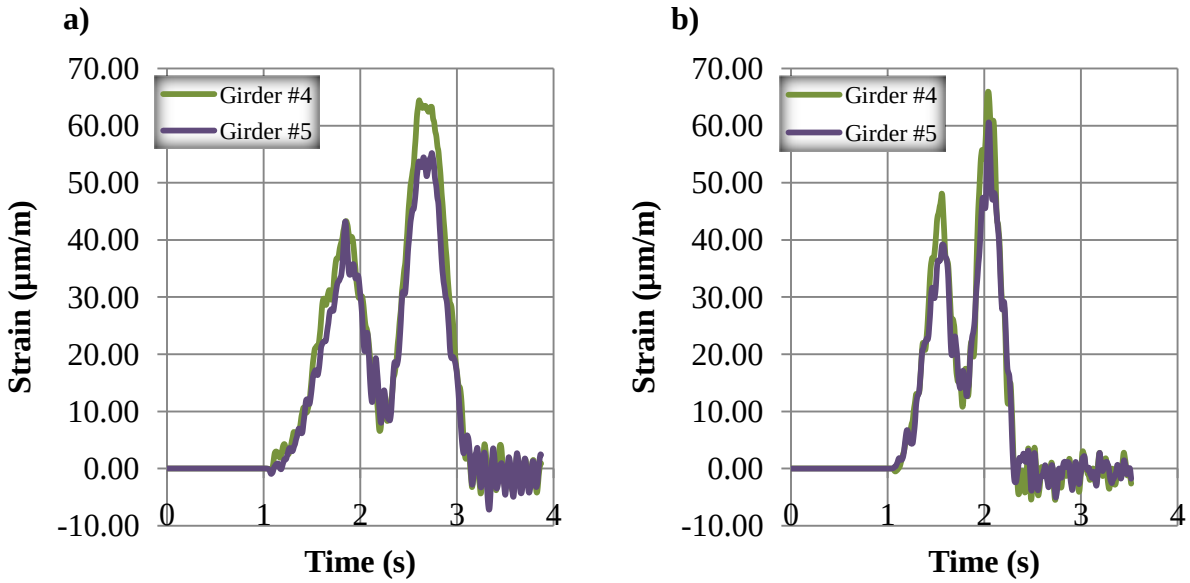

Figure 6.6. Longitudinal strain history from FE analyses at the bottom of the girders for the tractor-trailer in the center of the westbound lane at: a) 48 km/h (30 mph), b) 80 km/h (50 mph)

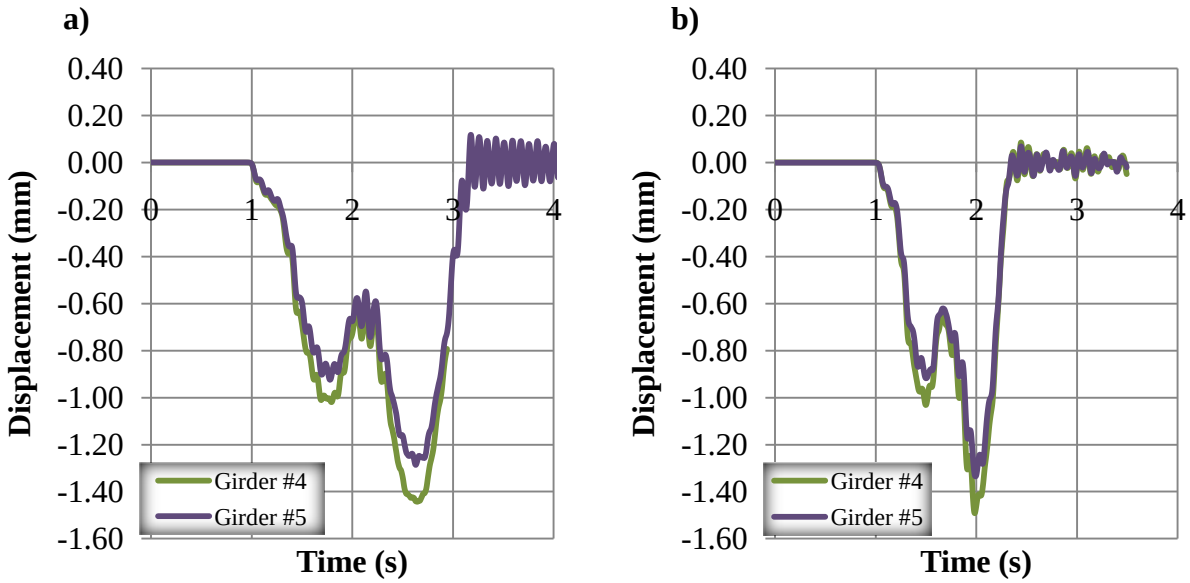

Figure 6.7. Vertical displacement from FE analyses at the bottom of the girders for the tractor-trailer in the center of the westbound lane at: a) 48 km/h (30 mph), b) 80 km/h (50 mph)

The shape of the time history of strains and displacements observed for this case is very characteristic in that it has two distinct peaks. The two peaks are a result of the long distance between the third and fourth axles of the tractor-trailer and the short length of the bridge. When the first three axles of the tractor-trailer approach the end of the bridge span, the last three axles

are just entering. This results in the relief of the load on the girders for a moment which is what differentiates this curve shape from the others.

DLA for each speed was calculated from the maximum strains on the fourth girder obtained from time histories. Maximum strains from fourth girder were critical, because they resulted in the worst case scenario due to the position of the vehicle. The results are summarized in Table 6.1 and presented in Figure 6.8 as a function of speed.

Table 6.1. DLA for tractor-trailer on No Name Creek Bridge

Speed (km/h) / (mph)	Strain (μm/m)	DLA
Static	62.9	0.00%
24 / 15	64.7	2.86%
32 / 20	66.3	5.41%
40 / 25	65.6	4.29%
48 / 30	64.5	2.54%
56 / 35	66.2	5.25%
64 / 40	67.1	6.68%
72 / 45	65.1	3.50%
80 / 50	65.9	4.77%
88 / 55	65.5	4.13%
96 / 60	64.6	2.70%

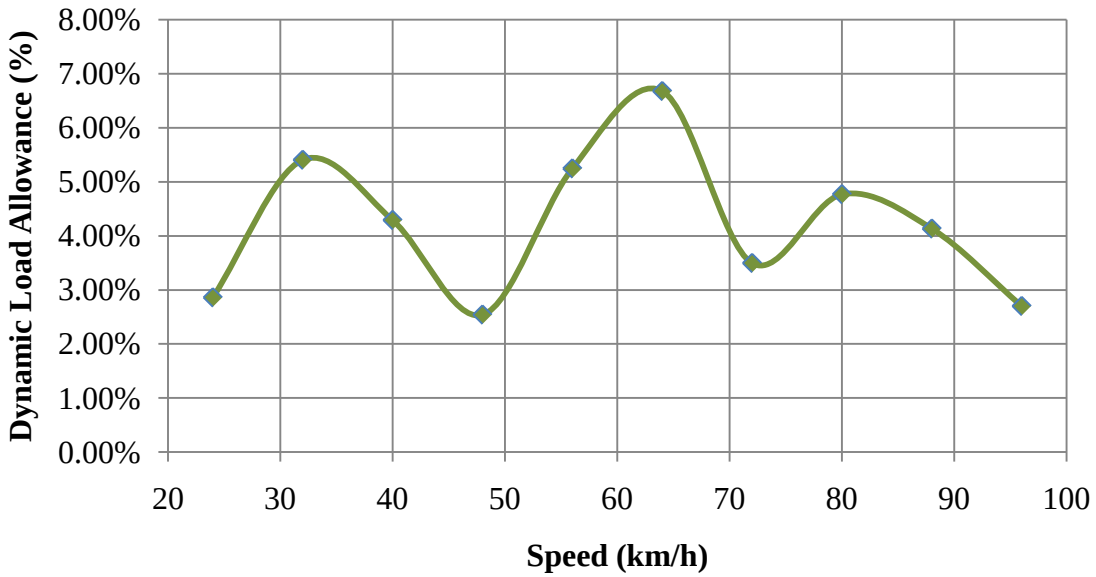

Figure 6.8. DLA vs. speed based on maximum strain on the bottom of girder #4, for the tractor-trailer in the center of the westbound lane

6.1.3. FE Analysis of the Terex Crane

The analysis was the same as for the tractor-trailer, with eleven runs including static and dynamic cases. Longitudinal strains obtained from the analysis for all the vehicle speeds are presented in Figure 6.9. The strains range from 38 to 56 μm/m, without a strong correlation to the vehicle speed. Selected time histories for the fourth and fifth girders are presented in Figures 6.10 and 6.11.

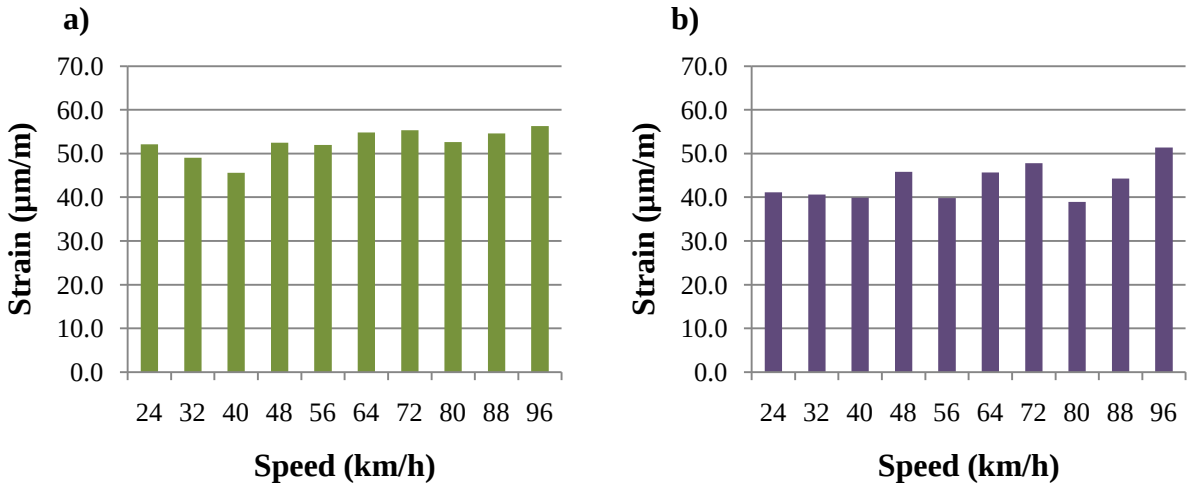

Figure 6.9. Longitudinal strains from FE analyses in the bottom of the girder for the Terex crane in the center of the westbound lane: a) girder #4, b) girder #5

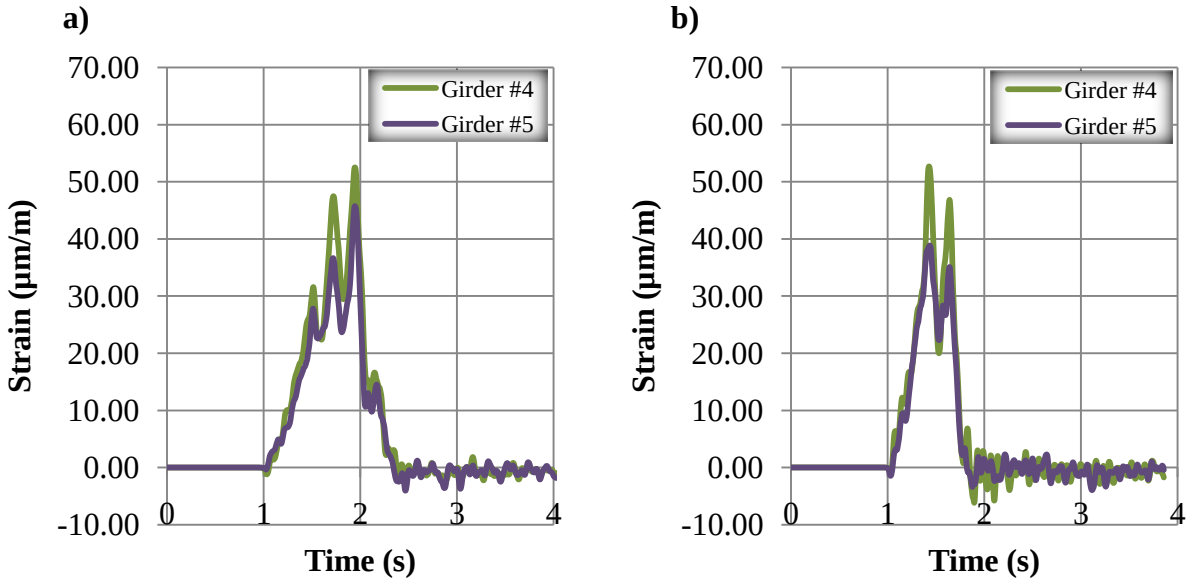

Figure 6.10. Longitudinal strain from FE analyses at the bottom of the girders for the Terex crane in the center of the westbound lane at: a) 48 km/h (30 mph), b) 80 km/h (50 mph)

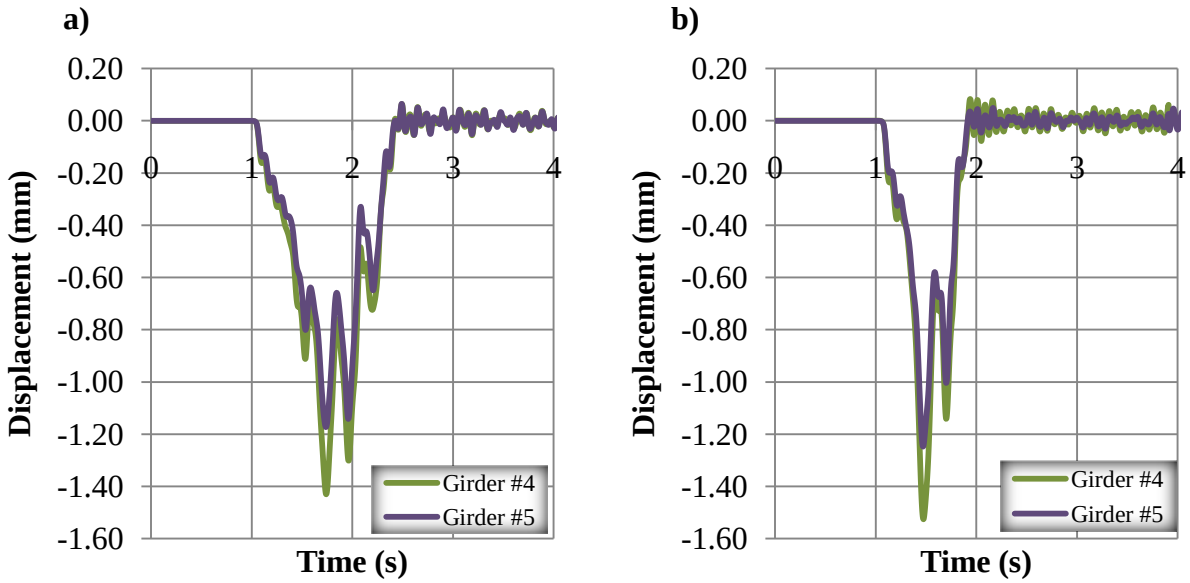

Figure 6.11. Vertical displacement from FE analyses at the bottom of the girders for the Terex crane in the center of the westbound lane at: a) 48 km/h (30 mph), b) 80 km/h (50 mph)

The results obtained from the FE analysis are characterized by higher values in the fourth girder. The strain history from the interaction of the crane and the bridge may be described with three specific peaks for the lower speed and two peaks for the faster speed, with both having a low-frequency vibration. At a lower speed, the bridge is subject to a longer forced vibration phase due to the longer time the vehicle takes to travel across the bridge, thus the higher number of peaks.

From the results of maximum strains in the fourth girder, calculation of the DLA is summarized in Table 6.2 and presented in Figure 6.12.

Table 6.2. DLA for Terex crane on No Name Creek Bridge

Speed (km/h) / (mph)	Strain (μm/m)	DLA
Static	42.1	0.00%
24 / 15	52.1	23.75%
32 / 20	49	16.39%
40 / 25	45.6	8.31%
48 / 30	52.5	24.70%
56 / 35	52	23.52%
64 / 40	54.8	30.17%
72 / 45	55.3	31.35%
80 / 50	52.6	24.94%
88 / 55	54.6	29.69%
96 / 60	56.3	33.73%

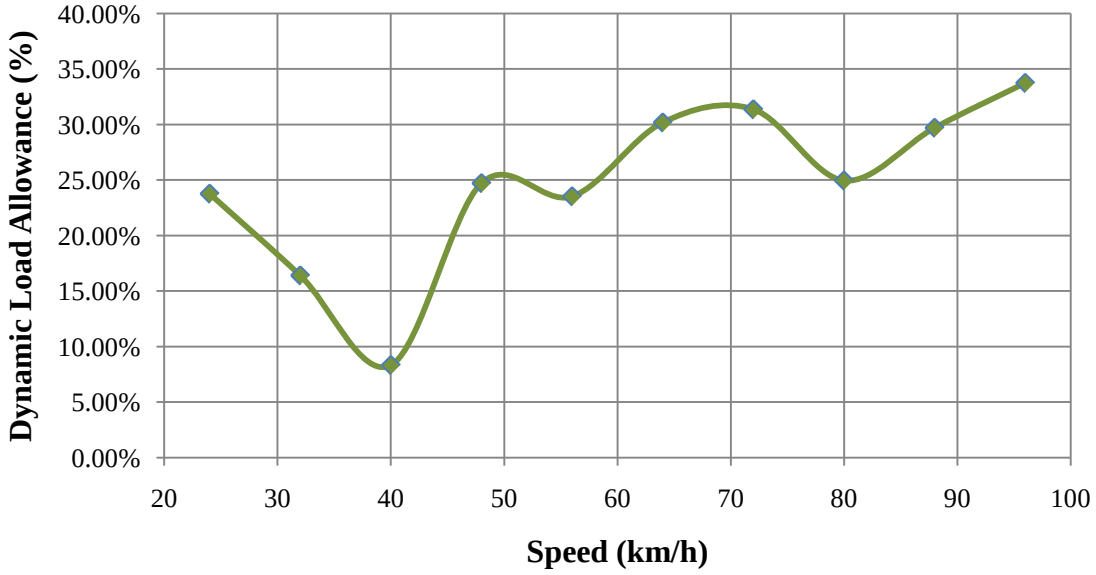

Figure 6.12. DLA vs. speed based on maximum strain on the bottom of girder #4, for the Terex crane in the center of the westbound lane

6.1.4. FE Analysis of the FDOT Truck

The analysis included eleven runs for the static and dynamic cases. Longitudinal strains obtained from the analysis for all the vehicle speeds are presented in Figure 6.13. The strains range from 32 to 51 μm/m, without a strong correlation to the vehicle speed. Selected time histories for the fourth and fifth girders are presented in Figures 6.14 and 6.15.

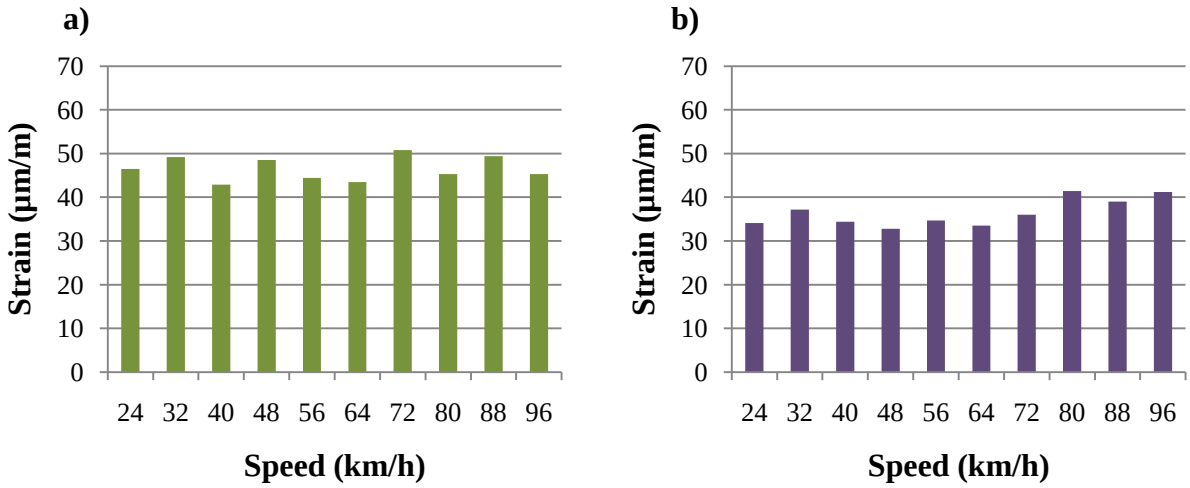

Figure 6.13. Longitudinal strains from FE analyses in the bottom of the girder for the FDOT truck in the center of the westbound lane: a) girder #4, b) girder #5

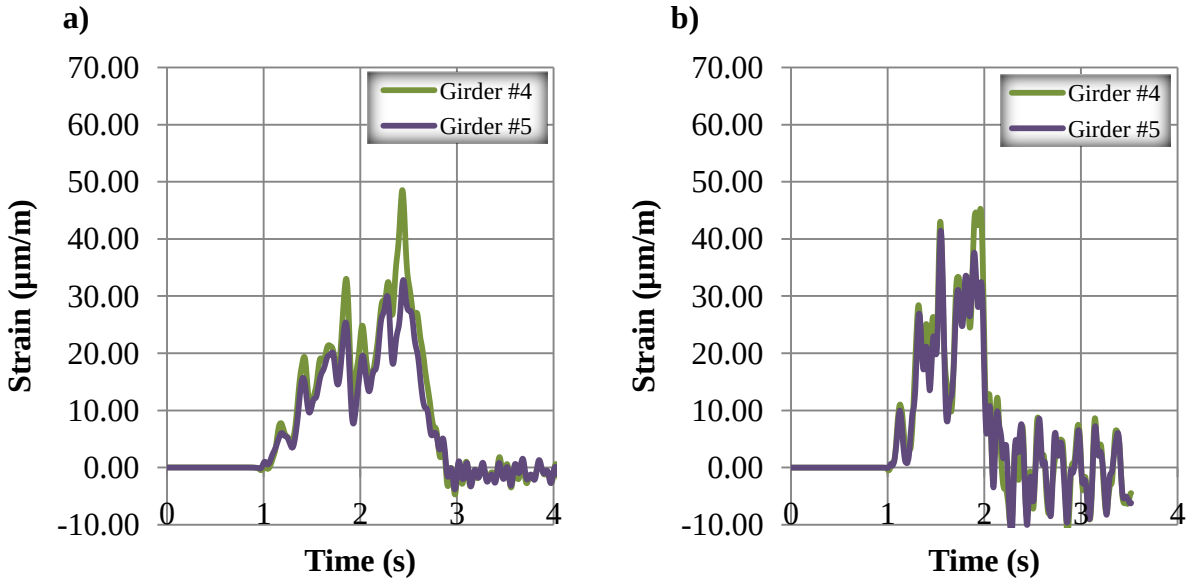

Figure 6.14. Longitudinal strain from FE analyses at the bottom of the girders for the FDOT truck in the center of the westbound lane at: a) 48 km/h (30 mph), b) 80 km/h (50 mph)

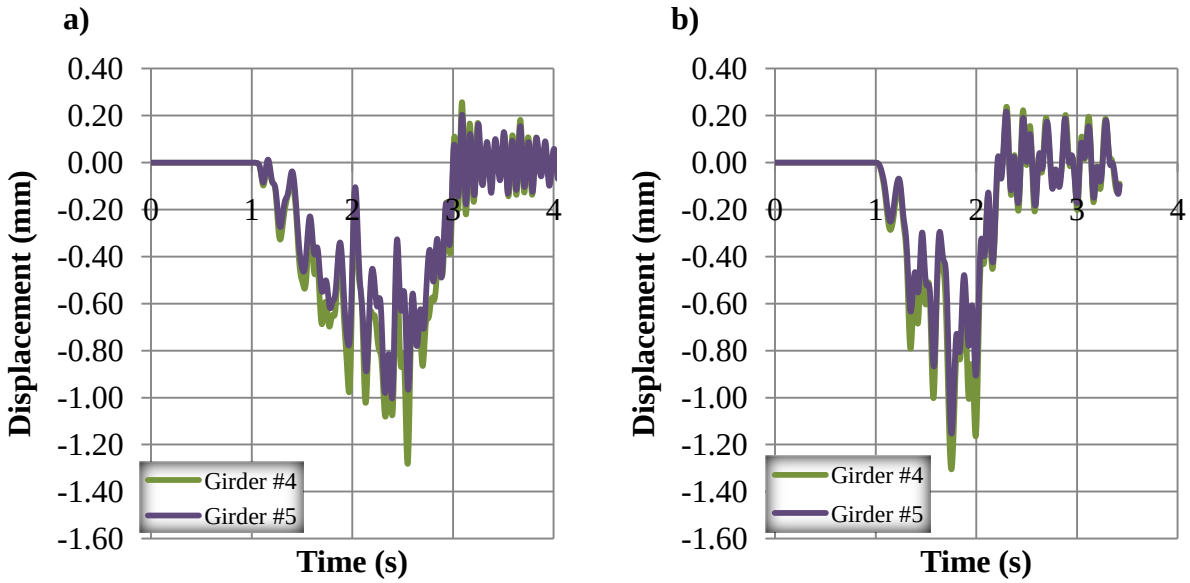

Figure 6.15. Vertical displacement from FE analyses at the bottom of the girders for the FDOT truck in the center of the westbound lane at: a) 48 km/h (30 mph), b) 80 km/h (50 mph)

The results obtained from the FE analysis are characterized by high frequency vibrations generated by the motion of the truck while driven over the bridge. The strains were higher in the fourth girder, due to the vehicle position on the analysis.

From the results of maximum strains, the calculation of the DLAs is summarized in Table 6.3 and presented in Figure 6.16 as function of speed.

Table 6.3. DLA for FDOT truck on No Name Creek Bridge

Speed (km/h) / (mph)	Strain (μm/m)	DLA
Static	39.2	0.00%
24 / 15	46.5	18.62%
32 / 20	49.2	25.51%
40 / 25	42.9	9.44%
48 / 30	48.5	23.72%
56 / 35	44.4	13.27%
64 / 40	43.5	10.97%
72 / 45	50.8	29.59%
80 / 50	45.3	15.56%
88 / 55	49.4	26.02%
96 / 60	45.3	15.56%

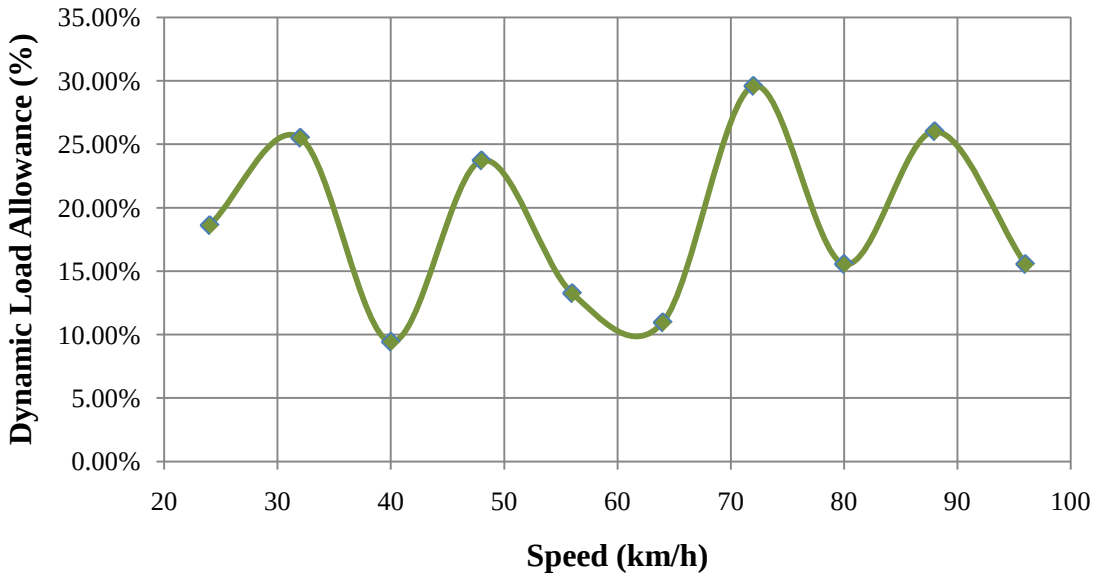

Figure 6.16. DLA vs. speed based on maximum strain on the bottom of girder #4, for the FDOT truck in the center of the westbound lane

6.2. FE Analysis of Chattahoochee Bridge (#500133)

The dynamic analysis of the FE model of the Chattahoochee Bridge follows the same methodology as for the No Name Creek, with the same amount of runs per case.

6.2.1. Longitudinal Position for Static Test

The static tests for the Chattahoochee Bridge followed the same methodology as the static tests for the No Name Creek Bridge.

Tractor-trailer. For the tractor-trailer – bridge system, the maximum moment in the middle of the span occurs when the fourth axle is located in the centerline of the span. The location of the tractor-trailer in the FE model of the Chattahoochee Bridge for the static test is presented in Figure 6.17.

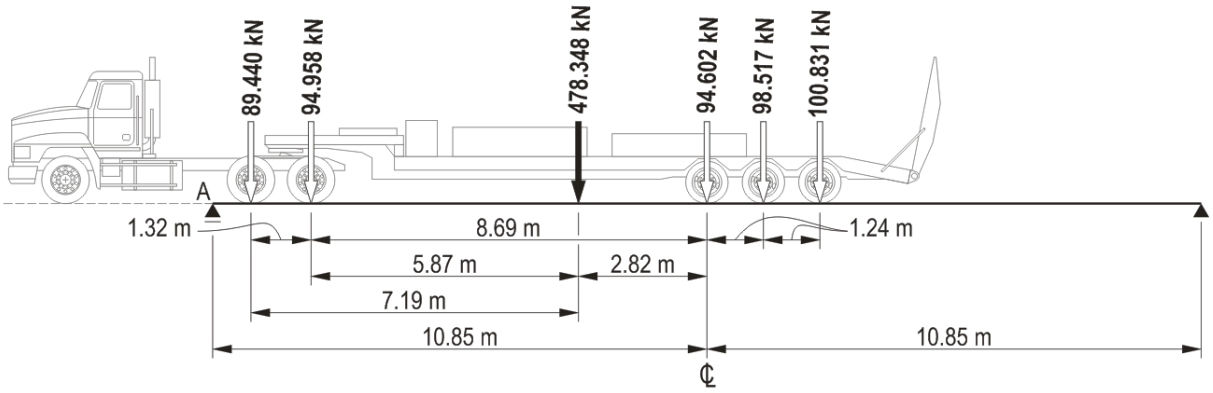

Figure 6.17. Position of the tractor-trailer in the Chattahoochee Bridge FE model resulting in the maximum moment in the middle of the span with the resultant force shown as a black arrow

The resultant force, its location and all other necessary calculations for all three vehicles followed the same methodology as the No Name Creek Bridge, and are summarized in Table 6.4.

Terex crane. For the Terex crane – bridge system, the maximum moment in the middle of the span occurs when the third axle is located in the centerline of the span. The location of the tractor-trailer in the FE model of the Chattahoochee Bridge for the static test is presented in Figure 6.18.

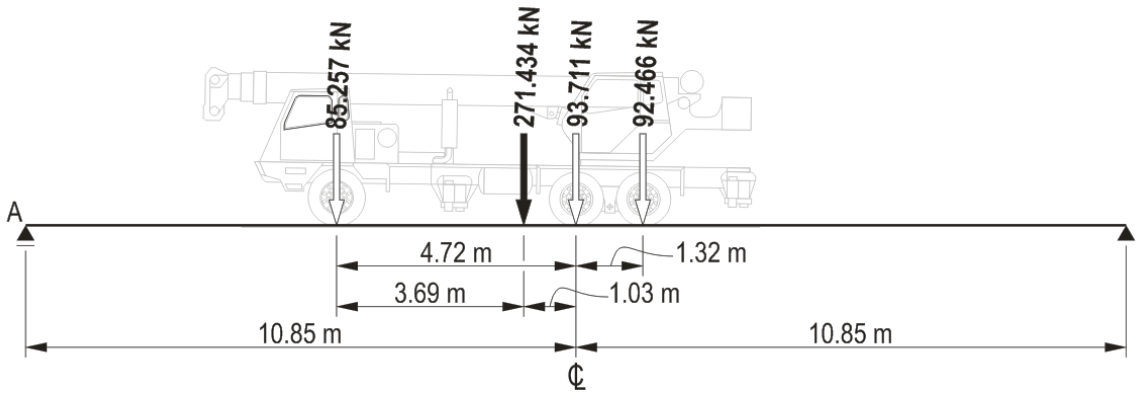

Figure 6.18. Position of the Terex crane in the Chattahoochee Bridge FE model resulting in the maximum moment in the middle of the span with the resultant force shown as a black arrow

FDOT truck. For the Terex crane – bridge system, the maximum moment in the middle of the span occurs when the third axle is located in the centerline of the span. The location of the tractor-trailer in the FE model of the Chattahoochee Bridge for the static test is presented in Figure 6.19.

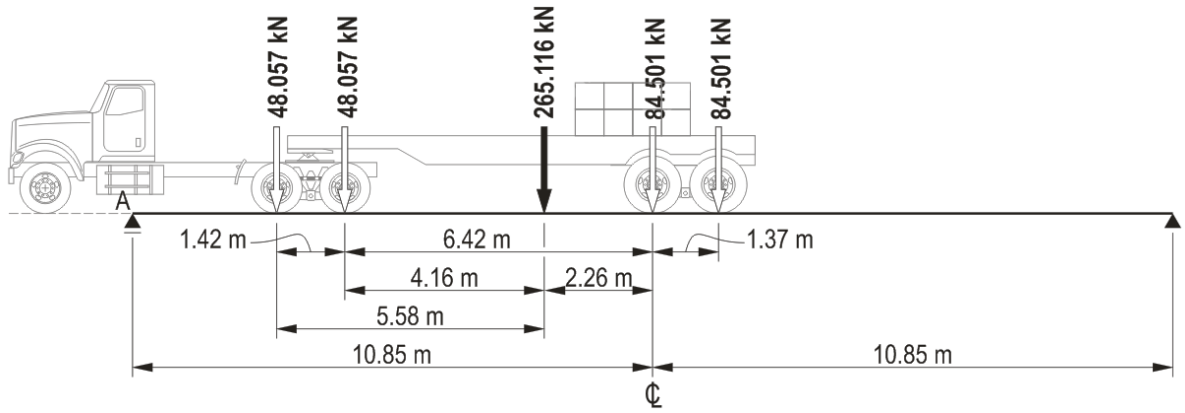

Figure 6.19. Position of the FDOT truck in the Chattahoochee Bridge FE model resulting in the maximum moment in the middle of the span with the resultant force shown as a black arrow

Table 6.4. Static position results on Chattahoochee Bridge

Vehicle	Resultant Force, FR (kN / Kips)	FR defined from axle	Distance to FR from axle (m / ft)	Reaction, Ay (kN / Kips)	Moment (kN·m / Kips·ft)
Tractor-trailer	478.35 / 107.54	3rd	5.87 / 19.26	301.34 / 67.74	1549.03 / 1142.51
Terex crane	271.43 / 61.02	1st	3.69 / 12.11	148.60 / 33.41	1209.91 / 892.38
FDOT truck	265.12 / 59.60	2nd	5.58 / 18.31	160.17 / 36.01	1052.54 / 776.31

6.2.2. FE Analysis of the Tractor-Trailer

Longitudinal strains were obtained from the analysis for all the vehicle speeds and are summarized in Figure 6.20. The strains range from 63 to 69 μm/m, without a good correlation to the vehicle speed. The range of the strains is very small compared to other cases. Selected time histories for the fourth and fifth girders are presented in Figures 6.21 and 6.22.

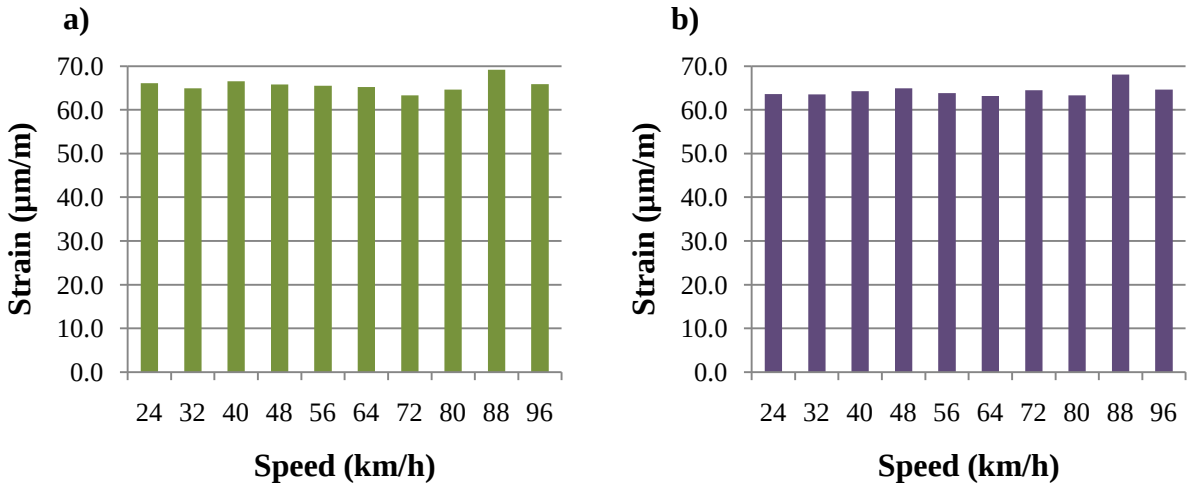

Figure 6.20. Longitudinal strains from FE analyses in the bottom of the girder for the tractor-trailer in the center of the westbound lane: a) girder #4, b) girder #5

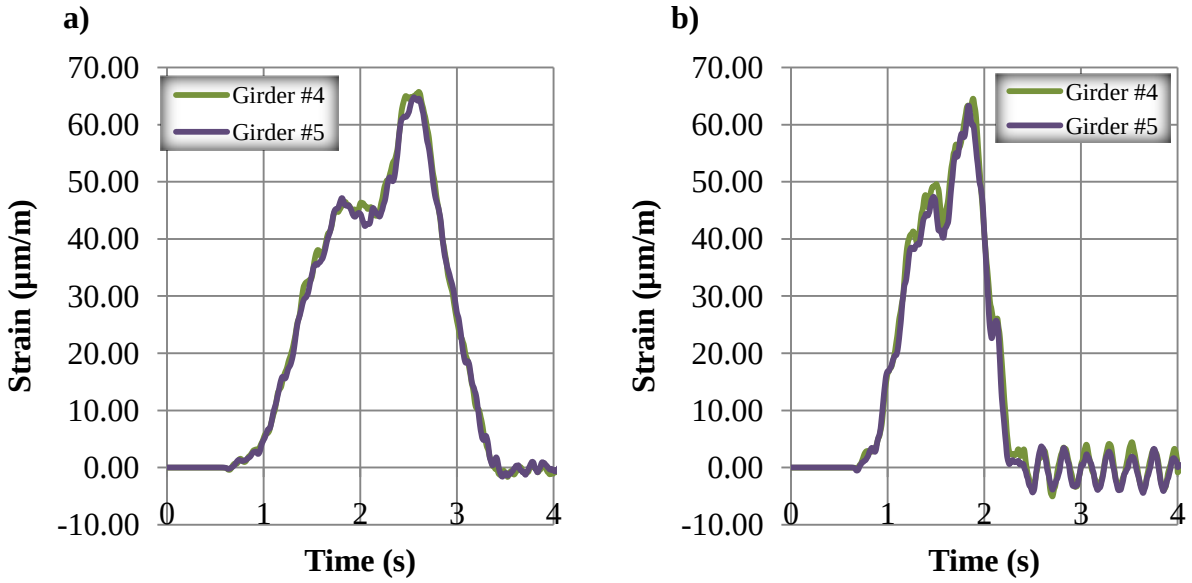

Figure 6.21. Longitudinal strain from FE analyses at the bottom of the girders for the tractor-trailer in the center of the westbound lane at: a) 48 km/h (30 mph), b) 80 km/h (50 mph)

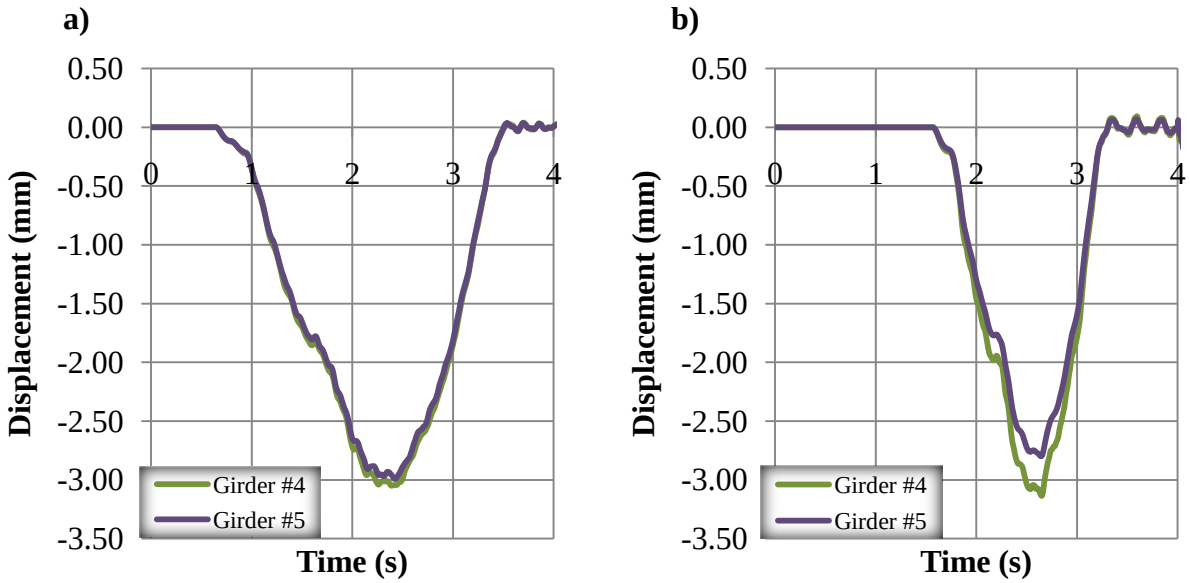

Figure 6.22. Vertical displacement from FE analyses at the bottom of the girders for the tractor-trailer in the center of the westbound lane at: a) 48 km/h (30 mph), b) 80 km/h (50 mph)

The results obtained from the FE analysis are described mainly by a low frequency response of the bridge to the interaction with the tractor-trailer. The strains and displacements were very similar in both the fourth and fifth girder, but once again were higher in the fourth girder due to the vehicle position on the analysis.

Calculation of the DLAs is summarized in Table 6.5 and presented in Figure 6.23 as function of speed.

Table 6.5. DLA for tractor-trailer on Chattahoochee Bridge

Speed (km/h) / (mph)	Strain (μm/m)	DLA
Static	60.59	0.00%
24 / 15	66.1	9.09%
32 / 20	64.9	7.11%
40 / 25	66.5	9.75%
48 / 30	65.8	8.60%
56 / 35	65.5	8.10%
64 / 40	65.2	7.61%
72 / 45	63.3	4.47%
80 / 50	64.6	6.62%
88 / 55	69.2	14.21%
96 / 60	65.9	8.76%

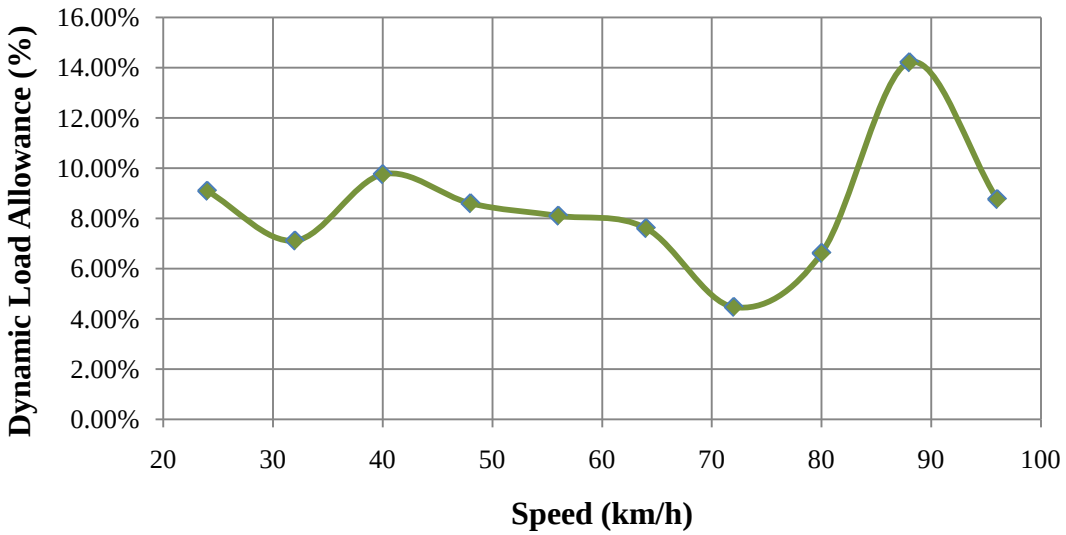

Figure 6.23. DLA vs. speed based on maximum strain on the bottom of girder #4, for the tractor-trailer in the center of the westbound lane

6.2.3. FE Analysis of the Terex Crane

The analysis included all the eleven runs as for the other cases. Longitudinal strains obtained from the analysis for all the vehicle speeds are summarized in Figure 6.24. The strains range from 48 to 66 μm/m, without a good correlation to the vehicle speed. Selected time histories for the fourth and fifth girders are also presented in Figures 6.25 and 6.26.

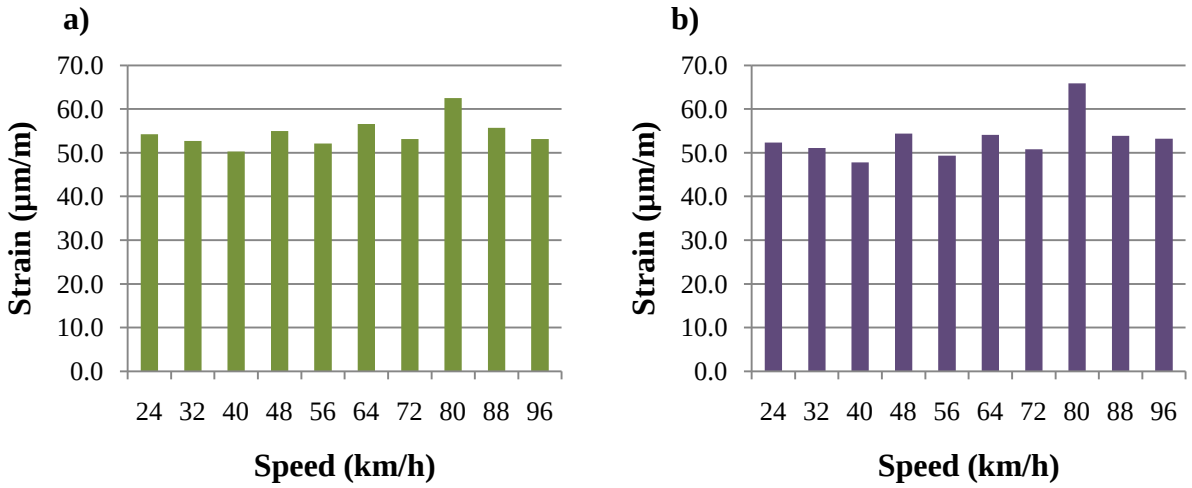

Figure 6.24. Longitudinal strains from FE analyses in the bottom of the girder for the Terex crane in the center of the westbound lane: a) girder #4, b) girder #5

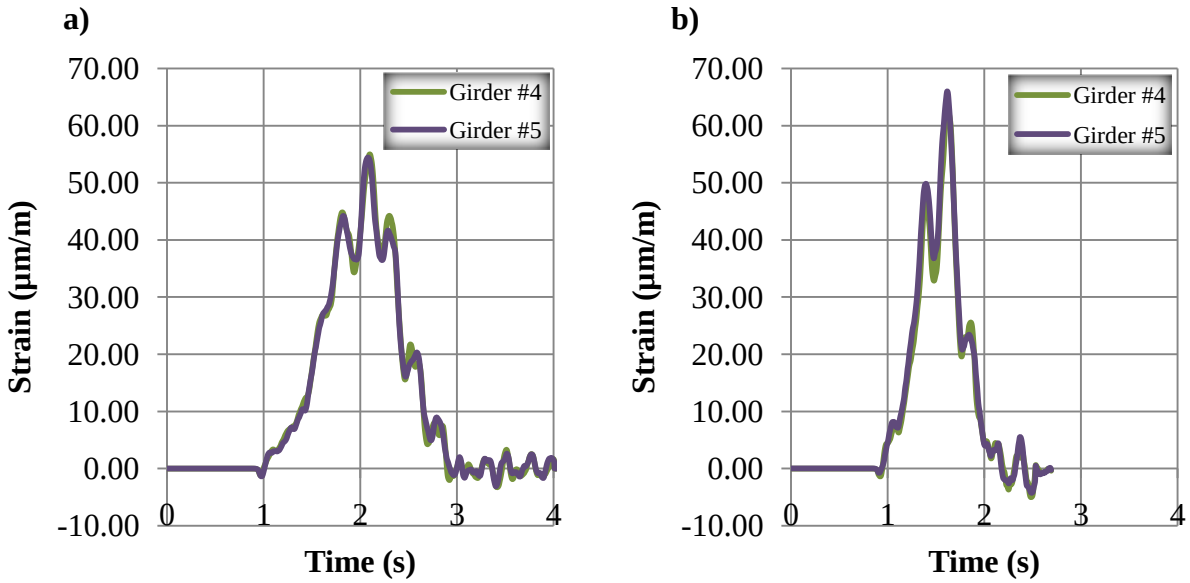

Figure 6.25. Longitudinal strain from FE analyses at the bottom of the girders for the Terex crane in the center of the westbound lane at: a) 48 km/h (30 mph), b) 80 km/h (50 mph)

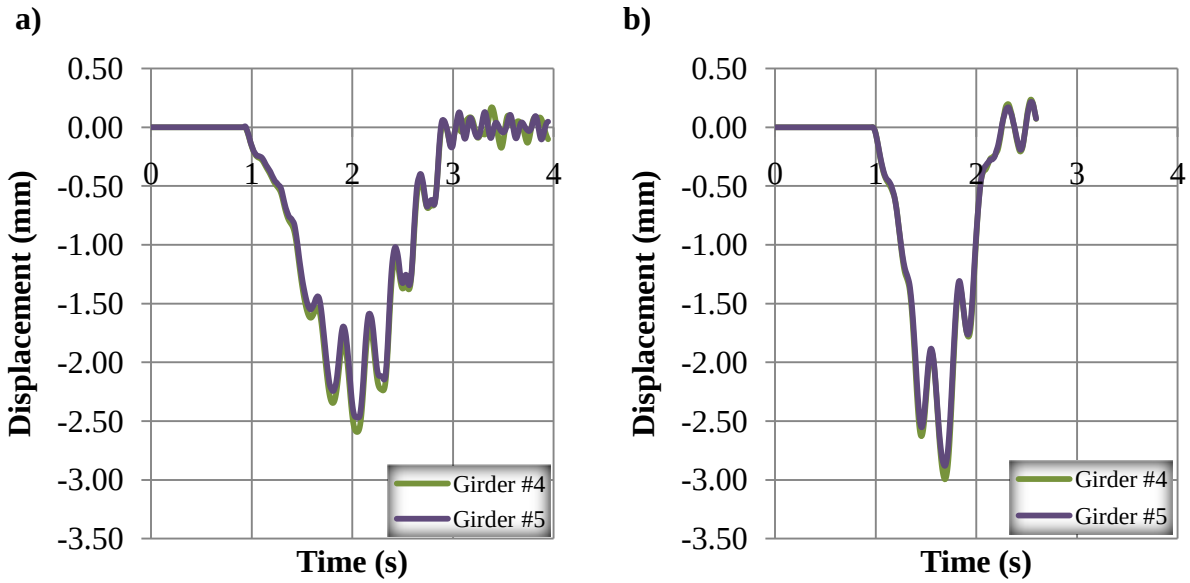

Figure 6.26. Vertical displacement from FE analyses at the bottom of the girders for the Terex crane in the center of the westbound lane at: a) 48 km/h (30 mph), b) 80 km/h (50 mph)

There is a high level of conformity between the time histories of the two girders, even more than for the other vehicles which might be due to the compact setup of the crane. The

interaction is described with low frequency vibrations. DLA calculations are summarized in Table 6.6 and presented in Figure 6.27 as a function of speed.

Table 6.6. DLA for Terex crane on Chattahoochee Bridge

Speed (km/h) / (mph)	Strain (μm/m)	DLA
Static	47.1	0.00%
24 / 15	54.2	15.07%
32 / 20	52.7	11.89%
40 / 25	50.3	6.79%
48 / 30	55	16.77%
56 / 35	52.1	10.62%
64 / 40	56.6	20.17%
72 / 45	53.1	12.74%
80 / 50	62.5	32.70%
88 / 55	55.7	18.26%
96 / 60	53.1	12.74%

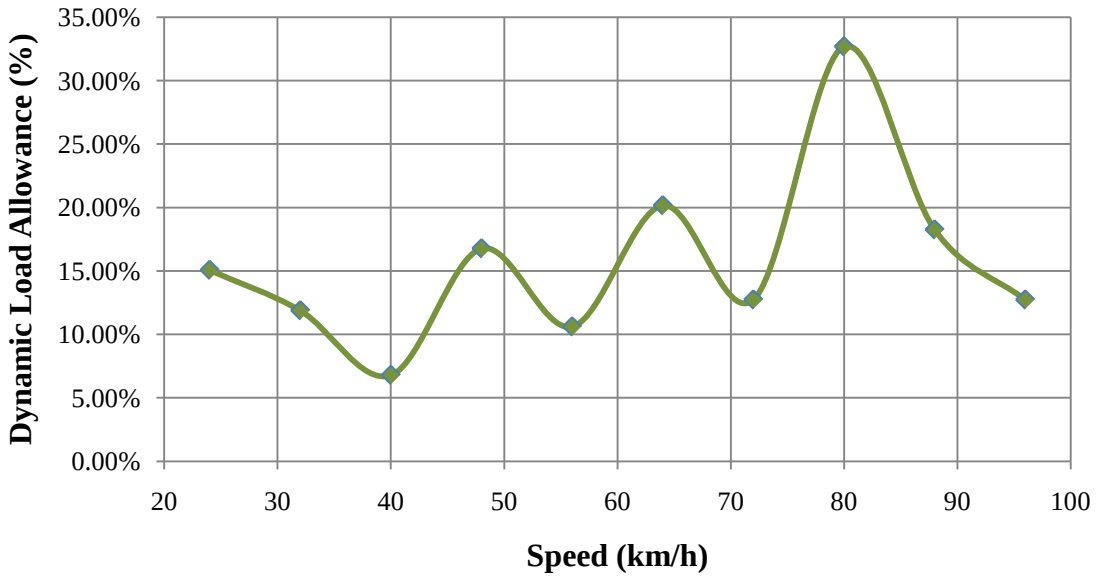

Figure 6.27. DLA vs. speed based on maximum strain on the bottom of girder #4, for the Terex crane in the center of the westbound lane

6.2.4. FE Analysis of the FDOT Truck

Longitudinal strains obtained from the analysis for all the vehicle speeds are presented in Figure 6.28. The strains do not show a strong correlation to the vehicle speed, and they range from 44 to 58 μm/m. Selected time histories for the fourth and fifth girders are also presented in Figures 6.29 and 6.30.

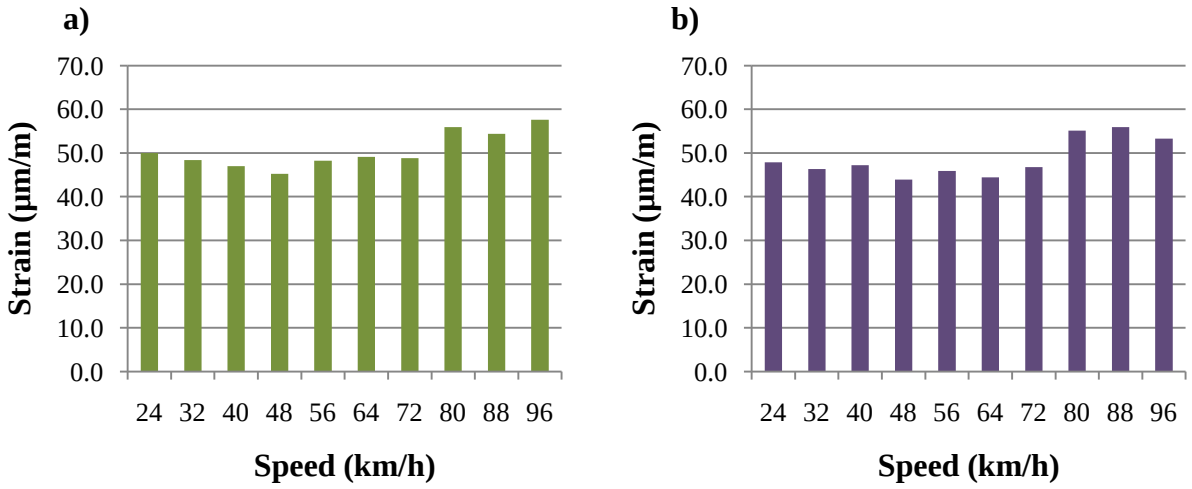

Figure 6.28. Longitudinal strains from FE analyses in the bottom of the girder for the FDOT truck in the center of the westbound lane: a) girder #4, b) girder #5

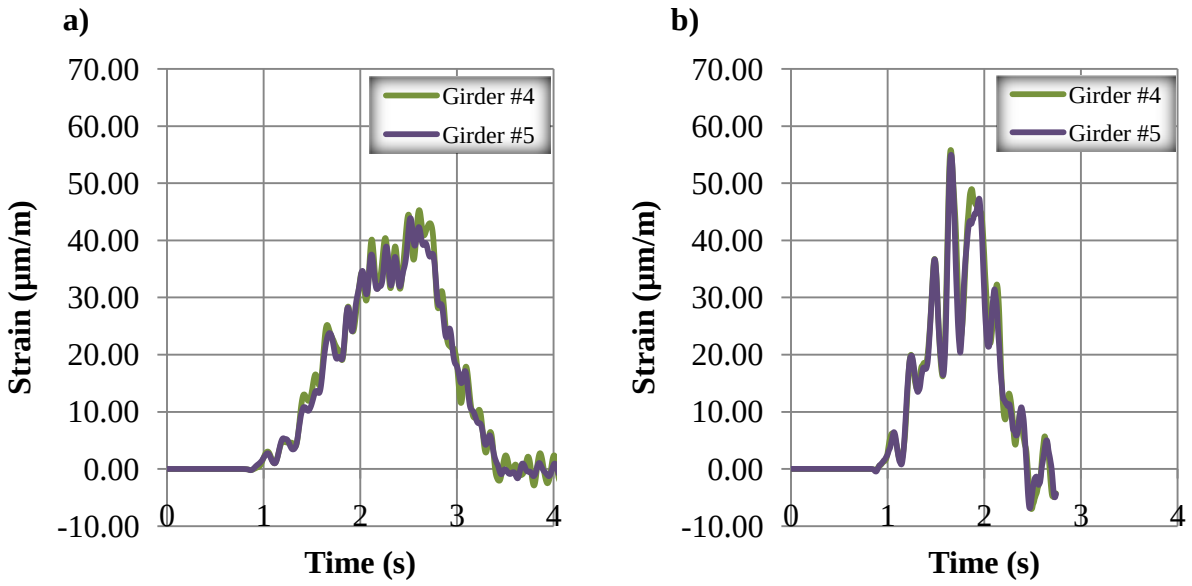

Figure 6.29. Longitudinal strain from FE analyses at the bottom of the girders for the FDOT truck in the center of the westbound lane at: a) 48 km/h (30 mph), b) 80 km/h (50 mph)

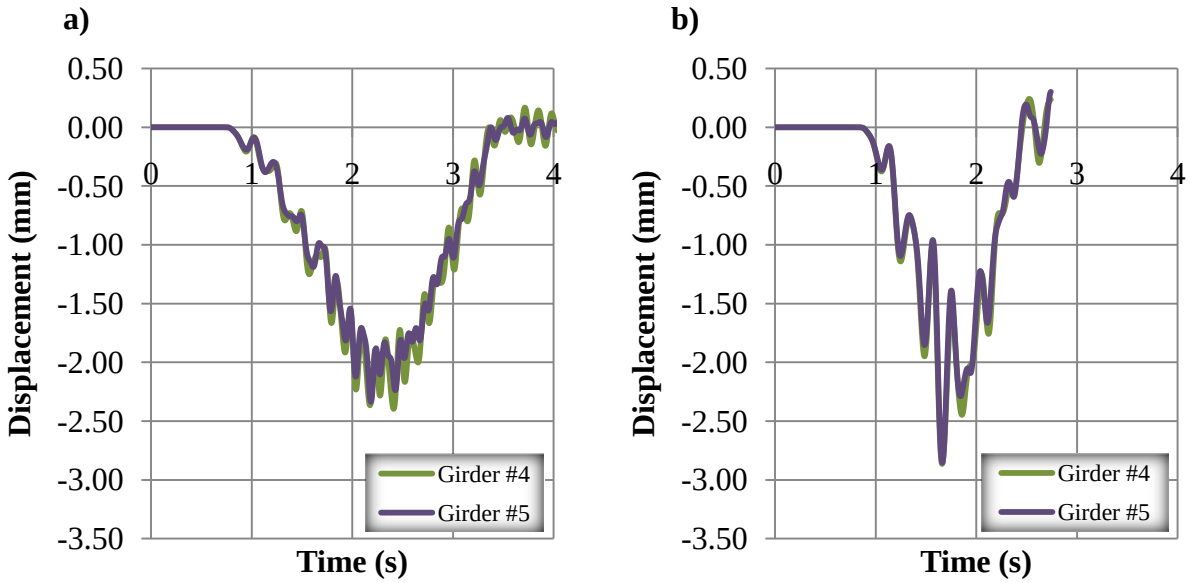

Figure 6.30. Vertical displacement from FE analyses at the bottom of the girders for the FDOT truck in the center of the westbound lane at: a) 48 km/h (30 mph), b) 80 km/h (50 mph)

From analysis of the three vehicles the FDOT truck induces the lowest strains and displacements on the bridge girders. The interaction may be described by the high frequency vibrations induced in the bridge girders. Calculations of DLAs are summarized in Table 6.7 and presented in Figure 6.31 as a function of speed.

Table 6.7. DLA for FDOT truck on Chattahoochee Bridge

Speed (km/h) / (mph)	Strain (μm/m)	DLA
Static	41.3	0.00%
24 / 15	50	21.07%
32 / 20	48.4	17.19%
40 / 25	47	13.80%
48 / 30	45.2	9.44%
56 / 35	48.2	16.71%
64 / 40	49.1	18.89%
72 / 45	48.8	18.16%
80 / 50	55.9	35.35%
88 / 55	54.4	31.72%
96 / 60	57.6	39.47%

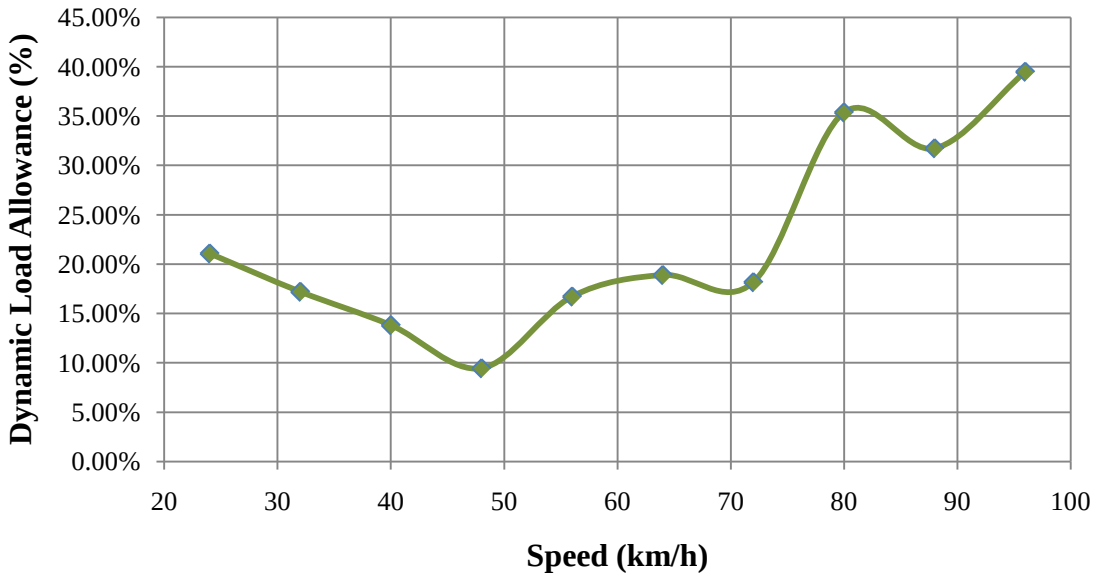

Figure 6.31. DLA vs. speed based on maximum strain on the bottom of girder #4, for the FDOT truck in the center of the westbound lane

6.3. FE Analysis of St. Mark's Bridge (#590056)

The dynamic analysis of the FE model of the St. Mark's follows the same methodology as for the No Name Creek, with the same amount of runs per case.

6.3.1. Longitudinal Position for Static Test

The static tests for the St. Mark's Bridge followed the same methodology as the static tests for the No Name Creek Bridge. The vehicle position is described below for the static tests.

Tractor-trailer. For the tractor-trailer – bridge system, the maximum moment in the middle of the span occurs when the fourth axle is located in the centerline of the span. The location of the tractor-trailer in the FE model of the St. Mark's Bridge for the static test is presented in Figure 6.32.

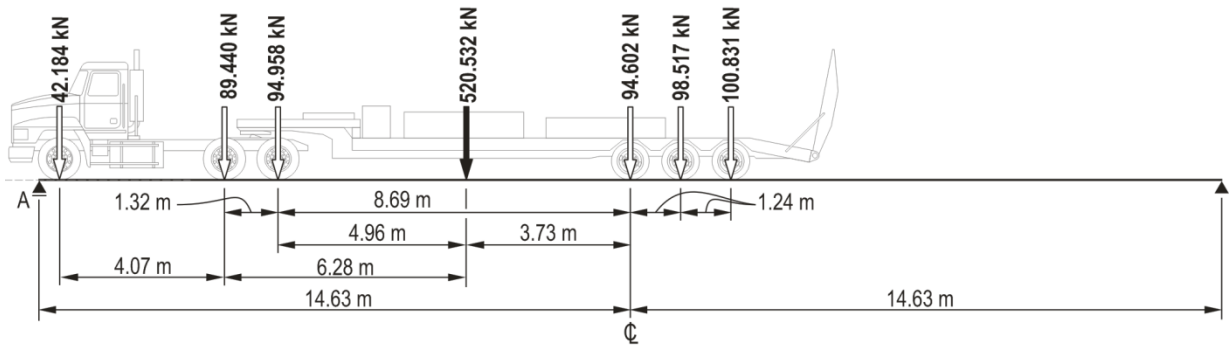

Figure 6.32. Position of the tractor-trailer in the St. Mark's Bridge FE model resulting in the maximum moment in the middle of the span with the resultant force shown as a black arrow

The resultant force, its location and all other necessary calculations for all three vehicles followed the same methodology as the No Name Creek Bridge, and are summarized in Table 6.8.

Terex crane. For the Terex crane – bridge system, the maximum moment in the middle of the span occurs when the third axle is located in the centerline of the span. The location of the tractor-trailer in the FE model of the St. Mark's Bridge for the static test is presented in Figure 6.33.

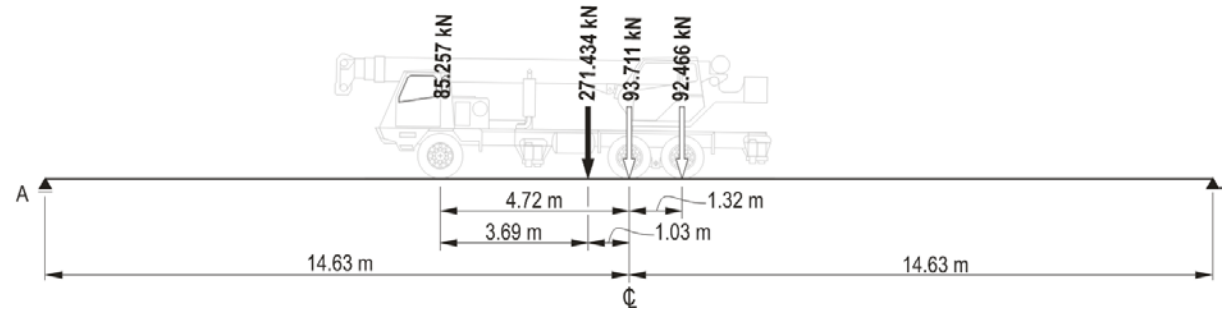

Figure 6.33. Position of the Terex crane in the St. Mark's Bridge FE model resulting in the maximum moment in the middle of the span with the resultant force shown as a black arrow

FDOT truck. For the Terex crane – bridge system, the maximum moment in the middle of the span occurs when the fourth axle is located in the centerline of the span. The location of the tractor-trailer in the FE model of the St. Mark's Bridge for the static test is presented in Figure 6.34.

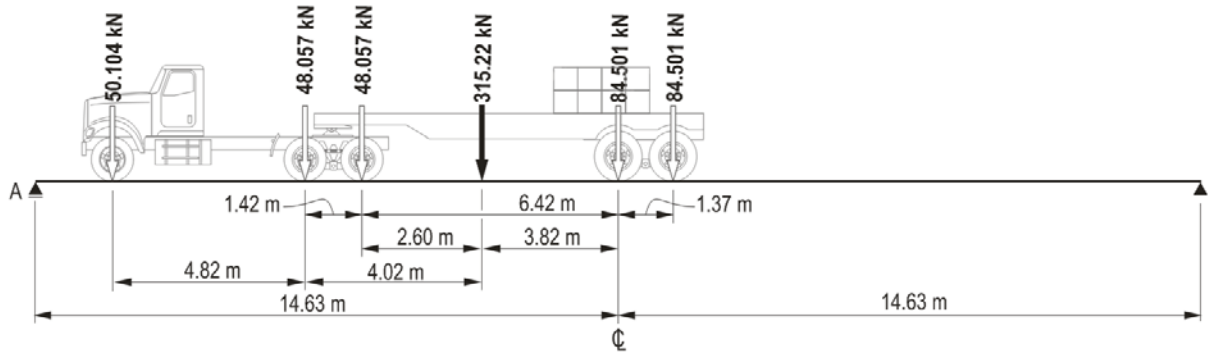

Figure 6.34. Position of the FDOT truck in the St. Mark's Bridge FE model resulting in the maximum moment in the middle of the span with the resultant force shown as a black arrow

Table 6.8. Static position results on St. Mark's Bridge

Vehicle	Resultant Force, FR (kN / Kips)	FR defined from axle	Distance to FR from axle (m / ft)	Reaction, Ay (kN / Kips)	Moment (kN·m / Kips·ft)
Tractor-trailer	520.53 / 117.02	3rd	4.96 / 16.27	326.62 / 73.43	2464.05 / 1817.39
Terex crane	271.43 / 61.02	1st	3.69 / 12.11	145.27 / 32.66	1722.92 / 1270.76
FDOT truck	315.22 / 70.86	3rd	2.60 / 8.53	198.76 / 44.68	1588.30 / 1171.47

6.3.2. FE Analysis of the Tractor-Trailer

Longitudinal strains obtained from the analysis for all the vehicle speeds are summarized in Figure 6.35. Strain values have a small range from 55 to 58 μm/m but they do not show a strong correlation to vehicle speed. Selected time histories for the fourth and fifth girders are presented in Figures 6.36 and 6.37.

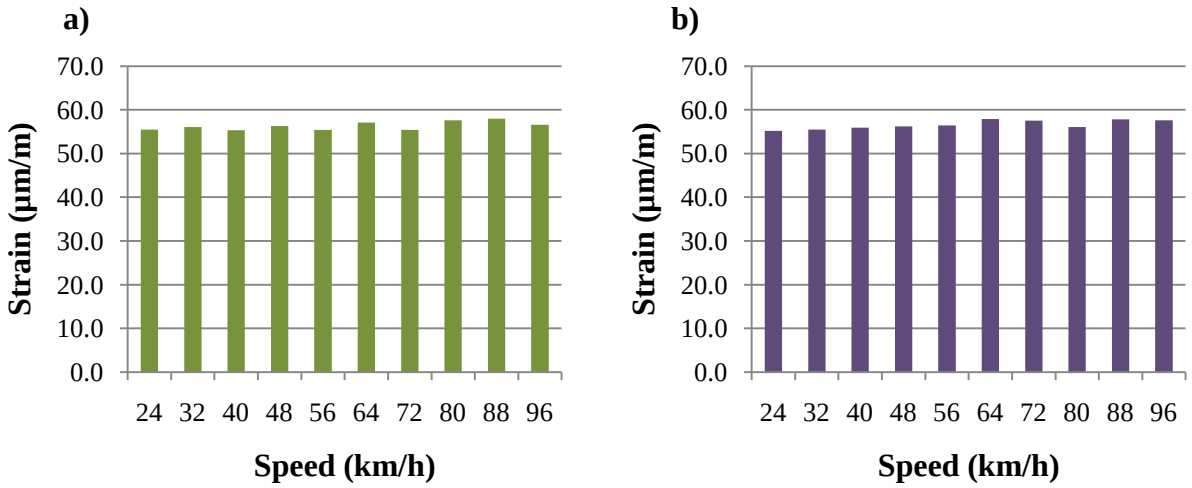

Figure 6.35. Longitudinal strains from FE analyses in the bottom of the girder for the tractor-trailer in the center of the westbound lane: a) girder #4, b) girder #5

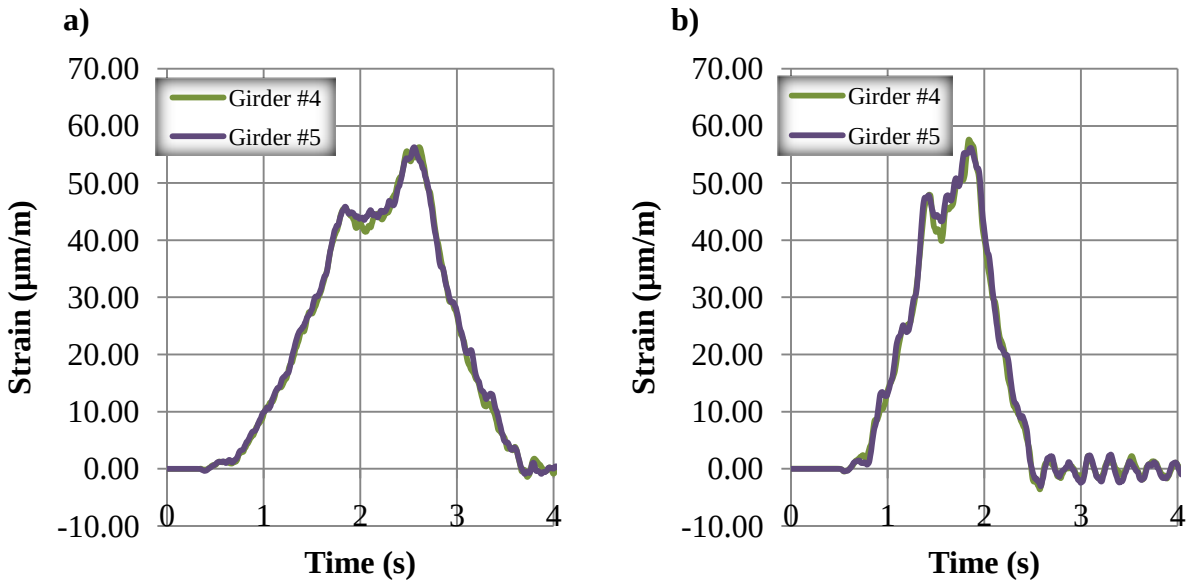

Figure 6.36. Longitudinal strain from FE analyses at the bottom of the girders for the tractor-trailer in the center of the westbound lane at: a) 48 km/h (30 mph), b) 80 km/h (50 mph)

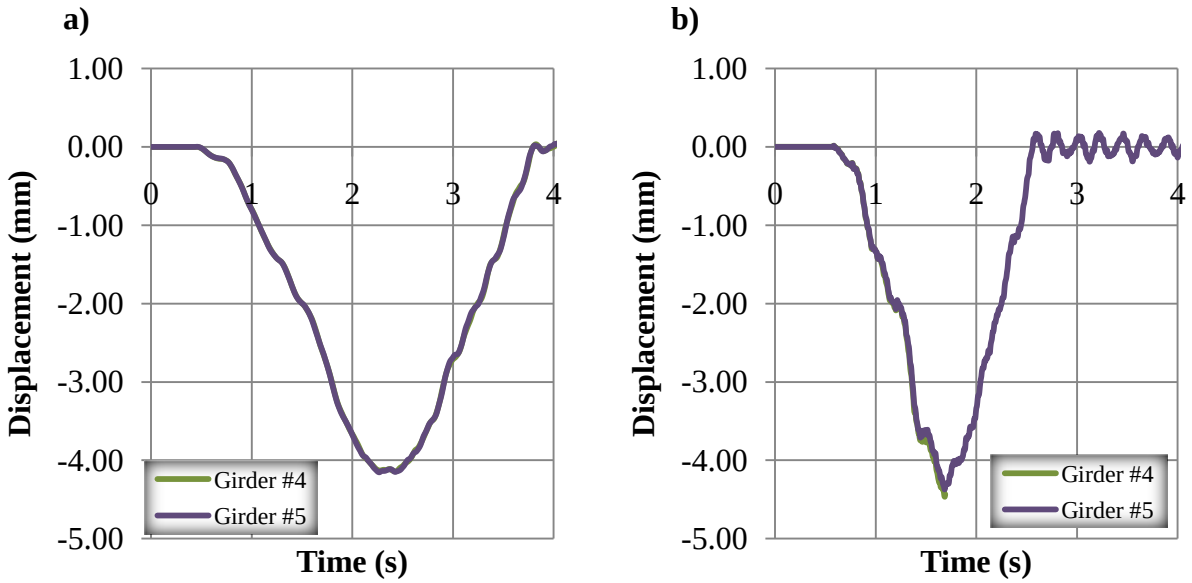

Figure 6.37. Vertical displacement from FE analyses at the bottom of the girders for the tractor-trailer in the center of the westbound lane at: a) 48 km/h (30 mph), b) 80 km/h (50 mph)

Time histories for the FE analysis, is described with low frequency vibrations. Calculation of the DLAs is summarized in Table 6.9 and presented in Figure 6.38 as function of speed.

Table 6.9. DLA for tractor-trailer on St. Mark's Bridge

Speed (km/h) / (mph)	Strain (μm/m)	DLA
Static	54.1	0.00%
24 / 15	55.5	2.59%
32 / 20	56.1	3.70%
40 / 25	55.3	2.22%
48 / 30	56.3	4.07%
56 / 35	55.4	2.40%
64 / 40	57.1	5.55%
72 / 45	55.4	2.40%
80 / 50	57.6	6.47%
88 / 55	58	7.21%
96 / 60	56.6	4.62%

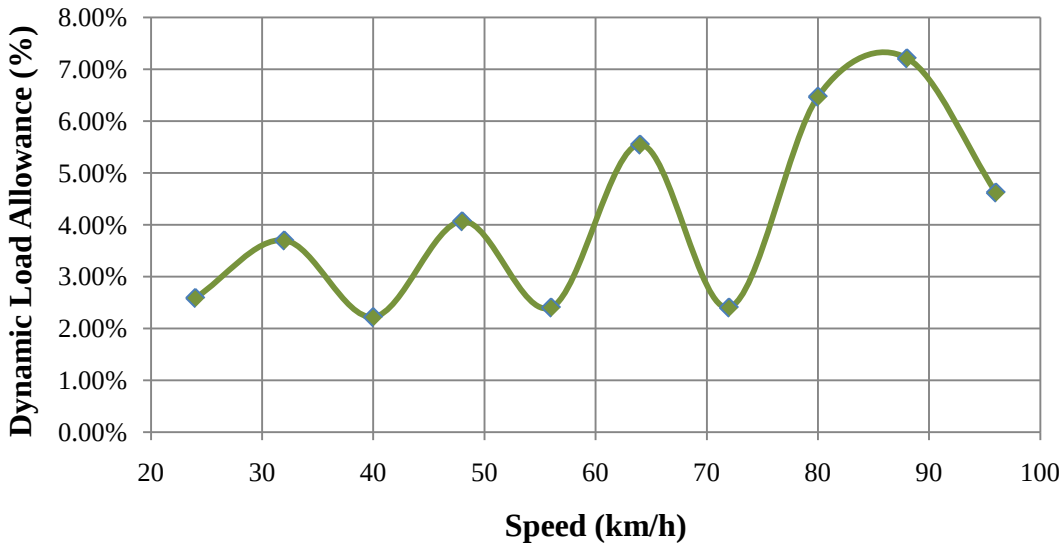

Figure 6.38. DLA vs. speed based on maximum strain on the bottom of girder #4, for the tractor-trailer in the center of the westbound lane

6.3.3. FE Analysis of the Terex Crane

Longitudinal strains obtained from the analysis for all the vehicle speeds are summarized in Figure 6.39. Strain values range from 41 to 54 μm/m but they do not show a strong correlation to vehicle speed. Selected time histories for the fourth and fifth girders are presented in Figures 6.40 and 6.41.

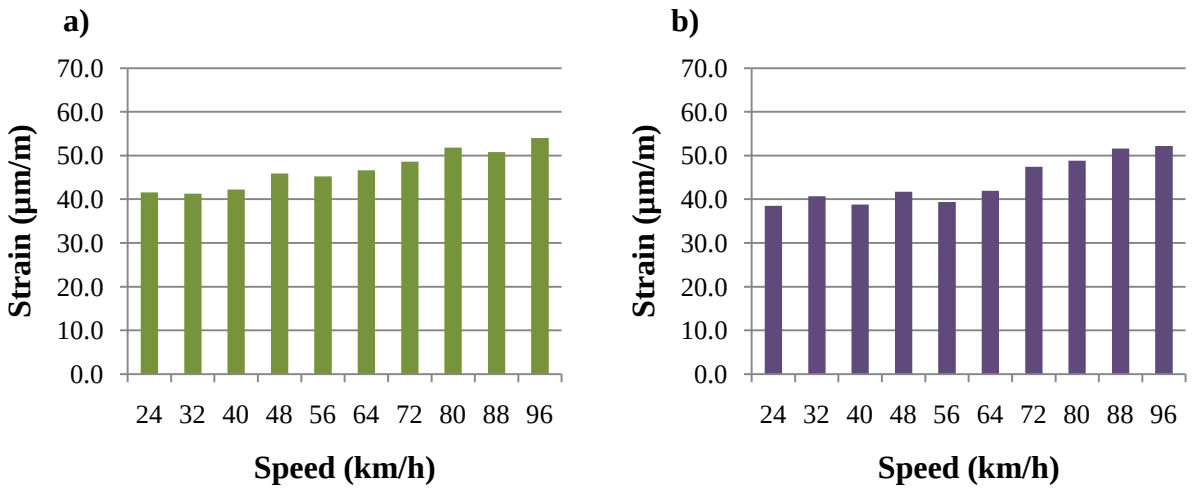

Figure 6.39. Longitudinal strains from FE analyses in the bottom of the girder for the Terex crane in the center of the westbound lane: a) girder #4, b) girder #5

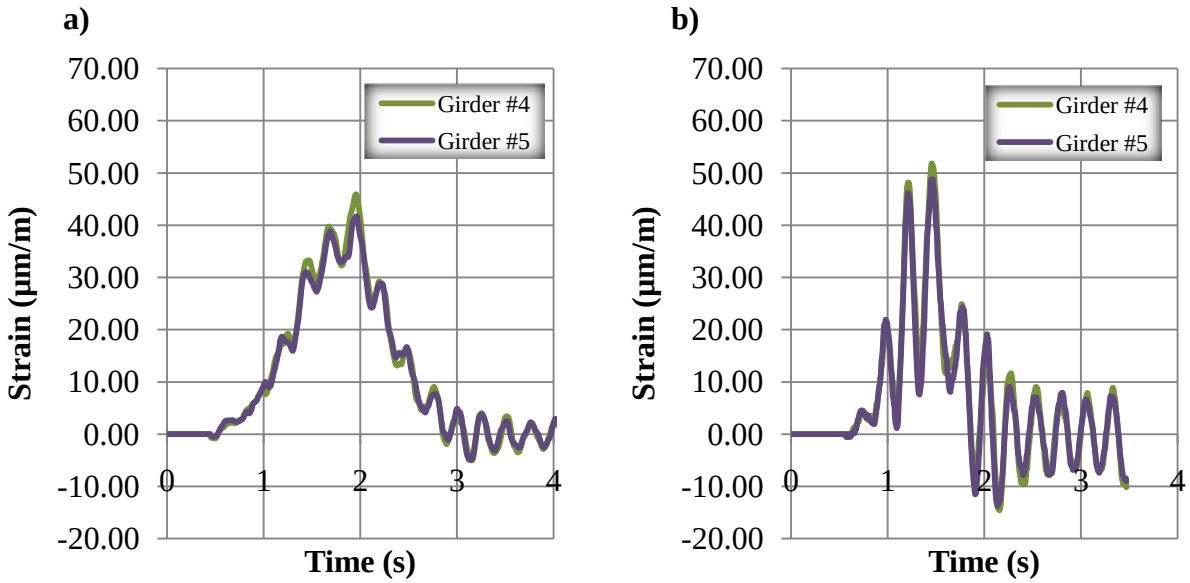

Figure 6.40. Longitudinal strain from FE analyses at the bottom of the girders for the Terex crane in the center of the westbound lane at: a) 48 km/h (30 mph), b) 80 km/h (50 mph)

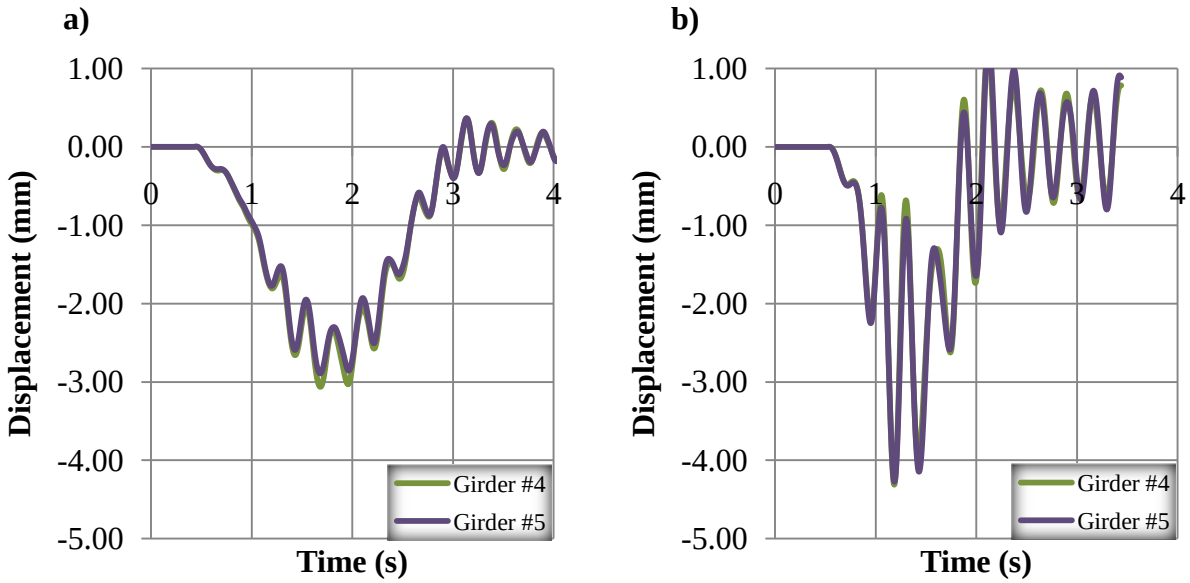

Figure 6.41. Vertical displacement from FE analyses at the bottom of the girders for the Terex crane in the center of the westbound lane at: a) 48 km/h (30 mph), b) 80 km/h (50 mph)

The time histories for the FE analysis are characterized by high frequency vibrations. Calculation of the DLAs is summarized in Table 6.10 and presented in Figure 6.42 as function of speed.

Table 6.10. DLA for Terex crane on St. Mark's Bridge

Speed (km/h) / (mph)	Strain (μm/m)	DLA
Static	38.8	0.00%
24 / 15	41.6	7.22%
32 / 20	41.3	6.44%
40 / 25	42.2	8.76%
48 / 30	45.9	18.30%
56 / 35	45.2	16.49%
64 / 40	46.6	20.10%
72 / 45	48.6	25.26%
80 / 50	51.8	33.51%
88 / 55	50.8	30.93%
96 / 60	54	39.18%

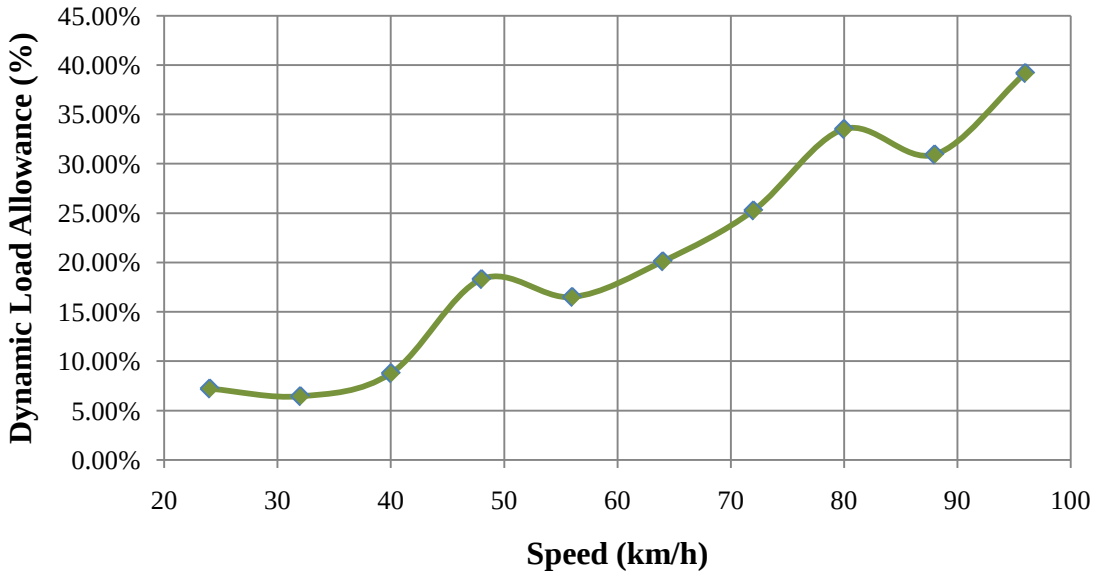

Figure 6.42. DLA vs. speed based on maximum strain on the bottom of girder #4, for the Terex crane in the center of the westbound lane

6.3.4. FE Analysis of the FDOT Truck

Longitudinal strains obtained from the analysis for all the vehicle speeds are summarized in Figure 6.43. Strains range from 37 to 47 μm/m, without a strong correlation to the vehicle speed. Selected time histories for the fourth and fifth girders are presented in Figures 6.44 and 6.45.

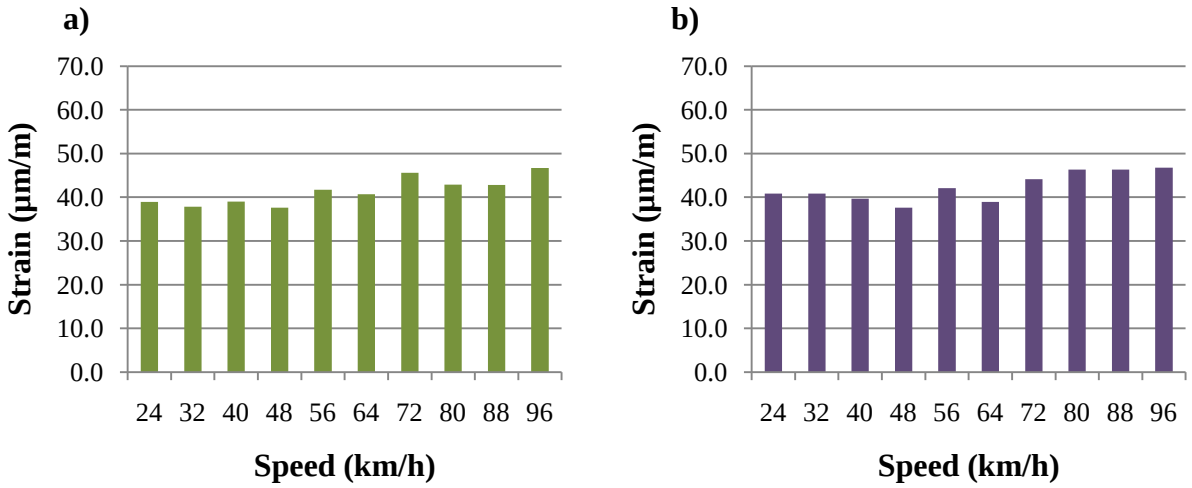

Figure 6.43. Longitudinal strains from FE analyses in the bottom of the girder for the FDOT truck in the center of the westbound lane: a) girder #4, b) girder #5

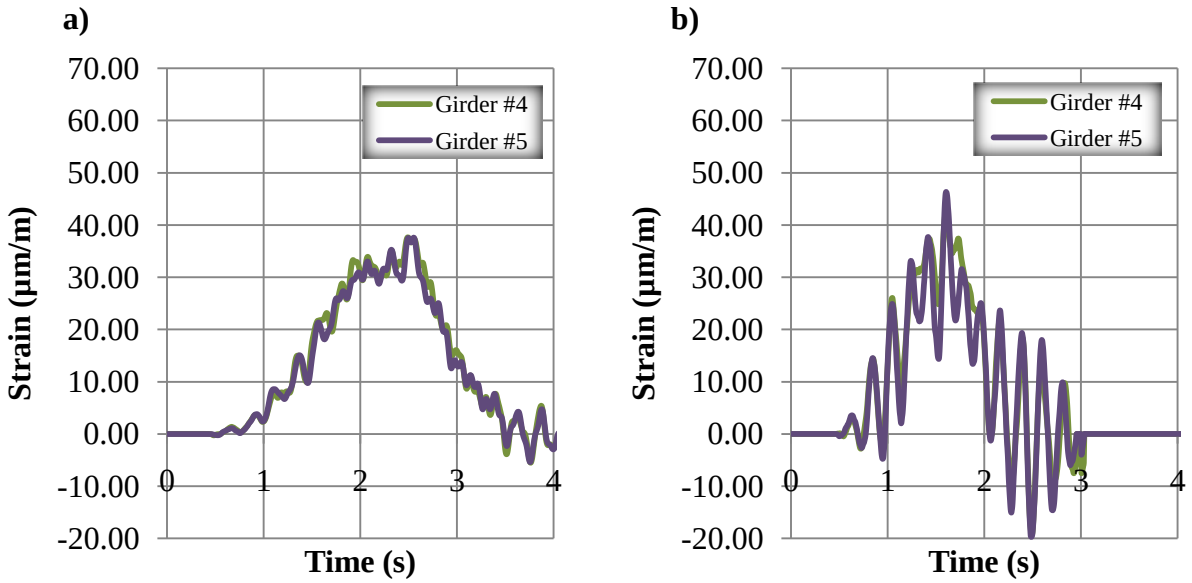

Figure 6.44. Longitudinal strain from FE analyses at the bottom of the girders for the FDOT truck in the center of the westbound lane at: a) 48 km/h (30 mph), b) 80 km/h (50 mph)

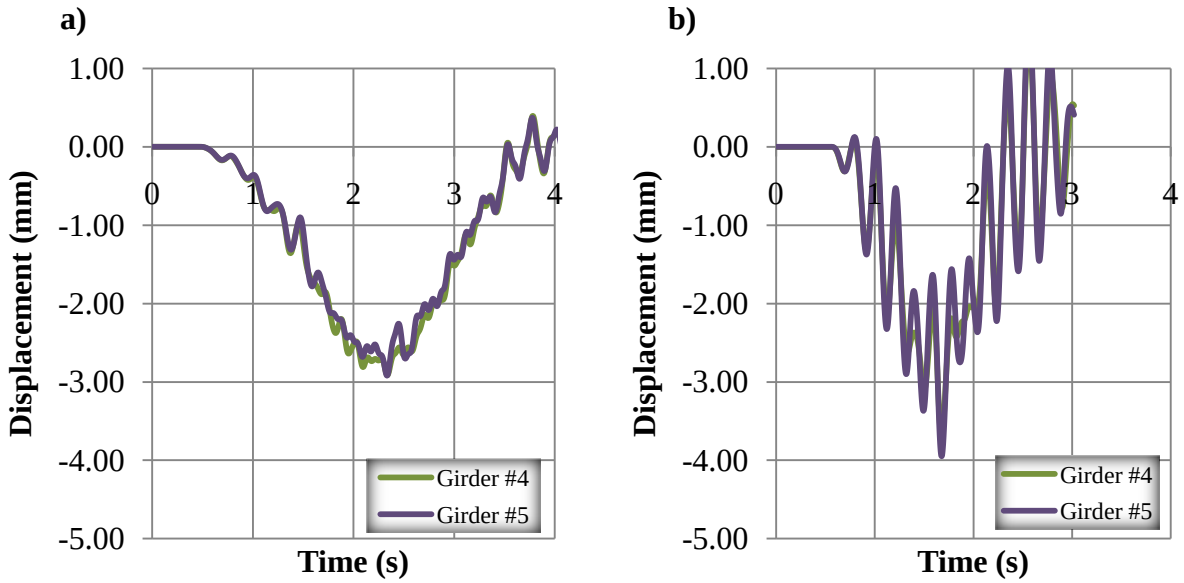

Figure 6.45. Vertical displacement from FE analyses at the bottom of the girders for the FDOT truck in the center of the westbound lane at: a) 48 km/h (30 mph), b) 80 km/h (50 mph)

The results for the time histories are described by the high frequency vibrations, the highest of the three vehicles. Calculation of the DLAs is summarized in Table 6.11 and presented in Figure 6.46 as function of speed.

Table 6.11. DLA for FDOT truck on St. Mark's Bridge

Speed (km/h) / (mph)	Strain (μm/m)	DLA
Static	34.7	0.00%
24 / 15	38.9	12.10%
32 / 20	37.8	8.93%
40 / 25	39	12.39%
48 / 30	37.6	8.36%
56 / 35	41.7	20.17%
64 / 40	40.7	17.29%
72 / 45	45.6	31.41%
80 / 50	42.9	23.63%
88 / 55	42.8	23.34%
96 / 60	46.7	34.58%

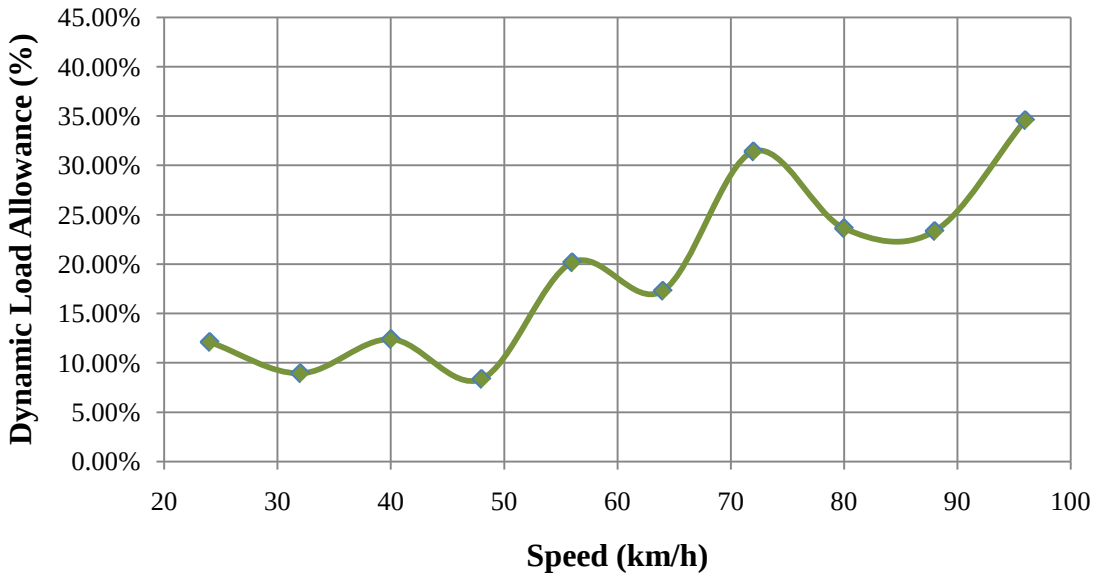

Figure 6.46. DLA vs. speed based on maximum strain on the bottom of girder #4, for the FDOT truck in the center of the westbound lane

6.4. FE Analysis of Bridge Flat Approach

To study the effect of the bridge approach surface on the dynamic response of the bridge, a run with a flat approach surface at 80 km/h (50 mph) in the center of the westbound lane for the Terex crane on the Chattahoochee Bridge was performed. Two analyses were performed using the original model with a bridge approach depression, and a modified model with a flat approach surface. The strain and displacement history for the fourth girder in both models are presented in Figure 6.47 and 6.48.

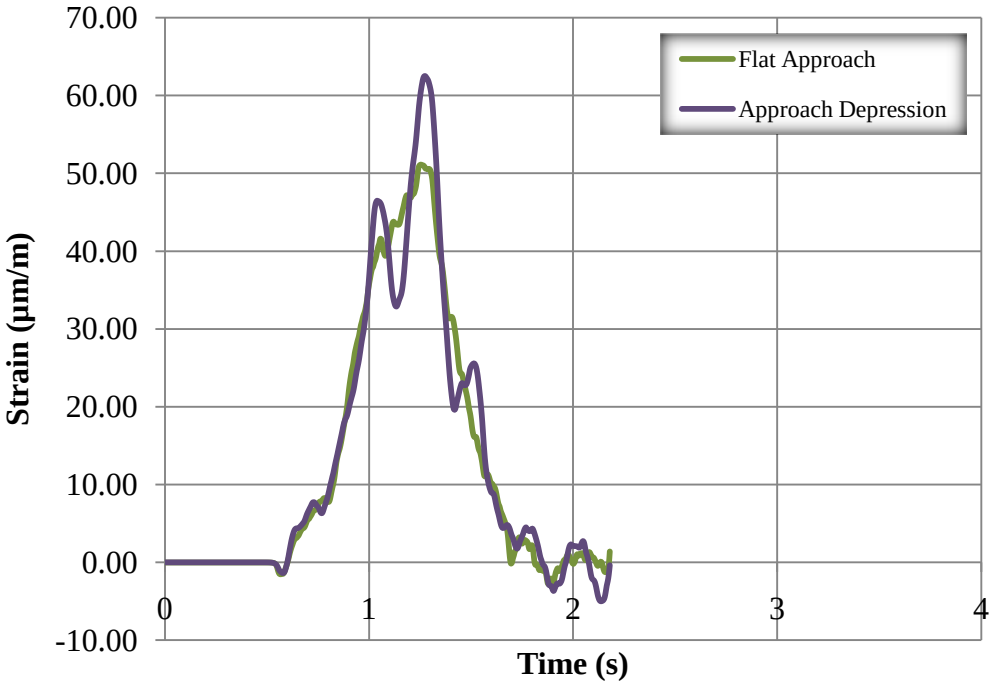

Figure 6.47. Longitudinal strains from FE analyses at the bottom of the fourth girder for the Terex crane in the center of the westbound lane at 80 km/h (50 mph)

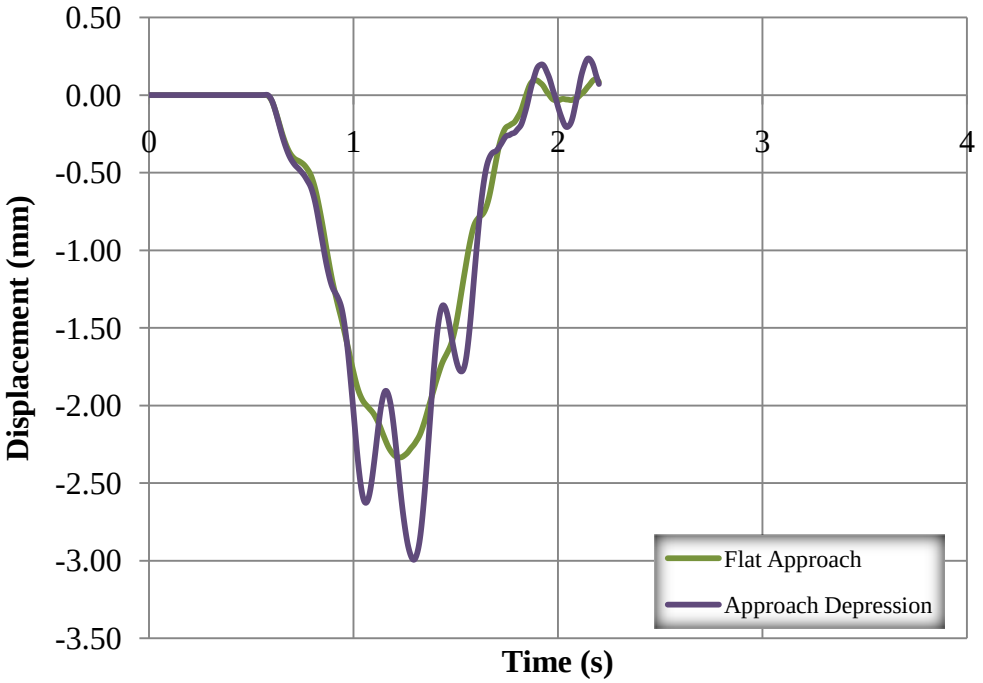

Figure 6.48. Displacements from FE analyses at the bottom of the fourth girder for the Terex crane in the center of the westbound lane at 80 km/h (50 mph)

The maximum strain observed in the model with the flat approach surface is 52.0 μm/m compared to 61.5 μm/m in the original model. While it is still just a 9.5 μm/m difference, it has a considerable difference when calculating DLA, as presented in Table 6.12. There is a decrease in DLA of 194% when the vehicle crosses the bridge with a flat approach surface. From the displacement history it is also observed that the vehicle running on a flat approach has a decreased dynamic response on the bridge.

Table 6.12. Comparison of original and modified FE models

Model	Max. Strain Static (μm/m)	Max. Strain Dynamic (μm/m)	DLA	Percentage Difference	Max. Displacement (mm)
Flat Approach	47.1	52	10.40%	193.94%	-2.29
Approach Depression	47.1	61.5	30.57%		-2.95

The effect of the approach surface is considerable in the interaction of vehicles and bridges. The strain history for the flat approach also has lower frequency vibrations than the original model. It may be explained by the fact that a bad approach surface may trigger vibrations in the vehicle, which results in higher dynamic responses of bridges.

6.5. Analysis of Results

The complete FE analyses included nine cases, runs of three different vehicles in three different bridges. Time histories taken at the bottom of the fourth girder for speeds of 80 km/h (50 mph) of the three vehicles in each bridge are presented in Figures 6.49, 6.50 and 6.51.

The tractor-trailer induces the highest strains in all the bridges, which is because it has the highest weight of all the three vehicles. The strains in all bridges are described by low frequency vibrations, due to the good distribution of the weight in the axles, and the well-designed suspension system.

The Terex crane induces the second highest strains on all the bridges, due to its compact setup. The strains are described by mid to high frequency vibrations due to the bad distribution of the loads in a short vehicle span, and the not so well designed suspension system.

The FDOT truck induces the least strains in all three bridges, due to low weight and the distribution of the weight. The FDOT truck time histories are described by high frequency vibrations, which is a result of the very stiff suspension system it is equipped with.

The strains induced by each vehicle on the bridge, do not directly reflect the DLA, because each vehicle DLA is calculated by a comparison with its static case. Therefore a higher strain does not necessarily result in a higher DLA.

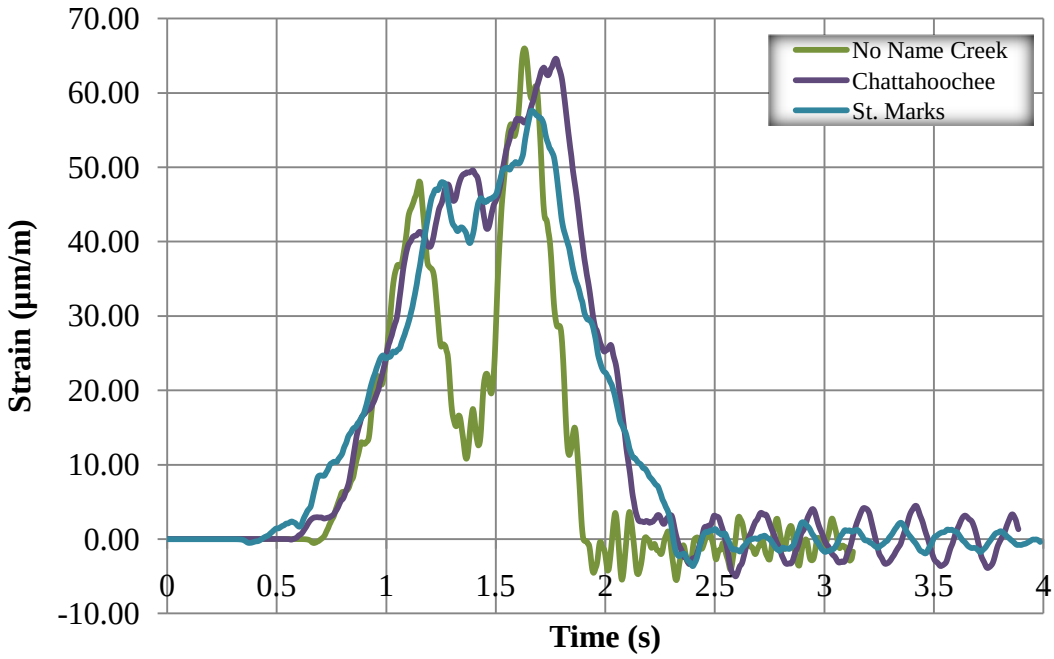

Figure 6.49. Strain histories for the tractor-trailer on the three bridge FE models in the center of the westbound lane at 80 km/h (50 mph)

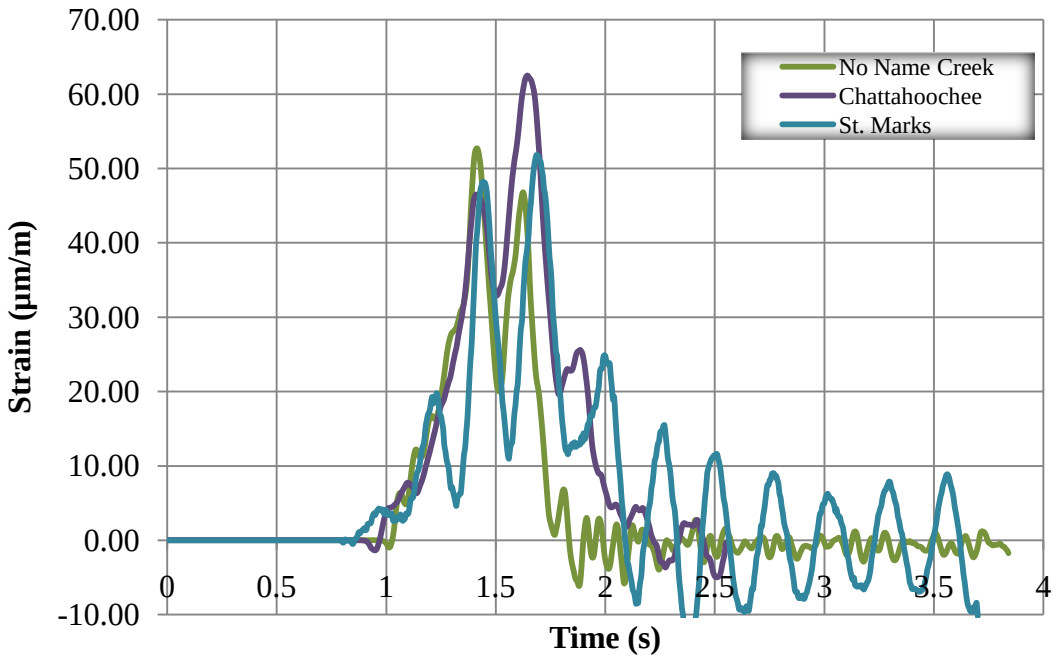

Figure 6.50. Strain histories for the Terex crane on the three bridge FE models in the center of the westbound lane at 80 km/h (50 mph)

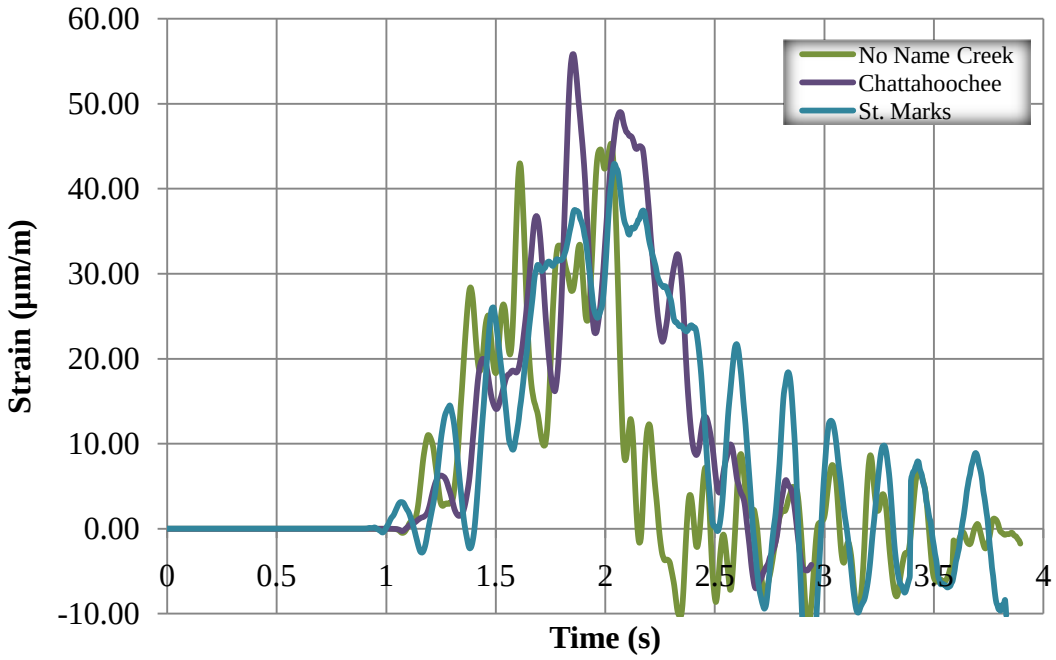

Figure 6.51. Strain histories for the FDOT truck on the three bridge FE models in the center of the westbound lane at 80 km/h (50 mph)

The bridge behavior under loading is commonly said to be controlled by the size of the girders. The DLA calculations for a selected case of the FDOT truck, summarized in Table 6.13, suggest that the span of the bridge also has a considerable effect on the dynamic response. These two factors have to be considered together when making assumptions about the dynamic response of a bridge loaded with vehicle loads.

Table 6.13. Summary of DLA for FDOT truck on the three bridge models

Bridge Name	AASHTO Girder Type	Span Length (m) / (ft.)	Max. Strain (μm/m)	DLA (%)
No Name Creek	II	12.1 / 40.0	45.3	15.56
Chattahoochee	III	21.0 / 69.0	55.9	35.35
St. Mark's Bridge	IV	29.3 / 96.0	42.9	23.63

The case for the Chattahoochee Bridge, with the AASHTO type III girders, represents the worst case scenario of the three bridges when interacting with the FDOT truck. The No Name Creek Bridge has the lowest DLA of the three bridges for this case. There are several bridge components that have to be considered when calculating DLA such as bridge span length and AASHTO girder type both of which in this case differ for all three bridges. DLA results from a combination of factors therefore due to the difference in the bridges components it is not easy to make conclusions on the results.

CHAPTER 7

BOUNCING LOAD EFFECT ON DYNAMIC RESPONSE OF THE BRIDGE

An important factor to account for in the vehicle bridge interaction comes from the effect of the loose cargo which can bounce on top of the vehicle. The bouncing load phenomenon produces an amplified structural response of the bridge, due to the additional dynamic load from hammering effect of the bouncing cargo. The original model of the tractor-trailer was modified to allow for the bouncing of the cargo. Time histories were obtained from both the original model of the tractor-trailer and the modified model and then compared, to assess the influence of the bouncing cargo on the interaction between the bridge and the vehicle.

7.1. Modifications of the Tractor-Trailer Model

The FE model of the tractor-trailer was developed with the additional cargo distributed across the trailer, as was used in the bridge experimental testing [12], [20]. In the original FE models of the tractor-trailer, the cargo and the trailer ended up sharing nodes which prevented the cargo from bouncing on the top of the trailer. Modifications of the FE model were made so that the model could allow the bouncing of the cargo to occur.

LS-Prepost preprocessor was used for modifying the existing model of the tractor-trailer. The shared nodes from the cargo and the trailer were detached. The chains used to tie the cargo were introduced as two different components. Four-node type 16 fully integrated shell elements were used to represent most of the chain body. The chain ends were modeled using seatbelt elements which include 1-D elements. Two-point seatbelt elements were of specific interest because they allow for introduction of a tensional force [15], to avoid having a loose chain. The chain was assumed to be a high-test steel chain with trade size of 3/8 inches, and material properties were defined accordingly. Physical properties were found from available information on general tying chains [4]. The vehicle cargo in the trailer is presented in Figure 7.1.

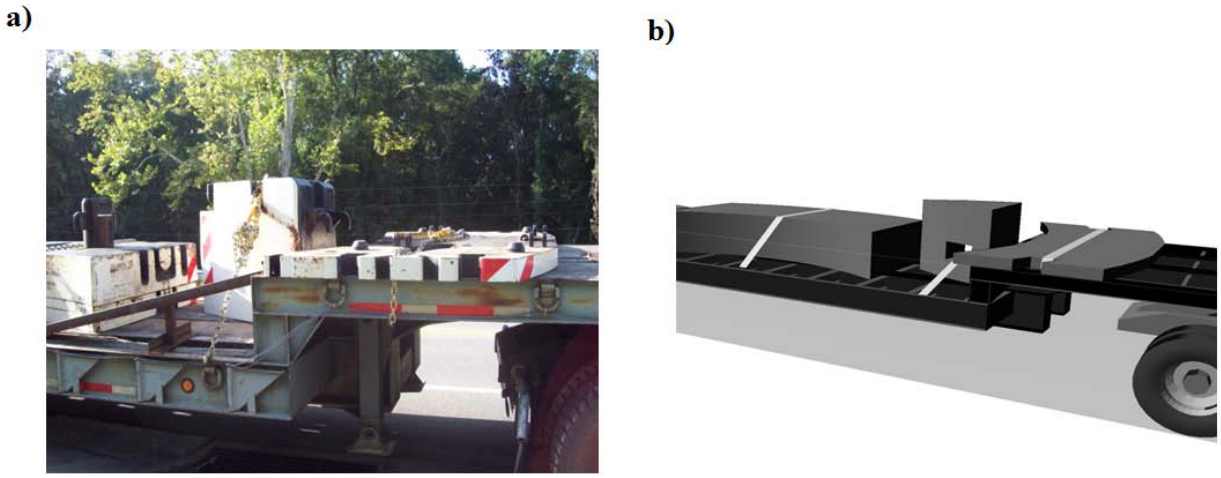

Figure 7.1. Vehicle cargo with tying chains in: a) experimental test, b) FE model

A special material model for seatbelts, MAT_SEATBELT, was used for the seatbelt elements. This material model allows for a force versus strain curve to be used to introduce tension in the seatbelts. The load curve in the loading face introduces tension between both ends of the chain, making the cargo tight. The initial tension introduced in the chain FE model was 1 kN. The yield force of the chain was calculated from the Young's modulus of elasticity and the cross sectional area of the chain. The tension introduced was chosen to allow for the slack of the tying chain in the FE model, considering the actual chain is not tensioned to the yield force when tied in real life. After initial tension loading, the seatbelt elements behave under the force versus strain curve, using the chain yield curve as strain is introduced in the chain. The chain properties are summarized in Table 7.1. The modified FE model of the tractor-trailer is presented in Figure 7.2.

Table 7.1. Material properties of seatbelt elements

	Weight per 30 m of chain (N)	Chain Diameter (mm)	Cross Sectional Area (mm^2)	Young's Modulus (GPa)	Calculated Yield Force (kN)
Tying Chain	702.8	10.3	83.5	200	16700

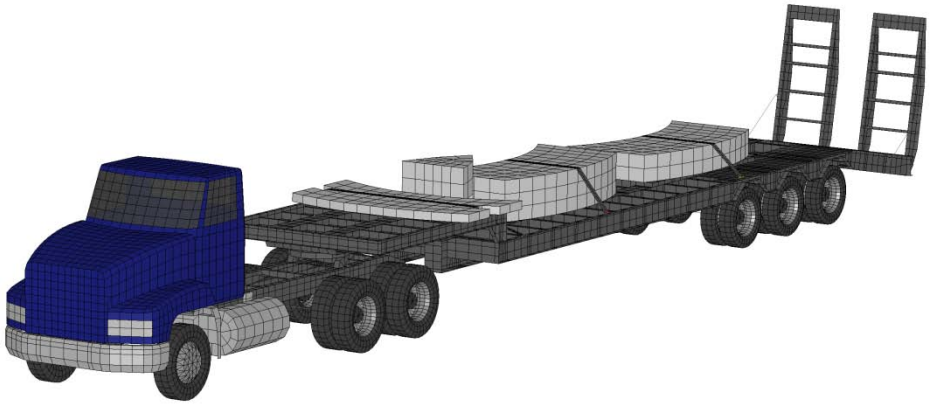

Figure 7.2. A modified FE model of the tractor-trailer, including chains to tie the cargo

7.2. FE Analyses of Hammering Effect

The FE study of the interaction between the bridge and the vehicle with the modified tractor-trailer included static and dynamic analyses. Data from experimental results were obtained from earlier tests and were reported in [20]. Girder numbering and one westbound transverse position of the tractor-trailer across the bridge width was considered, as presented in Figure 7.3.

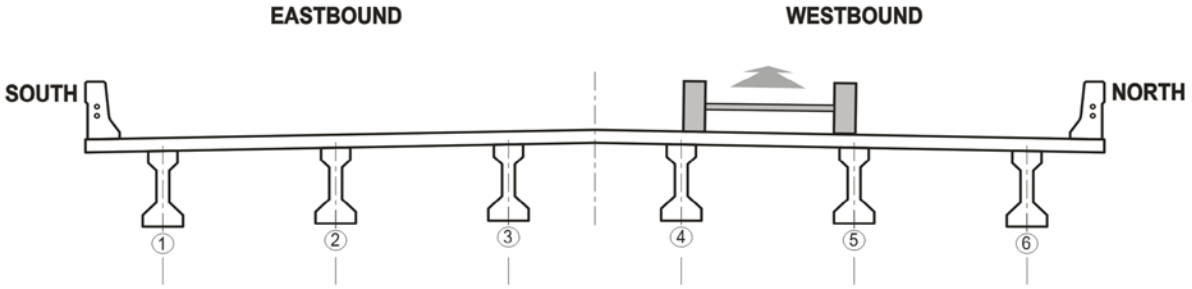

Figure 7.3. Transverse position of tractor-trailer on the bridge for FE analysis

The analysis of both FE models provided results of the maximum displacements and strains of each of the bridge girders. The values obtained from the modified FE model analysis were compared to the original FE analysis of the tractor-trailer. Strains and displacements obtained from analysis with the bouncing load were higher as compared with those when bouncing of the load was prevented.

Maximum displacements were obtained from the fourth and fifth girder, shown in Table 7.2. These two cases were considered because they resulted in the highest displacements. The

results obtained for the displacements are as expected, with the higher response obtained from the modified FE model. Time histories of displacement for both cases were also obtained from analyses and are shown in Figure 7.4. The time history of the displacement obtained from the FE analysis of the modified tractor-trailer has an overall shape and values similar to the original model, but with an additional frequency of about 4.8 cycles per second (hertz). This pounding frequency was consistent with those observed earlier during the test of bridge #500133. The differences between the results might seem very small but this additional frequency, subsequently results in an increased DLA factor, due to the additional displacement in the middle of the girder.

Table 7.2. Comparison of the deflection (mm) of the FE analyses

	Girder #4	Girder #5
Original	-3.22	-3.16
Modified	-3.34	-3.25

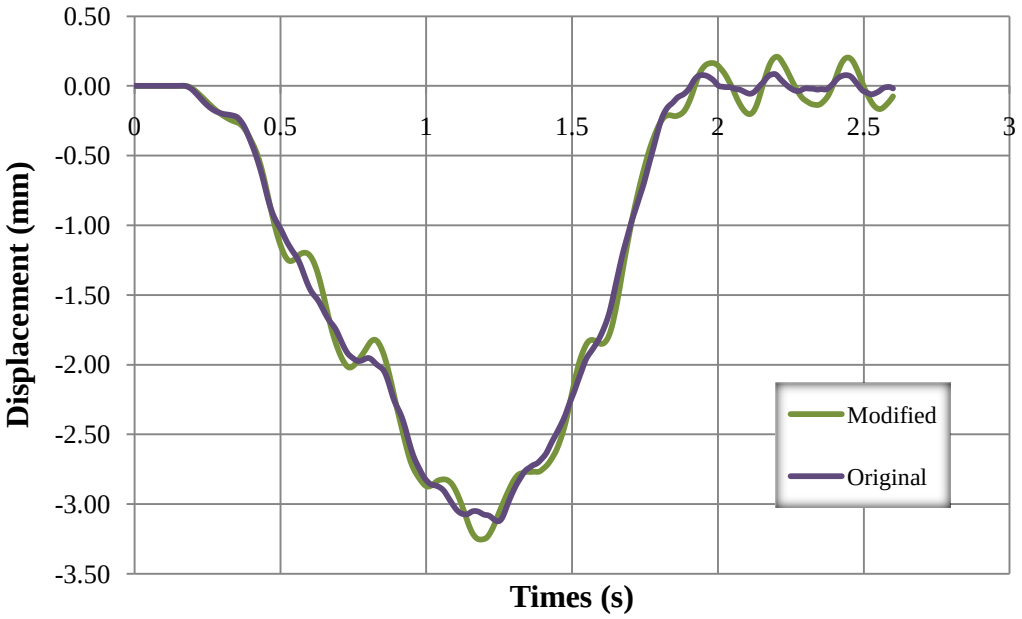

Figure 7.4. Deflection of the bridge girder #4 from FE analyses for the tractor-trailer in the center of the westbound traffic lane at 80 km/h (50mph)

Comparison of longitudinal strains from both analyses at a specified speed of 80 km/h (50 mph) is shown in Figure 7.5. The resulting strains in all girders of the modified FE model are

higher than those in the original model. The maximum strains as well as maximum displacements occur in girder number four of the bridge, due to the position of the vehicle in the analyses. Time histories of strains for the analyses are also shown in Figure 7.6. The time histories show an additional response of the bridge for the modified FE model.

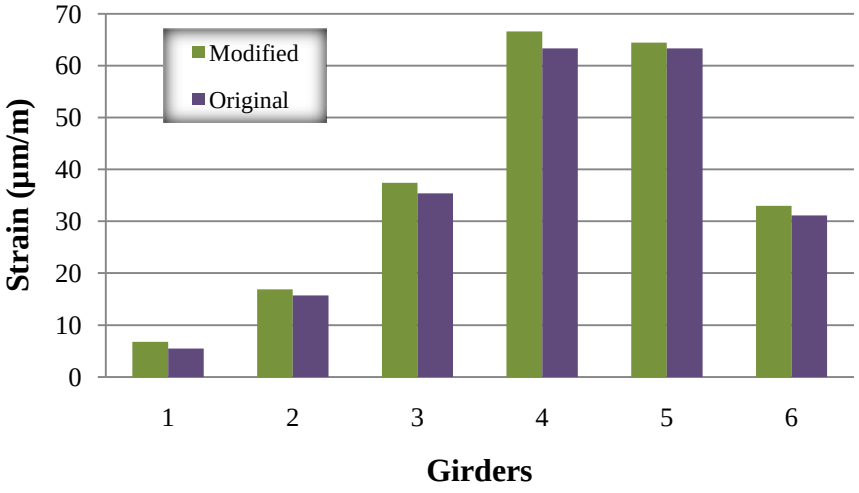

Figure 7.5. Longitudinal strain from the FE analyses in the bottom of the girder for the tractor-trailer in the center of the westbound lane at 80 km/h (50mph)

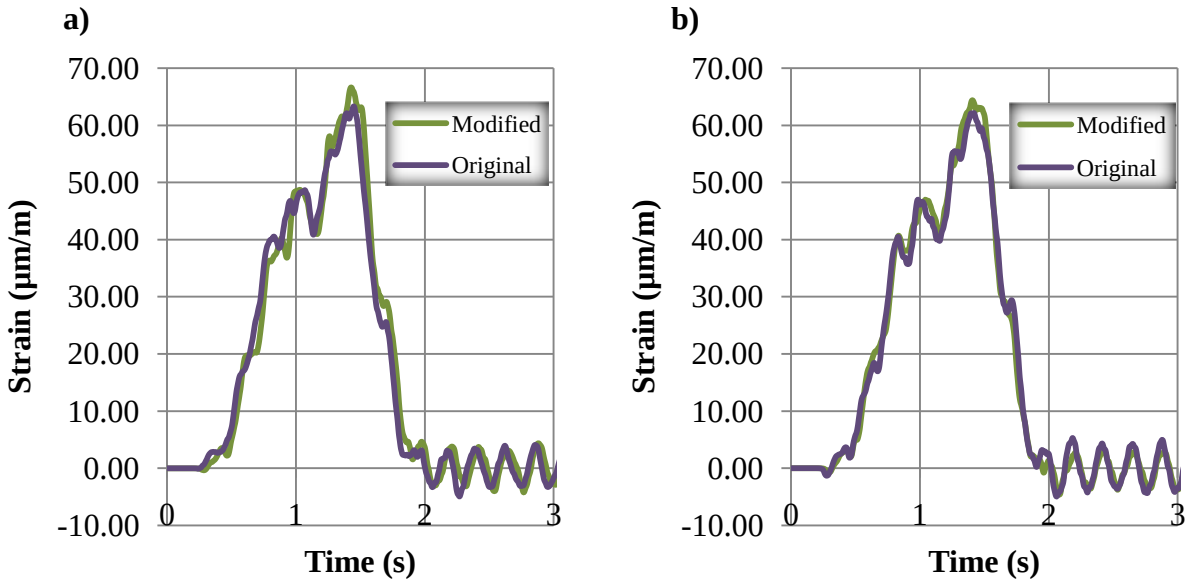

Figure 7.6. Longitudinal strain from the FE analyses at the bottom of the girder for the tractor-trailer in the center of the westbound lane at 80 km/h (50mph) a) girder #4, b) girder #5

The dynamic analyses included an analysis of DLA with varying speeds. It included over twenty runs with speeds varying from 24 km/h (15 mph) to 96 km/h (60 mph) on the center of the westbound lane of traffic. Results for the analyses of both FE models were compared and summarized in Table 7.3.

Table 7.3. Results of analysis for modified and original FE models

Speed (km/h)/(mph)	Modified Strain (μm/mm)	Modified DLA	Original Strain (μm/mm)	Original DLA
Static	60.59	0.00%	60.59	0.00%
24 / 15	66.9	10.41%	66.1	9.09%
32 / 20	66.3	9.42%	64.9	7.11%
40 / 25	66.8	10.25%	66.5	9.75%
48 / 30	66.8	10.25%	65.8	8.60%
56 / 35	66.3	9.42%	65.5	8.10%
64 / 40	67.3	11.07%	65.2	7.61%
72 / 45	67.6	11.57%	63.3	4.47%
80 / 50	66.6	9.92%	64.6	6.62%
88 / 55	71.6	18.17%	69.2	14.21%
96 / 60	71.4	17.84%	65.9	8.76%

The results from the FE analyses show that the modified FE model of the tractor-trailer results in higher DLA for most of the cases. The strain values for the two cases seem to be very close to one another, but with very small values for strain, small differences result in significant increase or decrease of the DLA.

The DLA factors are shown as a function of the vehicle speed in Figure 7.7 for both models of the cargo attachments. The FE model that allows for the bouncing of the cargo resulted in higher DLA factors. Even though analyses of both cases included the same mass and vehicle characteristics, with only the bouncing cargo effect added, they behave as two completely different systems. The curves are not symmetric, and one might show an increase of DLA while the other is a reduction in the 55 to 70 km/h speed range.

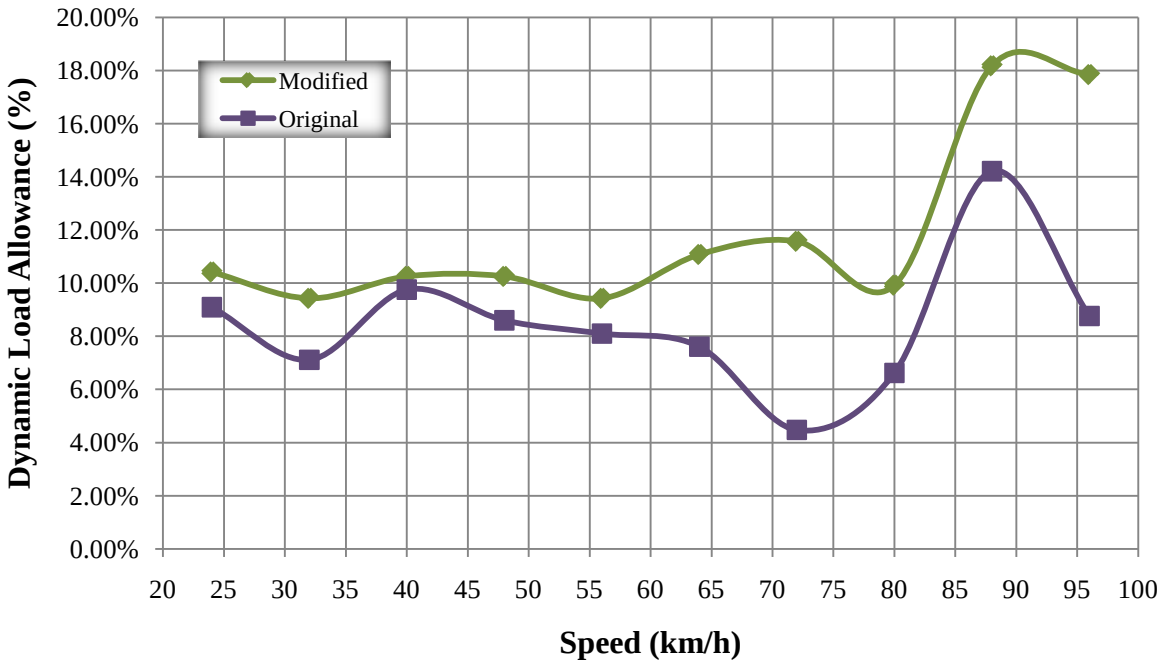

Figure 7.7. DLA vs. speed based on maximum strain on the bottom of girder #4, for modified and original FE models of the tractor-trailer in the center of the westbound lane of traffic

The results obtained from the FE analyses are characterized by a general increase in the response of the bridge when allowing the cargo to bounce on top of the trailer. One explanation is that the tractor-trailer with the bouncing cargo, as mentioned before, induces different frequencies on the bridge than the original tractor-trailer. Therefore each case behaves as a different dynamic system having a different response on the bridge.

CHAPTER 8

SIMPLIFIED FE ANALYSIS OF BRIDGE DYNAMIC RESPONSE

A simplified FE model consisting of the Chattahoochee Bridge and the loads of each of the Terex crane's axles applied as constant moving point loads was developed. The simplified FE model was developed specifically to have a different approach on the interaction between the two parts and to provide a model for comparison. The new model provided a simpler approach to the interaction, with faster calculations, while still being reliable. Two models were used for this analysis, one with the vehicle's axle loads, the simplified, and one with the actual vehicle, the original. Time histories were obtained from the simplified model and the original model to compare and draw conclusions on the effect of the bridge approach surface and the vibration frequencies resulting from the interaction with the vehicle at different speeds.

8.1. Development of Simplified Vehicle and Bridge Interaction Model

The original FE model of the Chattahoochee Bridge was taken, and the RAIL_TRACK and RAIL_TRAIN options from LS-Prepost were introduced. The rail track and train are intended to have a model with moving point loads sliding along a predefined pathway [15]. The two track parts were developed as 1-D beam elements and defined through the original pathway of the Terex crane on the Chattahoochee Bridge as the rail track. Three 1-D beam elements were attached to the tracks with the distance between them being the same as for the axles of the Terex crane. These three parts represented the Terex crane's axle loads moving on the tracks, and were defined as the rail train. The new parts for the track and train system were modeled as rigid materials using the material model MAT_NULL thus providing faster calculations for the simulation. Velocities were introduced to the model as initial velocities, to avoid the need for acceleration time. The final simplified FE model is presented in Figure 8.1.

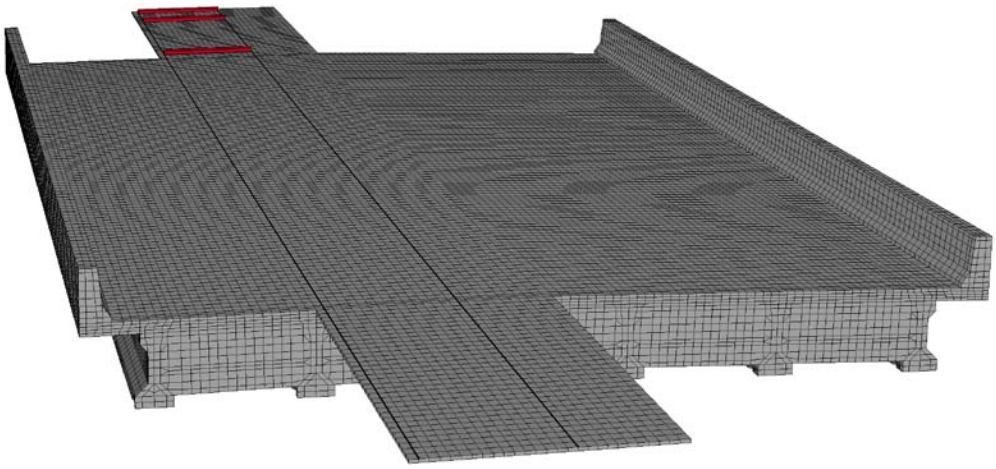

Figure 8.1. A Simplified FE model of vehicle – bridge interaction

8.2. FE Analysis of Simplified Interaction Model

The interaction between the bridge and the vehicle loads in the simplified FE model provided information about the effect of the vehicle speed and the bridge approach surface on the dynamic response of the bridge. The rail system used, provided a method for sliding the constant loads along a defined pathway, but the complex interaction between the vehicle and the bridge that includes the vehicle's suspension system and bouncing masses is disregarded.

The FE analysis included an analysis of DLA with varying speeds for dynamic cases and a static case totaling eleven simulations. The girder numbering and the transverse position of the vehicle for the FE analysis are presented in Figure 8.2.

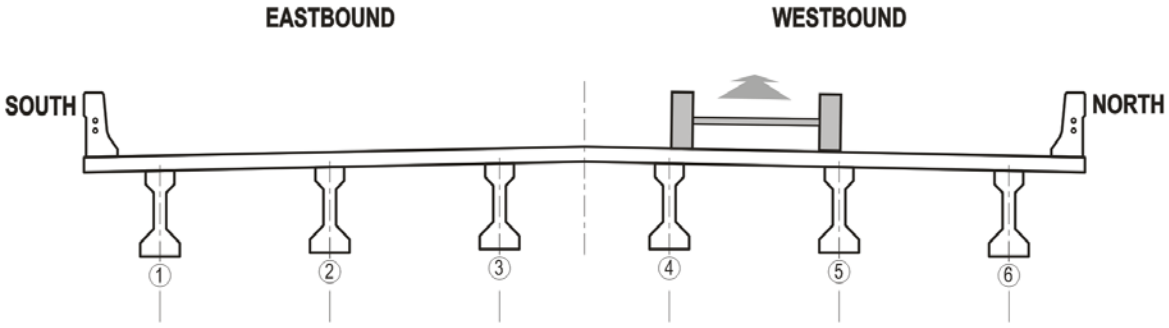

Figure 8.2. Transverse position of the axles and moving loads for FE analysis

From the FE analyses, maximum strains were obtained for each of the girders, as presented in Figure 8.3. The maximum strains for the simplified model are considerably lower

than for the original model. Time histories of the longitudinal strain and displacement in the bottom of the fourth girder for the original and the simplified models are presented in Figure 8.4 and 8.5.

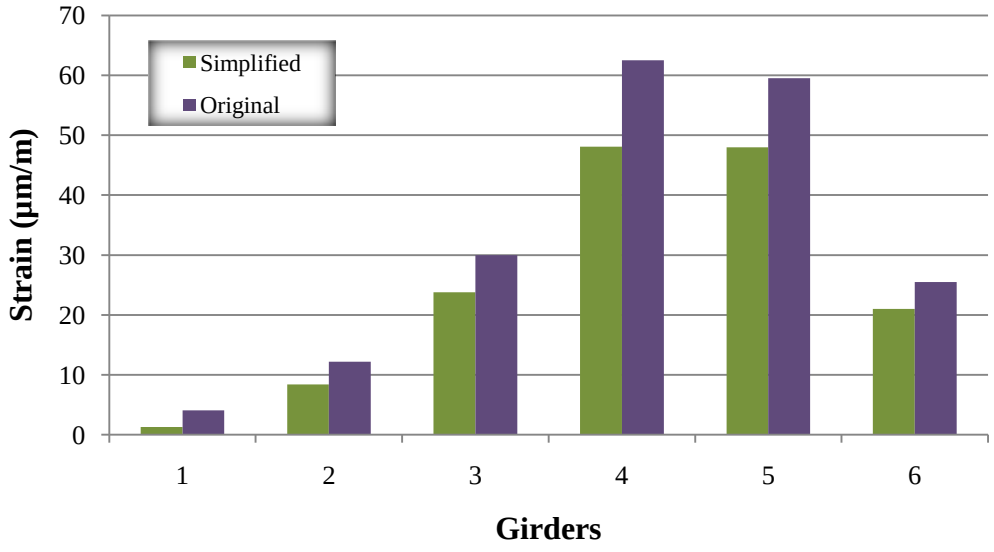

Figure 8.3. Longitudinal strain from FE analyses in the bottom of the girder for the Terex crane in the center of the westbound lane at 80 km/h (50 mph)

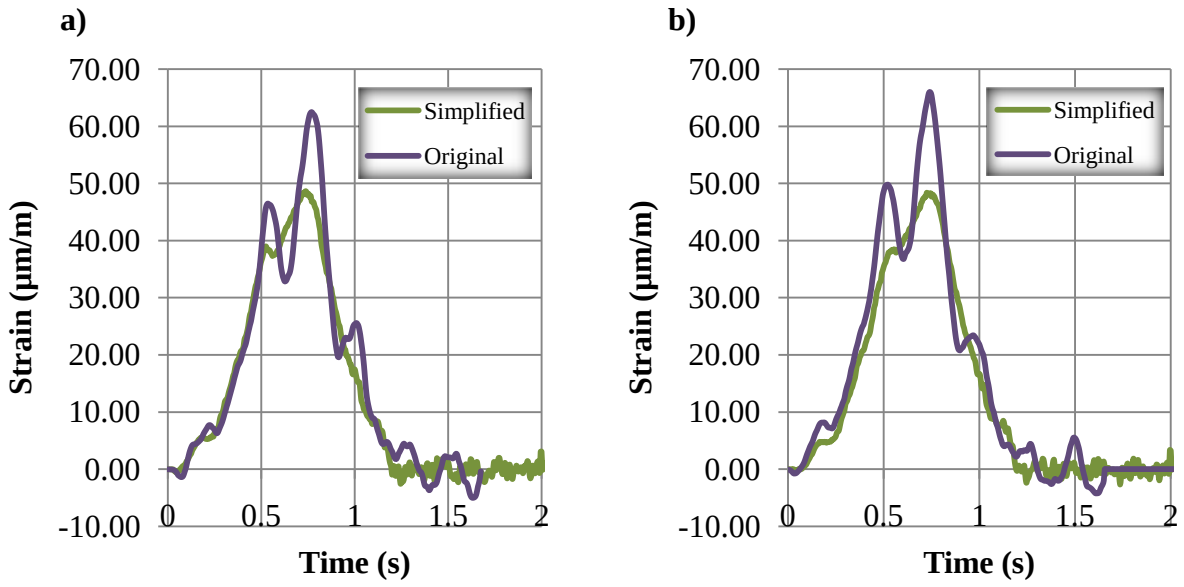

Figure 8.4. Longitudinal strain from FE analyses of both FE models at the bottom of the girder in the center of the westbound lane at 80 km/h (50mph) a) girder #4, b) girder #5

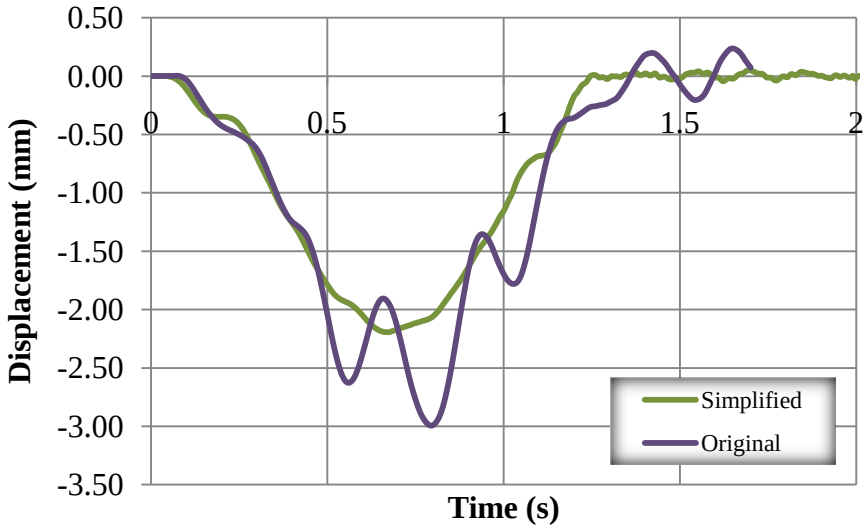

Figure 8.5. Deflection of the bridge girder #4 from FE analyses for both FE models in the center of the westbound traffic lane at 80 km/h (50mph)

From the time histories of strains and displacements, lower frequency vibrations can be observed in the results of the simplified model. Results of the simplified model are explained by the fact that the complex vibrations of the vehicle's mass and the suspension system are disregarded in this case. The loads in the simplified model are applied directly to the bridge as constant moving point loads that do not vary dynamically.

Dynamic analyses included an analysis with varying speeds. Maximum strains from the fourth girder were used to calculate DLA for each vehicle speed because they resulted in the highest strains from all the girders. Results for the analysis of both models were compared and summarized in Table 8.1, and presented in Figure 8.6 as a function of speed.

Table 8.1. Results of analysis for simplified and original FE models

Speed (km/h) / (mph)	Simplified Strain (μm/m)	Simplified DLA	Original Strain (μm/m)	Original DLA
Static	47.1	0.00%	47.1	0.00%
24 / 15	48.6	3.18%	54.2	15.07%
32 / 20	49.5	5.10%	52.7	11.89%
40 / 25	48.7	3.40%	50.3	6.79%
48 / 30	48.3	2.55%	55	16.77%
56 / 35	48.5	2.97%	52.1	10.62%
64 / 40	48.3	2.55%	56.6	20.17%
72 / 45	48.9	3.82%	53.1	12.74%
80 / 50	48.3	2.55%	62.5	32.70%
88 / 55	49.8	5.73%	55.7	18.26%
96 / 60	49.2	4.46%	53.1	12.74%

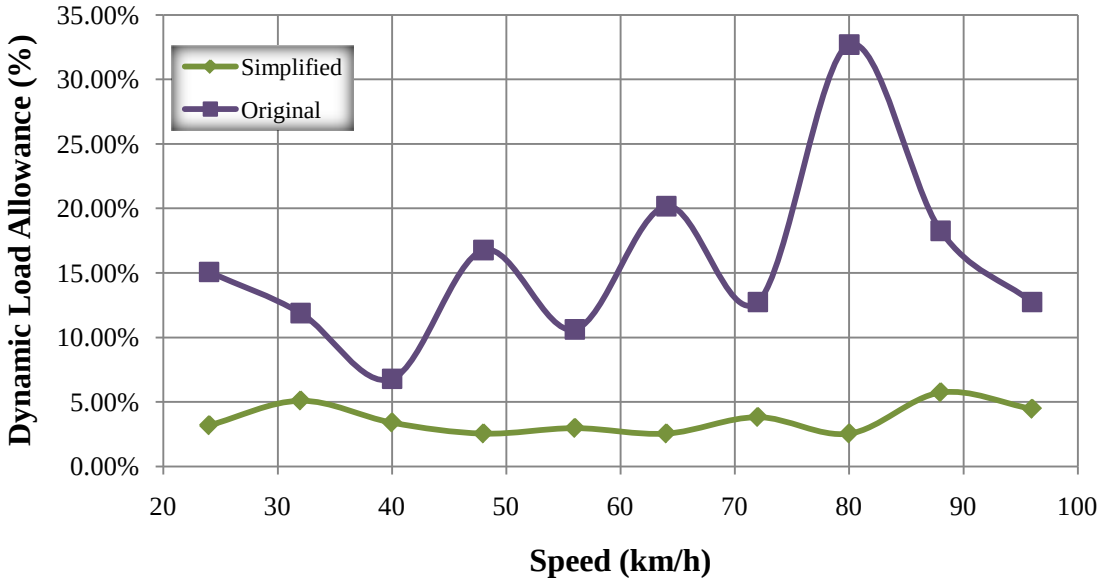

Figure 8.6. DLA vs. speed based on maximum strain on the bottom of girder #4, for both FE models in with vehicle traveling in the center of the westbound lane of traffic

The simplified FE model resulted in DLA factors ranging from 2 to 6 percent, while the original model has DLA ranging from 5 to 35 percent. The analysis of DLA versus speed for the simplified model has a very small range of DLA values, resulting from the small variation of strains induced by the loads in the bridge. For the simplified model neither the speed of the vehicle or the bridge approach surface have a big effect in the dynamic response of the bridge.

The results for the original model have a larger range of DLA values resulting from the different vibrations from the complexity of the complete vehicle-bridge interaction. The model of the vehicle's wheels and suspension system are desired to obtain more realistic results of the FE analysis, as was proven in [26].

CHAPTER 9

FUTURE RESEARCH PLANS

Current and past research projects supported by the FDOT Structures Research Laboratory have resulted in development of research tools that may be helpful in future research. Making use of these tools, there are several different research plans for the future.

9.1. Dynamic Load Allowance for Florida DOT Bridges

Looking to get more insight into some of the results obtained from the current research project, more investigation on the interaction between the heavy vehicles and the FDOT bridges is planned. The variation of DLA with varying speeds, where lower DLA was observed at higher speeds in most cases is of specific interest. A specific case for the Terex crane crossing over the Chattahoochee Bridge is presented in Figure 9.1, showing results from the numerical analysis and experimental test.

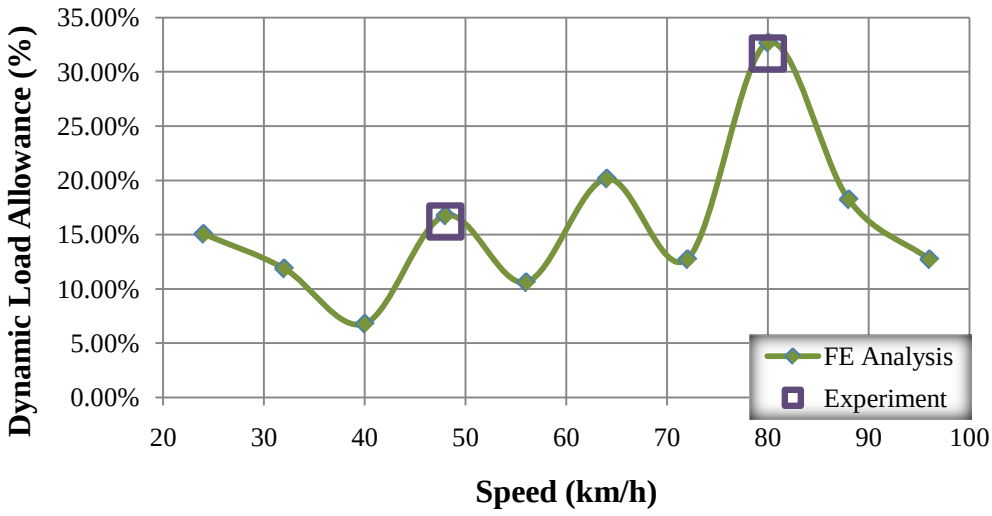

Figure 9.1. An example of DLA as a function of speed

Similar results from both tests suggest that the numerical analysis is highly reliable. The phenomenon may be explained by further testing of the FE models, with additional tools including the simplified model with the rail system as discussed in chapter 8. Also applying

different mathematical algorithms including Fast Fourier Transform (FFT) may shed some light into the frequencies transferred to the bridge, and the reason why lower speeds may result in higher DLA.

Another part of the research would include a continuous monitoring program in the Chattahoochee Bridge using wireless technology and an automatic data recording system. The system would include sensors for strains, displacements and accelerations at selected points, and provide information on passing vehicles like speed, number of axles, etc. Additional experimental data would provide more information on the complexity of this type of research.

9.2. Impacts of Heavy Trucks on the Highway Bridge Substructures

Reports on crashes of heavy tankers or trucks with highway overpasses are relatively common. A crash that occurred on May 23, 2003 where a semi-truck left the interstate and struck the main support post of a county road overpass on I-80, near Big Springs, NE is presented in Figure 9.2.

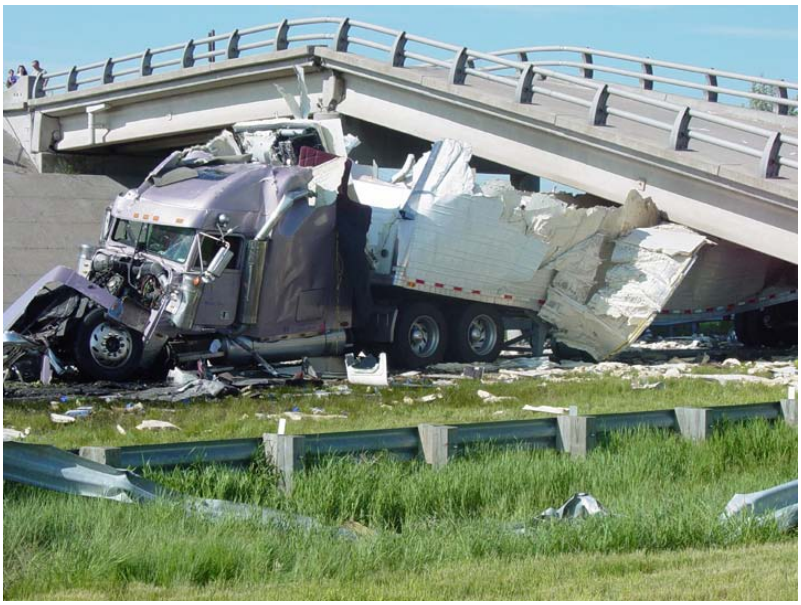

Figure 9.2. An example of the extensive damage resulting from an accident on I-80

This is a very serious problem, requiring research on improved crash resistance of overpasses. According to a recent survey, Florida reports 40 to 55 impacts, mostly to multi-

girder bridges, with 3 to 5 of these impacts resulting in major damages. The major goal of the research would be to assess the use of New Jersey barriers as a method to preserve the structural integrity of an existing bridge substructure when accidentally impacted by heavy vehicles.

New models of a New Jersey barrier interconnected for improved efficiency, and a common overpass pier from existing blueprints and design documentation will be developed. The complete FE model for analysis would include a vehicle, the barrier, overpass pier, and a simple model of the highway bridge deck. The proposed computational mechanics efforts will be to assess the following:

1. The feasibility and effectiveness of such protection,
2. The amount of energy absorbed by the New Jersey barrier,
3. The remaining energy transferred to the pier, and
4. The extent of the damage to the pier due to such accidents.

The methodology applied is particularly attractive for this type of feasibility studies, when compared to experimental testing of overpasses which would be excessively expensive.

9.3. Impact of Over-height Vehicles with the Bridge Superstructure

According to a National Cooperative Highway Research Program study the average number of concrete bridges damaged each year in the USA is 200, approximately 80 percent of which are caused by impacts from over-height vehicles or loads. It was stated that reinforced concrete box girders are not susceptible to vehicle impact damage as much as the concrete I-beams. One of the common damages in existing highway bridges is the damage at the bottom corners or edges of the reinforced concrete beams or box girders induced by an impact of trucks exceeding the allowable height clearance of the bridges, as shown in Figure 9.3.

Figure 9.3. An example of damage from an over-height hit on a highway bridge

Overpasses that are most vulnerable to this type of impacts will be identified with cooperation of the project manager. Existing FE models will be modified as necessary for the specific research, and new FE models of girders from the selected highway bridges will be developed, and further validated using experimental data. One of the selected AASHTO girders will be tested experimentally for validation and verification of the entire FE model of the bridge span. The experimental testing will be conducted at the Florida DOT Structures Lab using the newly erected pendulum device.

The efforts of this project would be to analyze two different devices currently used to absorb energy during impacts and recommending the best solution to handle this type of impacts. The following devices will be analyzed using computational mechanics:

1. a bridge bumper consisting of a stiff rectangular or an angle section with additional layer of energy absorbing material, developed and implemented in Texas, and
2. The I-Lam (Impact Laminate) panels which are made of composite sandwich construction with multi-layer aluminum honeycomb core and top and bottom thin face sheets.

CHAPTER 10

SUMMARY AND CONCLUSIONS

The main purpose of the research project was to develop two new FE models of highway bridges with AASHTO type II and IV girders, for dynamic analysis of vehicle-bridge interaction. The two new models would complement an existing model of an AASHTO type III girder in the analyses. The two new models were developed, and dynamic and static analyses of the three bridges were performed with three existing FE models of heavy vehicles acquired from a previous research project. The maximum strains obtained from the analyses were used in every case to calculate the DLA.

Analysis of the interaction of each model of the vehicles with the three bridges was performed. The analyses were performed to study the influence of the bridge geometry and girder type in the dynamic response of the bridge. Analyses of DLA with varying speed were performed to study the influence of the vehicle speed in the calculation of DLA. The influence of the bridge girder size and the span length were considered together in the analysis due to the different girder types and spans in each of the three bridges.

The influence of the bridge approach surface on dynamic bridge response was also assessed. One case with a vehicle at a selected speed was reproduced with a perfectly flat bridge approach surface. The results for maximum strains and displacements for the modified bridge are relatively lower while also resulting in lower frequency vibrations.

An assessment of the influence of a vehicle cargo that is able to bounce on top of the tractor-trailer was also performed. The model of the tractor-trailer was modified to allow for the bouncing of the load. Analysis with varying speeds was performed and compared to the analysis of the original model. The results for maximum strains and displacements for the modified model are higher, as well as the frequency of vibrations in the response.

Additionally a different approach using a simplified FE model of one bridge with moving loads was performed. The model was used to assess the influence of the vehicle's complex mass and suspension system on the bridge's response. Analysis of DLA vs. speed for the model was compared to one of the vehicles, to assess the relation of the DLA to the vehicle speed. Results for the simplified model had a very small range of strain values with low frequency vibrations.

The results obtained from the analyses including all three vehicles and three bridges are summarized in Figure 10.1.

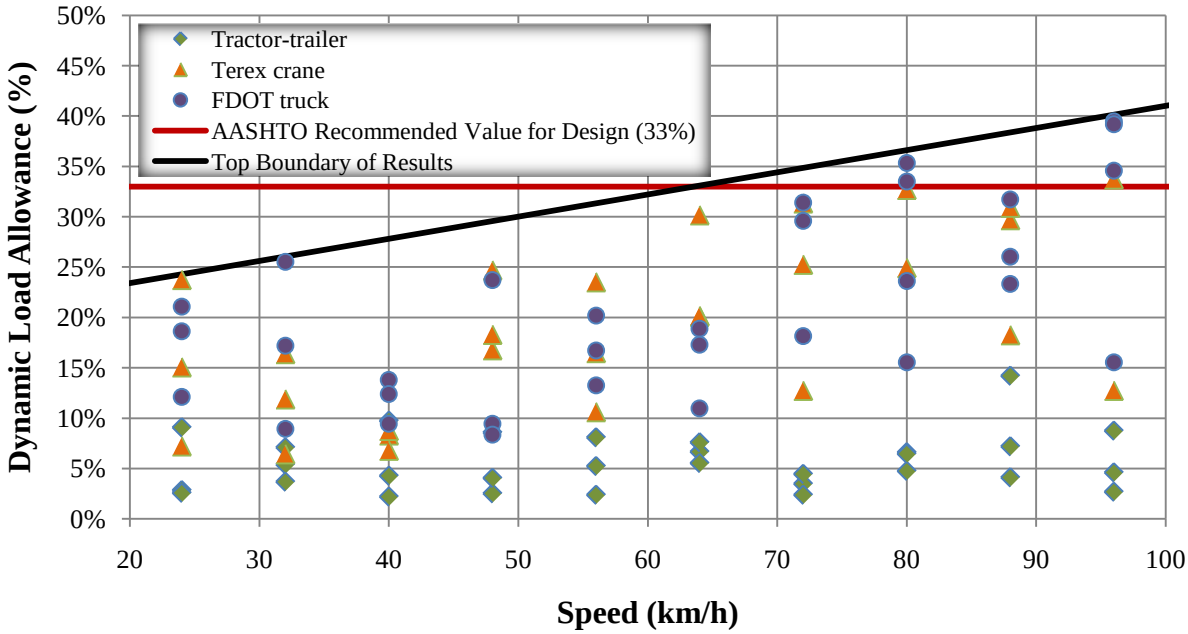

Figure 10.1. Summary of FE analyses of all the vehicle-bridge interactions

AASHTO specification. The DLAs obtained did not, in most cases, go above AASHTO recommendation for DLA. There are however cases in which the results did surpass AASHTO recommendation, although they are cases where excessive speeds are recorded.

From the top boundary of the DLA results a trend line was drawn, and equation 9.2 to calculate DLA was derived. Equation 9.2 offers a slightly better estimate of DLA than the AASHTO equation 9.1. The DLA for the two methods is:

(10.1)

(10.2)

where is equal to the vehicle speed in km/h.

Bridge geometry. The analyses performed provided information about the influence of the bridge's geometry on its dynamic response. The size of the girder is without a doubt a significant factor in the bridge's behavior. The bridge span also has an influence on the dynamic response of the bridge. No direct relationships were found between these two factors and the DLA measured.

Each bridge structure depending on the span, girder size, and other characteristics that make it one system, has independent natural frequencies. As may be seen from the results presented in Figure 10.1, showing a cloud of dispersed points with no direct relation to speed, the importance of the natural frequencies of the structure is considerable when assessing the interaction between vehicle and bridge.

Vehicle speed. The analyses also provided valuable information on the influence of the vehicle speed on the dynamic response of the bridge. Analyses at different speeds resulted in scattered points when increasing or decreasing speeds, showing a vague correlation. The DLA generally increases when the speed of the vehicle is increased, but the relation between these two is not nearly linear. Depending on the natural frequencies of the system, it is suspected that some speeds may trigger vibrations and lead the system close to resonance while other speeds are far from it. A lower vehicle speed in certain cases may result in higher DLA which suggests that the dynamic response of the bridge is somewhat independent of the vehicle speed. Still, the speed is clearly of some consideration, but the vehicle-bridge system is more complex, with the natural vibrations of each having much influence on the bridge's response.

Bouncing cargo. Tests of the bouncing cargo on the vehicle showed an increment in maximum strains and displacements on the bridge. Also, an additional frequency of about 4.8 hertz was observed. When the cargo is loosely fastened, it is able to pound the bridge with an additional dynamic force. The influence of the cargo that is able to bounce, on the dynamic response of a bridge is clearly visible, and when combined with a bad approach surface it may be even more damaging. Therefore cargo on top of heavy vehicles should be securely fastened to avoid introducing additional dynamic loading on bridges.

Road surface condition. Comparison of results from the same vehicle run on a bridge with a flat approach surface and a bridge with bad approach surface showed a decrease in DLA

of 194%. The road surface condition influence on the bridge is considerable, resulting in higher DLAs for bad surfaces. The bad road surface triggers vibrations in the vehicle during the interaction with the wheels which are transferred to the bridge.

The simplified model results provided more information about the influence of the bridge approach depression and vehicle suspension system on the bridge's response. The small range of strains from 48.3 to 49.8 μm/m from the results indicates that the interaction of the vehicle suspension with the bridge approach surface has considerable influence on the analysis. Low frequency vibrations are also observed in the results which are due to the lack of interaction between the loads and a bad approach surface. The vehicle suspension system is one factor that needs to be considered in depth when studying the interaction of vehicle and bridge. Very stiff suspensions, as for the FDOT truck, result in the worst possible case of DLA, because it is unable to dissipate vibrations through springs and dampers. Softer suspension, as for the tractor-trailer resulted in the lowest DLAs, proving its well-designed suspension system and good load distribution.

REFERENCES

[1] AASHTO. (2008). Bridge the Gap: Restoring and Rebuilding the Nation's Bridges. Report. Washington D.C.

[2] AASHTO (2002). Standard Specifications for Highway Bridges, 17th Edition, Washington D.C.

[3] Ansley, M. H. (2006). FDOT Design Standards. Florida Department of Transportation, Tallahassee, Florida.

[4] Armstrong Alar Chain Corporation (2010). Retrieved June, 2008, http://www.ncac.gwu.edu/vml/models.html.

[5] Cook, R. A., Allen, D. T. (2009). *Stiffness Evaluation of Neoprene Bearing Pads Under Long Term Loads.* Final Report, FDOT BD545-39. Structural Research Center, Florida Department of Transportation.

[6] Csikos, A., Hegedus, I. (1998). Torsion of Reinforced Concrete Beams. Technical University of Budapest, Department of Reinforced Concrete Structures, Budapest.

[7] Deng, L., Cai, C. S. (2010). *Development of Dynamic Impact Factor for Performance Evaluation of Existing Multi-girder Concrete Bridges*. Engineering Structures, vol. 32 (1), pages 21-31.

[8] Ding, L., Hao, H., Zhu, X. (2009). *Evaluation of Dynamic Vehicle Axle Loads on Bridges With Different Surface Conditions*. Journal of Sound and Vibration, vol. 323 (3-5), pages 826-848.

[9] Finite Element Model Archive. (2008). Retrieved December 16, 2008, from National Crash Analysis Center: http://www.ncac.gwu.edu/vml/models.html

[10] Gong, L., Cheung, M. S., (2008). *Computer Simulation of Dynamic Interactions between Vehicle and Long Span Box Girder Bridges*. Tsinghua Science & Technology, vol. 13 (1), pages 71-77.

[11] Hibbeler, R. C. (1998). *Structural Analysis* (4th ed.). Upper Saddle River, New Jersey: Prentice-Hall, Inc.

[12] Kwasniewski, L., Li, H., Wekezer, J. W., Malachowski, J. (2006). *Finite Element Analysis of Vehicle-Bridge Interaction*. Finite Elements in Analysis and Design, vol. 42 (11), pages 950-959.

[13] Lee, S., Yhim, S. (2005). *Dynamic Behavior of Long-span Box Girder Bridges Subjected to Moving Loads: Numerical Analysis and Experimental Verification*. International Journal of Solids and Structures, vol. 42 (18-19), pages 5021-5035.

[14] Li, H., Kwasniewski, L., Wekezer, J.W., (2008). *Dynamic Response of a Highway Bridge Subjected to Moving Trucks.* ASCE Journal of Bridge Engineering, vol. 13 (5), pages 439-448.

[15] LS-DYNA Keyword User's Manual (Vol. II). Livermore, California: Livermore Software Technology Corporation.

[16] Maupin, W., Brown, B.C., Abba, G. (1989). *Extending the Life of Bridges.* American Society for Testing and Materials, Lake Buena Vista, Florida.

[17] Mtenga, P. V. (2005). *Elastomeric Bearing Pads Under Combined Loading.* Final Report, FDOT BC352-16. Structural Research Center, Florida Department of Transportation.

[18] O'Brien, E. J., Keogh, D. L. (1999). *Bridge Deck Analysis*. New York, NY 10001.

[19] Ray, M., Mongiardini, M. (2009). *Roadside Safety Verification and Validation Program (RSVVP) User's Manual*. Worcester Polytechnic Institute (WPI). Worcester, Massachusetts.

[20] Szurgot, P., Kwasniewski, L., Wekezer, J. W. (2011). *Experimental Assessment of Dynamic Responses Induced by Permit Vehicles.* ASCE Journal of Bridge Engineering, Manuscript no. BEENG-2009, in press.

[21] Tan, G. H., Brameld, G. H., Tambiratnam, D. M. (1998). *Development of an Analytical Model for Treating Vehicle-Bridge Interaction*. Engineering Structure, vol. 20 (1-2), pages 54-61.

[22] Tedesco, J. W., Stallings, J. M., El-Mihimy, M. (1999). *Finite element method analysis of a concrete bridge repaired with fiber reinforced plastic laminates.* Computers and Structures, vol. 72, pages 379-407.

[23] Wang, T. L., Huang, D., Shahawy, M., Huang, K. (1996). *Dynamic Response of Highway Girder Bridge.* Computers and Structures, vol. 60 (6), pages 1021-1027.

[24] Wang, T., Liu, C. (2000). *Influence of Heavy Trucks on Highway Bridges*. Final Report, FDOT BC379. Structural Research Center, Florida Department of Transportation.

[25] Wekezer, J. W., Li, H., Kwasniewski, L., Malachowski, J. (2004). *Analytical and Experimental Evaluation of Existing Florida DOT Bridges*. Final Report, FDOT BD493. Structural Research Center, Florida Department of Transportation.

[26] Wekezer, J. W., Szurgott, P., Kwasniewski, L., Siervogel. (2008). *Investigation of Impact Factors for Permit Vehicles*. Final Report, FDOT BD543. Structural Research Center, Florida Department of Transportation.

[27] Yang, Y., Lin, B. H. (1995). *Vehicle-Bridge Interaction Analysis by Dynamic Condensation Method.* Journal of Structural Engineering, vol. 121 (11), pages 1636-1643.

[28] Yang, Y., Chang, C. H., Yau, J. D. (1999). *An Element for Analyzing Vehicle Bridge Systems Considering Vehicle's Pitching Effect*. International Journal for Numerical Methods in Engineering, vol. 46, pages 1031-1047.

APPENDIX A

RSVVP RESULTS OF EXISTING MODELS ASSESSMENT

In this appendix, results obtained from the RSVVP software used in the assessment of the existing FE models are presented. Apart from the values of the comparison metrics, the NCHRP 22-24 acceptance criteria states that it is important that the residual histogram has a bell shaped distribution and that the cumulative distribution has an "S" shape. The data presented in this appendix are the basis of the results which were presented in Chapter 3 for the comparison of experimental test and numerical analysis. The figures presented show the histograms and cumulative distributions obtained from the comparison of the experimental tests and numerical analysis results conducted in chapter 3.

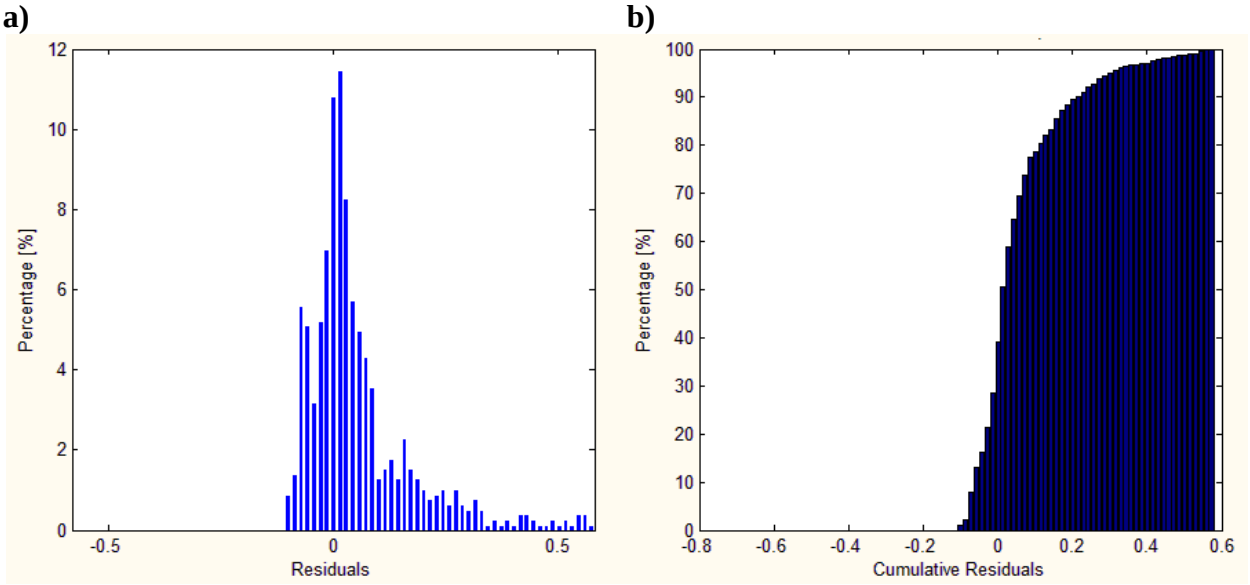

Figure A.1. Results of RSVVP for bridge strains with tractor-trailer at 80 km/h in westbound lane: a) histogram, b) cumulative residual

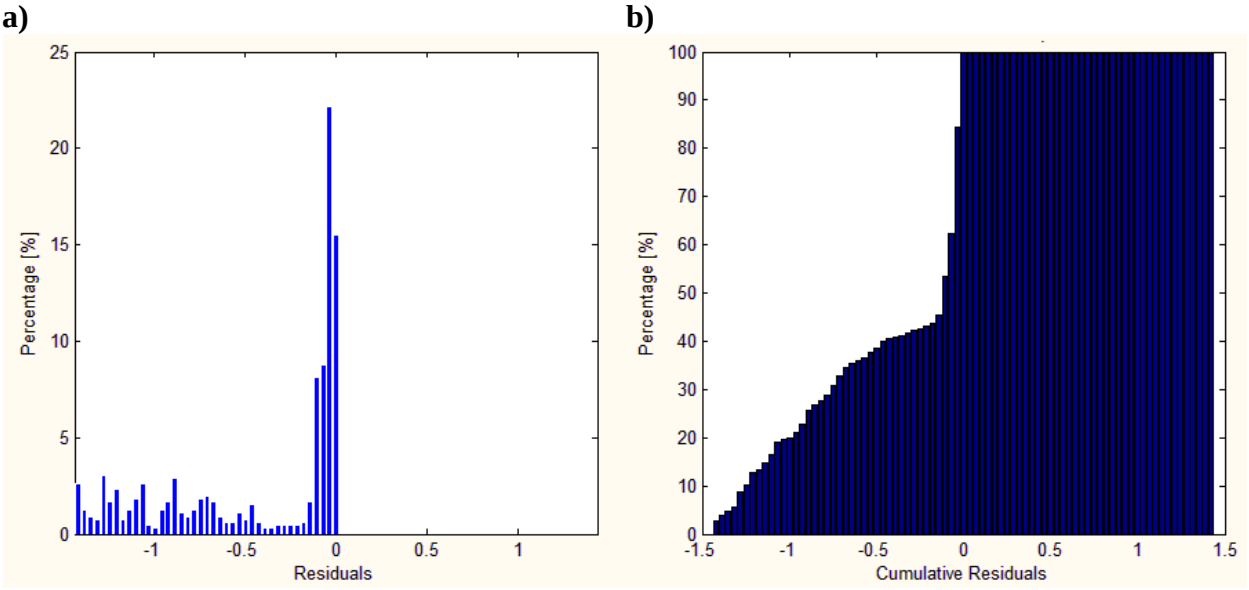

Figure A.2. Results of RSVVP for bridge displacements with tractor-trailer at 80 km/h in westbound lane: a) histogram, b) cumulative residual

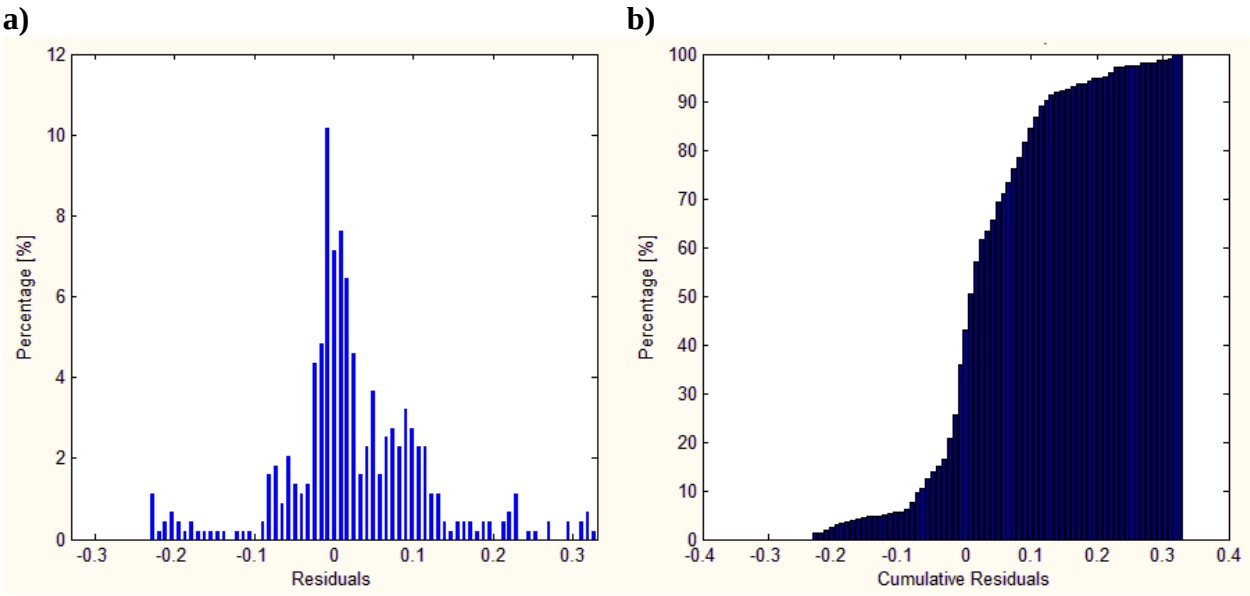

Figure A.3. Results of RSVVP for bridge strains with Terex crane at 80 km/h in westbound lane: a) histogram, b) cumulative residual

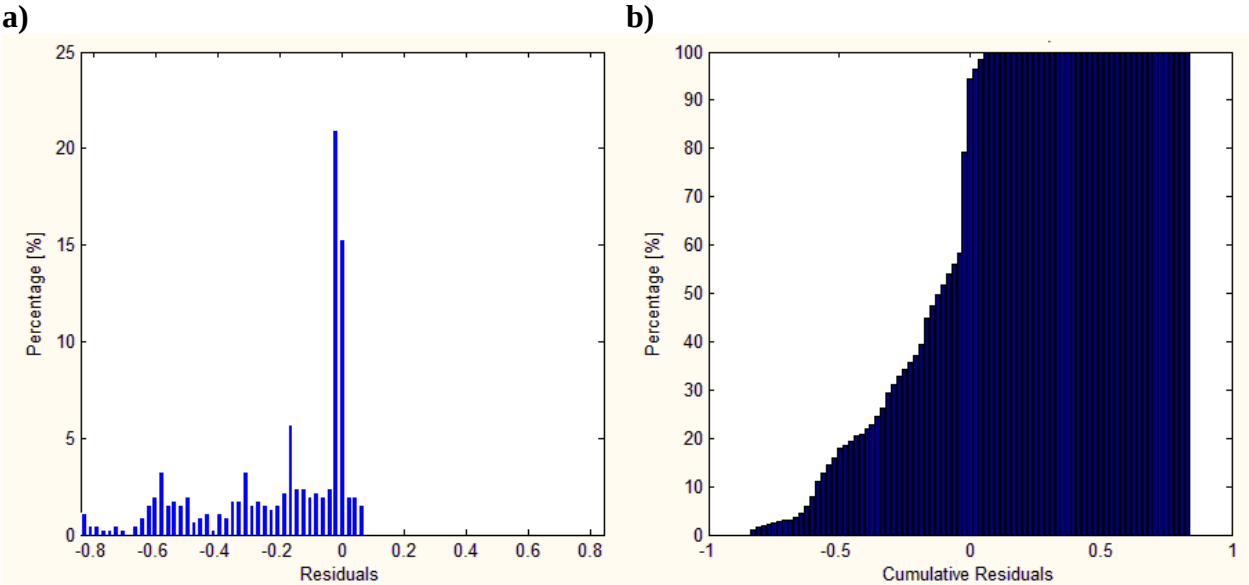

Figure A.4. Results of RSVVP for bridge displacements with Terex crane at 80 km/h in westbound lane: a) histogram, b) cumulative residual

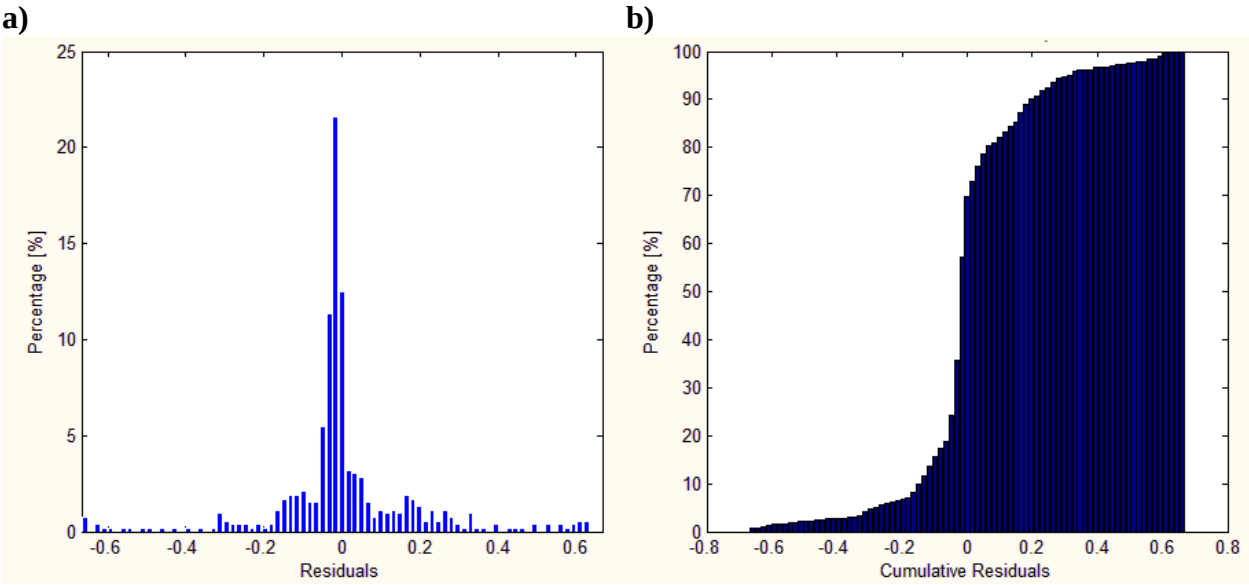

Figure A.5. Results of RSVVP for bridge strains with FDOT truck at 80 km/h in westbound lane: a) histogram, b) cumulative residual

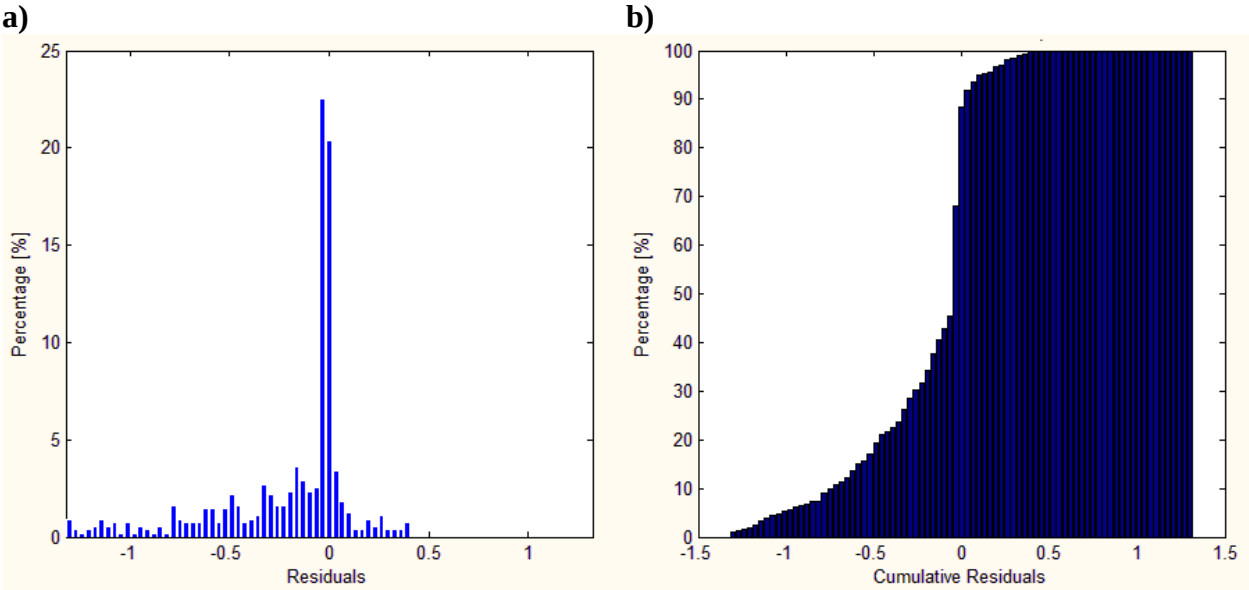

Figure A.6. Results of RSVVP for bridge displacements with FDOT truck at 80 km/h in westbound lane: a) histogram, b) cumulative residual

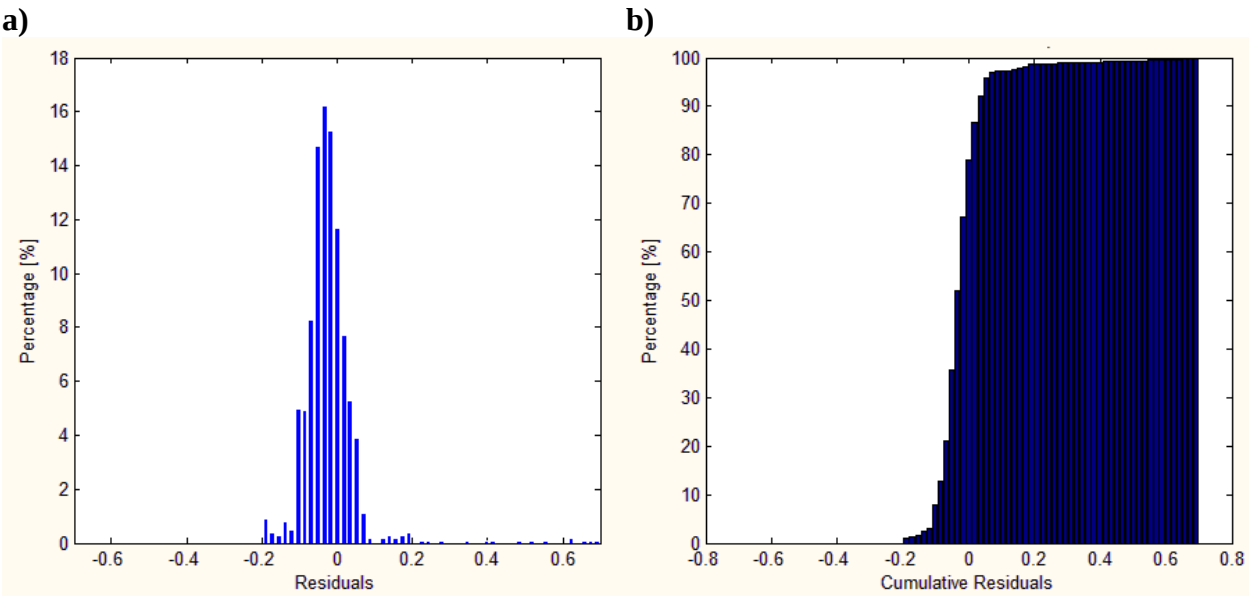

Figure A.7. Results of RSVVP for change in distance between axle and frame for tractor-trailer in the speed bump test at 24 km/h: a) histogram, b) cumulative residual

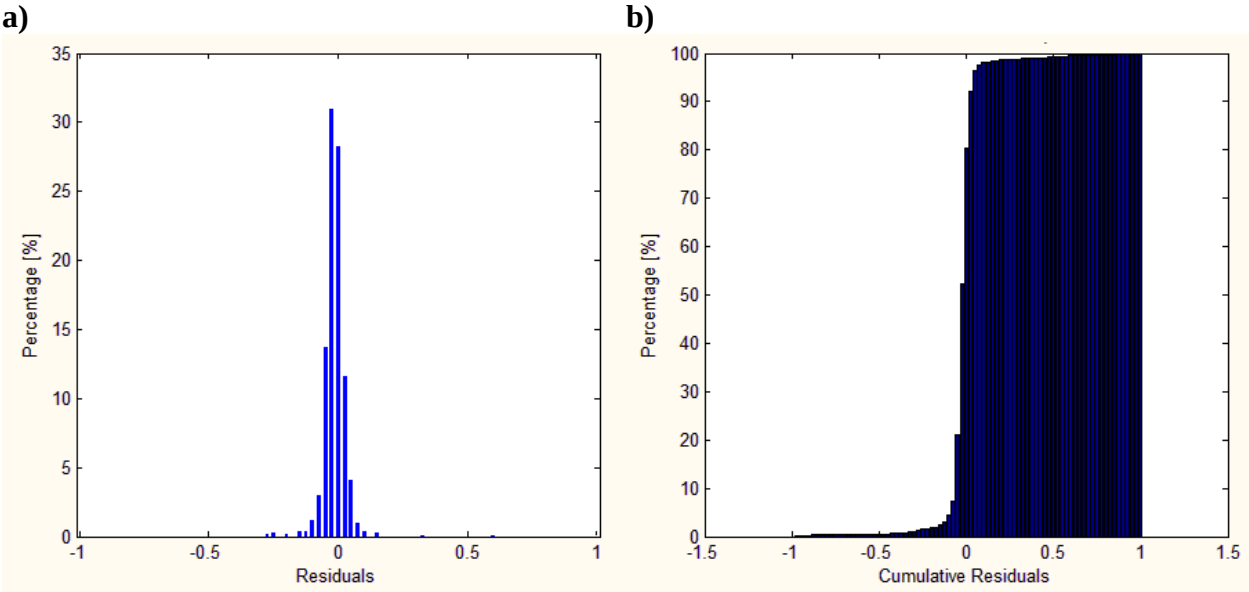

Figure A.8. Results of RSVVP for vertical acceleration of the tractor-trailer's front axle in the speed bump test at 24 km/h: a) histogram, b) cumulative residual

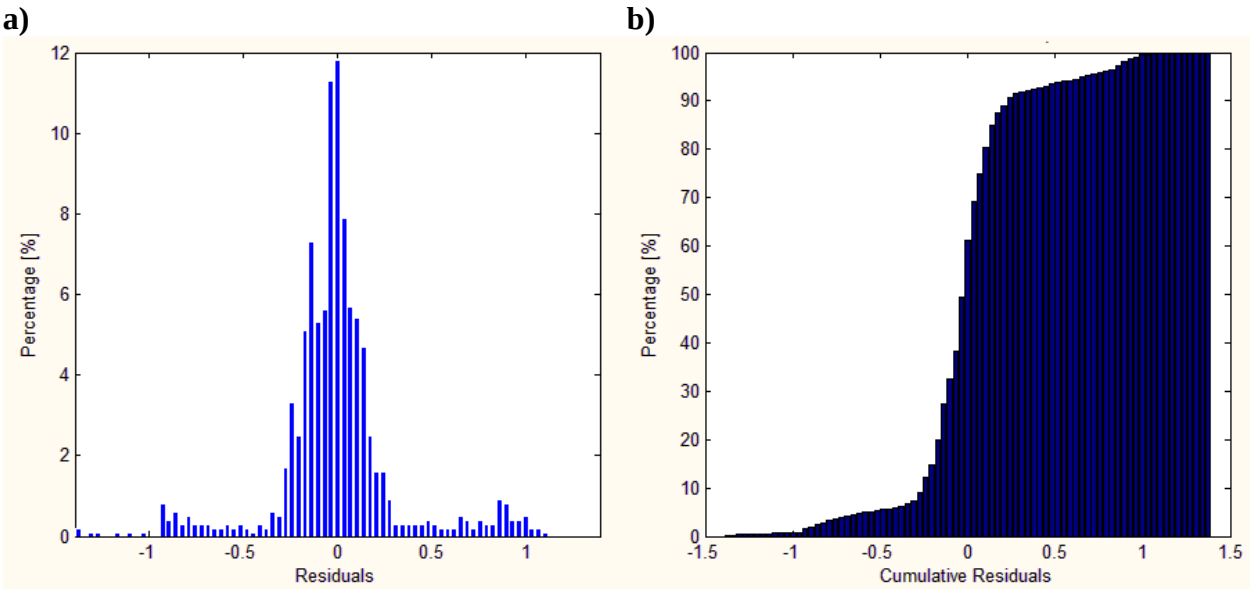

Figure A.9. Results of RSVVP for change in distance between axle and frame for Terex crane in the speed bump test at 24 km/h: a) histogram, b) cumulative residual

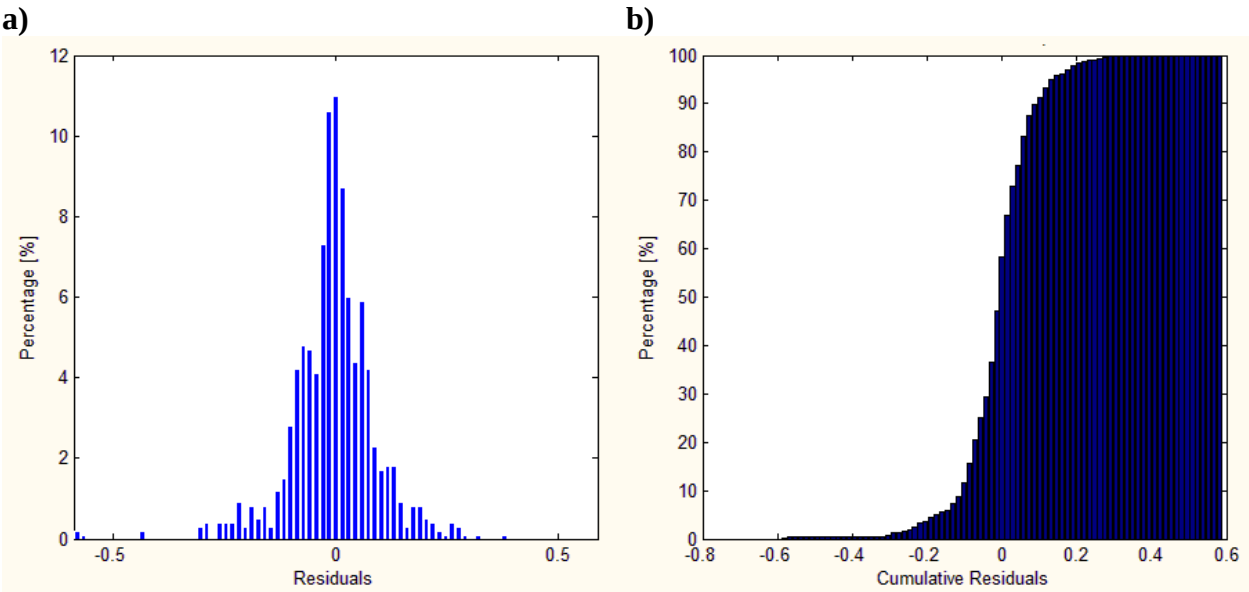

Figure A.10. Results of RSVVP for vertical acceleration of the Terex crane's front axle in the speed bump test at 24 km/h: a) histogram, b) cumulative residual